Mass spectrometry-based method development for glutathione determination and ^{13}C-tracer analysis in cultured cells

DISSERTATION ZUR ERLANGUNG DES DOKTORGRADES DER NATURWISSENSCHAFTEN (DR. RER. NAT.) DER FAKULTÄT CHEMIE UND PHARMAZIE DER UNIVERSITÄT REGENSBURG

Submitted by

Xueni Sun

from Qingdao, China

In 2020

Doctoral application submitted on: 25.06.2020

The dissertation was supervised by: PD Dr. Katja Dettmer-Wilde

Acknowledgements

I hereby sincerely thank everyone who provided support and advice during this doctoral work.

First, I would like to express my deepest appreciation to my supervisor PD. Dr. Katja Dettmer-Wilde for her continuous support of my PhD study and related research, for her patience and time that she spent on my work, and for the freedom, support, and trust during my time as a PhD student. The door to PD Dr. Katja Dettmer-Wilde's office was always open whenever I ran into a trouble with the instrument or had a question about my research or writing. Her guidance helped me tremendously during my research and writing of this thesis.

In addition, I would like to express my very profound gratitude to Prof. Peter Oefner for the opportunity and funding to accomplish this thesis at his institute and the constructive guidance in my work. I am gratefully indebted to his very valuable comments and revisions on each writing as well as on this thesis.

I also thank Prof. Wolfram Gronwald for his bioinformatical and statistical support, his instruction in NMR data analysis, as well as his participation in the discussion of my project.

Another "Thank you" goes to Lisa for her assistance in the lab, especially the sample preparation and performance of GC-MS analysis. She is a very considerate person and has always been responsive to my questions about sample preparation or instrument operation.

I would like to thank Raffaela for sharing knowledge of statistics, showing me how to do cell culture, and for her kind help in my doctoral work and life.

I would also like to thank Sharon for taking care of all paperwork, material submission, and contract preparation. And of course, I thank her for showing me how to bake German traditional cookies.

I would like to thank Paul for his instruction in the instrument operation at the beginning of my work, as well as his contributions on the project of GSH.

I would also like to thank Claudia for her help with NMR measurements and data analysis, thank Elke for her assistance in sample preparation, and thank Kathi for sharing knowledge of proteomics. Thanks also go to our lab boys: Fabian and Fadi. All people from the Institute of Functional Genomics are so nice and friendly. I was really happy to work with them.

Thanks also go to Christian for solving all problems with PCs, software, and so on. He is always patient to explain everything about the technique problems we met and how to solve it. And thanks go to all people from Prof. Rainer Spang group for their friendly cooperation on statistical matters.

I would like to thank Dr. Raquel Blazquez and Prof. Tobias Pukrop from the University Hospital Regensburg and Prof. Dieter Kube from the University Medical Centre Göttingen for the friendly cooperation.

I am grateful to Susanne, Jutta, Thomas, and Christoph from the Competence Center for Fluorescent Bioanalysis for their companionship. And thanks to all, whom I may have forgotten to name in person. Please do not take this as a sign of disrespect. Your support and help are appreciated sincerely.

My special thanks go to my friends Li, Suqi, Liangzi and her family with whom I could share all the ups and downs of the past four years, travel, and celebrate Chinese festivals together.

Last but not least, my deepest thanks go to my family: my parents, my brother, and sister in-law for supporting me spiritually throughout my doctoral work and my life. I love you all! My father used to be the one who supported me the most in my life. I will miss him forever!

This doctoral thesis was conducted at the Institute of Functional Genomics, University of Regensburg, from August 1st, 2016 until December 31st, 2019. It was financially supported by the Federal Ministry of Education and Research (Bundesministerium für Bildung und Forschung, BMBF) within the network eMed MMML-Demonstrator (BMBF-FKZ 031A428A) and Interreg V BY – CZ118.

Contents of Chapter 7 and Chapter 8 in this thesis were published in *Anal Chim Acta* with a slight alteration as the following research paper: *Quantification and ^{13}C-Tracer Analysis of Total Reduced Glutathione by HPLC-QTOFMS/MS,1080, 127-137.* Contents of Chapter 6 is a research paper in submission titled as "*Simultaneous determination of GSH and GSSG in cultured cells by LC-UV-QTOFMS after in situ derivatization with N-ethylmaleimide".* Contents in chapter 9 is an ongoing research paper with slight changes titled as "*Metabolomics studies regarding IDH mutation using ^{13}C-tracer analysis".* Paragraphs in this thesis (mainly in chapter 5, 6, 7, and 8) taken directly from the above publications are marked with quotation marks.

My contributions to this thesis include designing the project along with PD. Dr. Katja Dettmer-Wilde and Prof. Dr. Peter J. Oefner, carrying out the laboratory experiments, collecting and analyzing the data, as well as drafting the manuscript.

1 Table of Contents

2 Abbreviations and Acronyms

ANOVA	Analysis of variance
Ala	Alanine
Asp	Aspartic acid
α-KG	α-Ketoglutarate
bbCID	Broadband collision-induced dissociation
CID	Collision-induced dissociation
Cys	Cysteine
DTT	Dithiothreitol
Da	Dalton
EIC	Extracted ion chromatogram
ESI	Electrospray ionization
ER	Endoplasmic reticulum
FDA	Food and Drug Administration
GC	Gas chromatography
GCL	Glutamate cysteine ligase
Gln	Glutamine
Glu	Glutamate
Gly	Glycine
Glycerol-3-P	Glycerol-3-phosphate
GR	Glutathione reductase
GSH	Reduced form of glutathione

GSSG	Oxidized form of glutathione
D-2-HG	D-2-Hydroxyglutarate
IDH	Isocitrate dehydrogenase
IS	Internal standard
LLOQ	Lower limit of quantification
LOD	Limit of detection
MRM	Multiple reaction monitoring
MS	Mass spectrometry
MS/MS	Tandem mass spectrometry
m/z	Mass-to-charge ratio
NADPH	Nicotinamide adenine dinucleotide phosphate
NEM	N-ethylmaleimide
PBS	Phosphate-buffered saline
PCA	Principal component analysis
Pro	Proline
QTOFMS	Quadrupole-Time-of-Flight mass spectrometry
QqQ	Triple quadrupole
RSD	Relative standard deviation
S/N	Signal-to-noise ratio
SD	Standard deviation
Ser	Serine
TCA	Tricarboxylic acid
TCEP	Tris-(2-carboxyethyl)-phosphine

U-^{13}C	Uniform ^{13}C-labeled
2-VP	2-Vinylpridinne
WT	Wild type

3 Objectives

3.1 MS-based method development for glutathione determination

Glutathione is one of the most important endogenous antioxidants. Its level in the body is a useful indicator of oxidative stress status. Two forms of glutathione exist in vivo: the reduced form GSH and the oxidized form GSSG. A decrease in the ratio of GSH to GSSG is considered as an indicator of oxidative stress [1]. Several methods have been reported for GSH and GSSG determination in blood and tissues. However, studies regarding the determination of GSH and GSSG in cultured cells are scarce. In general, GSSG and GSH determination always suffers from autoxidation of GSH occurring at the -SH group which can result in overestimation of GSSG. This thesis aimed at developing and optimizing mass spectrometry-based methods for the simultaneous determination of GSH and GSSG in cultured cells, as well as total glutathione quantification.

In 2015, Giustarini *et al.* reported an HPLC-UV-based protocol for GSH and GSSG determination in cell culture employing NEM (*N*-ethylmaleimide) as the -SH masking agent [2]. NEM can rapidly permeate cells and react with GSH (Figure 1).

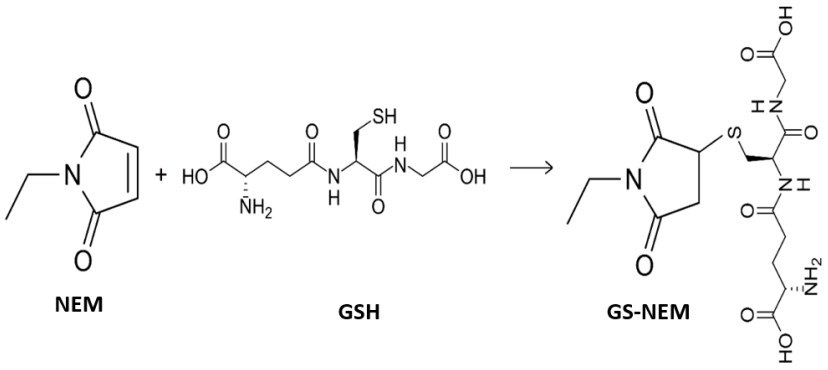

Figure 1. *Reaction of NEM with GSH. NEM quickly enters the cells and blocks the -SH group in GSH thereby preventing its auto-oxidation.*

Based on that protocol, an HPLC-UV-MS/MS method was developed and optimized in this thesis for the simultaneous determination of GSH and GSSG employing NEM derivatization. A major challenge in this context is the large gap between intracellular GSH and GSSG concentrations. While GSH is highly abundant, GSSG is only present in traces.

Hence, the linear range of many mass spectrometers might not allow the simultaneous determination of both species. Therefore, GSH was determined as the GS-NEM derivative adduct and detected by UV and the eluent from LC-UV was subsequently subjected to mass spectrometry for GSSG determination. In addition, an HPLC-MS/MS method was established to determine the total glutathione pool in cell culture samples with DTT reduction. Both methods were systematically validated in terms of LOD, LLOQ, inter-/intra-day precision, as well as recovery.

3.2 MS-based method development for ^{13}C tracer analysis of glutathione

Most of studies published on glutathione analysis to date have focused on its quantitative determination. However, knowledge of the metabolic pathways involved in glutathione biosynthesis is of equal importance. This thesis introduces an HPLC-MS/MS method for ^{13}C-tracer analysis of glutathione. We implemented a wide window MRM strategy on a QTOFMS instrument for the isotope labeling analysis of GSH, which yielded the full isotopologue profile of both parent and product ions resulting from the labeled substrates (see Figure 2). Compared to a triple quadrupole instrument, which requires tedious work to set up individual transitions, a QTOFMS can acquire all possible isotopologues of the analyte with high resolution simultaneously without the need to set up transitions. Additionally, the wide MRM window strategy can also reduce interferences as only ions within the *m/z* selection window can pass the first quadrupole, are fragmented in the collision cell, and subsequently detected.

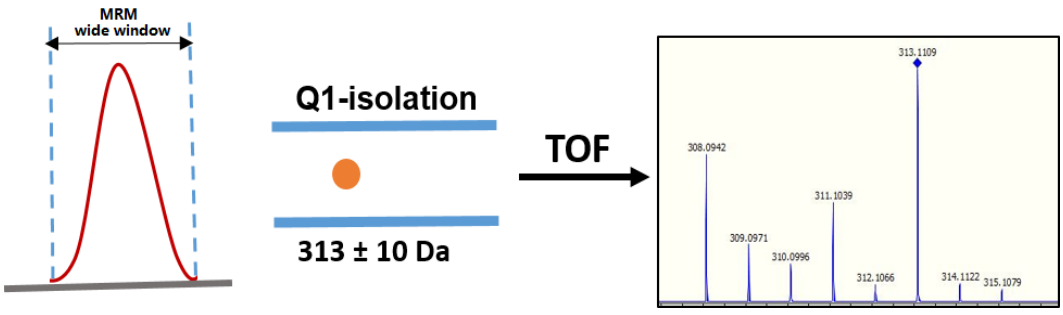

Figure 2. *"Scheme depicting the wide Q1-isolation window strategy on a QTOF instrument for comprehensive GSH isotopologue analysis." [3]*

3.3 Investigation of metabolic changes due to IDH1/2 mutation with ^{13}C-tracer analysis

The isocitrate dehydrogenase 1 & 2 (IDH1/2) are $NADP^+$-dependent enzyme involved in that catalyze the conversion of isocitrate to α-ketoglutarate. Mutations in *IDH1/2* have been found in several cancers such as certain types of gliomas [4]. The mutations result in a neomorphic activity of the enzyme, catalyzing the reduction of α-ketoglutarate (α-KG) to D-2-hydroxyglutarate (D-2-HG) concomitantly oxidizing NADPH to $NADP^+$. Metabolomic studies of IDH mutation have been frequently carried out and reported [5-8]. However, there is a continued need for more systematic investigations into the metabolic consequences of IDH mutation. In this thesis, using MS-based U-^{13}C-glucose and U-^{13}C-glutamine tracing, we investigated isotopic enrichment in a comprehensive set of metabolites including organic acids, amino acids, fatty acids, and endogenous antioxidant glutathione to elucidate the impact of different IDH1/2 mutations in the human colon cancer cell line HCT116 on cell metabolism.

4 Background

4.1 Glutathione

Glutathione is one of the most important intra- and extracellular antioxidants. Millimolar concentrations of glutathione are found in mammalian cells, whereas micromolar concentrations are typically detected in plasma [9]. Glutathione is synthesized in the cytosol and can be further distributed to different organelles, such as nucleus, mitochondria, and endoplasmic reticulum (ER) [10]. *De novo* biosynthesis occurs in two independent ATP-requiring steps, and uses L-cysteine, L-glycine, and L-glutamate as the substrates (see Figure 3). The first and rate-limiting step is the synthesis of the dipeptide γ-GluCys from cysteine and glutamate catalyzed by glutamate cysteine ligase (GCL), also called glutamylcysteine synthetase. Glutathione synthetase (GSS) catalyzes the second step whereby glycine is added to γ-GluCys to form the tripeptide glutathione.

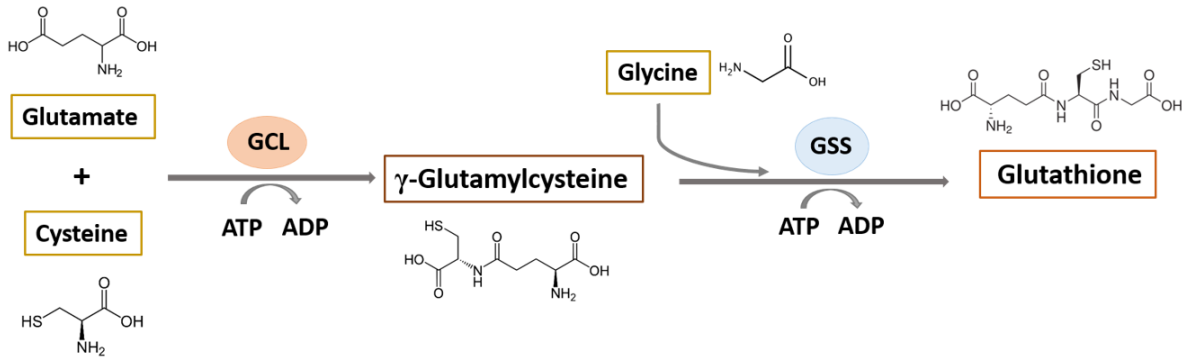

Figure 3. *"Scheme of de novo glutathione biosynthesis. Glutathione is a tripeptide that is synthesized in the cytosol from the precursor amino acids: glutamate, cysteine, and glycine. It can then be transported into mitochondria, endoplasmic reticulum or the nucleus to participate in distinct biological processes.* ***GCL****: glutamate cysteine ligase;* ***GSS****: glutathione synthetase." [3]*

Different forms of glutathione are present in cells, tissues, and plasma. Reduced glutathione (GSH) is the predominant form. Glutathione disulfide (GSSG), which is referred to as the oxidized form of glutathione, is formed by the oxidation of GSH. The ratio of GSH to GSSG within cells plays a crucial role in antioxidant defense. A decrease

of the ratio is considered indicative of oxidative stress [1]. Besides, other glutathione forms like sulfonates and glutathionylated proteins are also present in the body. However, in most cases, when speaking of total glutathione, only GSH and GSSG are included. Associations between the total intracellular glutathione level and various diseases have been observed in different experimental models [9]. The inhibition of glutathione *de novo* biosynthesis was found to sensitize tumor cells to chemotherapies [11], and to inhibit the generation of immune cytotoxic T lymphocytes [12]. This indicates the crucial role of glutathione in immune function and cancer therapy. Thus, glutathione has attracted increasing research interest.

4.2 Analysis of glutathione in biological samples

Over the years, numerous methods have been introduced to determine glutathione in biological samples. These methods can be divided into spectrophotometric- and HPLC-based methods. A ‘Recycling assay’, which is also called ‘Tietze recycling assay’, as the initial experiments were performed by Tietze in 1969, is one of the most popular spectrophotometric methods (see Figure 4) [13, 14]. It utilizes 5,5’-dithio-bis (2-nitrobenzoic acid) (DTNB) and glutathione reductase (GR), catalyzing the reduction of GSSG to GSH, to either determine GSSG only or to quantify the total glutathione pool (GSH + GSSG). Taking advantage of the specificity of GR, GSSG is reduced to GSH coupled with the generation of $NADP^+$ from NADPH. DTNB reacts with GSH and produces 5-thio-2-nitrobenzoate (TNB) which has a strong absorbance at 412 nm [15]. Another product GS-TNB (adduct of glutathione and TNB) is then reduced back to GSH by GR and NADPH, concomitantly the generation of TNB. Thus, the reaction circulates through the self-sustained closed cycle. The rate of TNB formation can be monitored by a spectrophotometer and compared to a standard curve and GSH is quantified. The recycling assay is generally used to quantify total glutathione (GSH + GSSG). To determine GSSG, it is necessary to first block the SH-group in GSH. 2-vinylpridine (2-VP) [16] and N-ethylmaleimide (NEM) are two commonly used blocking agents. In particular, NEM has been widely used due to its fast reaction with GSH as well as its high cell permeability [17]. However, since NEM is a potent inhibitor of GR, excess reagent has to be removed when a GR-based glutathione recycling assay is performed, which is

laborious and may introduce experimental errors. 2-VP is thus recommended in those cases. Alternatively, GSSG can also be measured by a GSSG-endpoint assay where NADH consumption is measured spectrophotometrically based on the specific reduction of GSSG by GR [18]. However, all of these enzymatic methods are indirect ways to determine glutathione and generally lack sufficient sensitivity for the determination of GSSG.

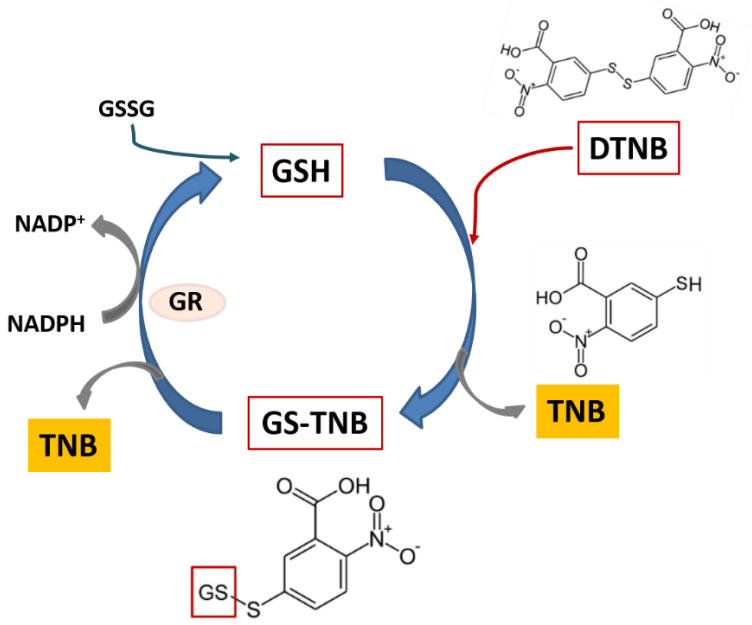

***Figure 4**. Scheme of glutathione recycling assay. GSSG is reduced to GSH by GR coupled with the conversion of NADPH into NADP⁺. GSH reacts with DTNB and produces TNB and GS-TNB. GS-TNB is then reduced back to GSH by GR and NADPH, entering a recycling reaction. The rate of TNB formation can be monitored by a spectrophotometer at 412 nm. It can be used to determine total glutathione. To determine GSSG only, GSH is quenched by blocking the -SH group with a derivatizing agent before the assay. The figure was redrawn and modified from previous reports [13, 15].*

HPLC-based methods for glutathione determination include HPLC-UV [19, 20], HPLC-fluorescence [21-23], and HPLC-MS detection [24-29]. Reed *et al.* reported an HPLC-UV method based on the derivatization of free thiol with iodoacetic acid (IAA) followed by derivatization of the *N*-terminal amino group with 1-fluoro-2,4-dinitrobenzene (DNFB) [30]. The method provided a linear response over a GSH working range of 0.1 to 5 nmol. However, it takes five hours to prepare the samples for analysis: 1 hour for IAA to react

with thiols and 4 hours for DNFB to react with the amino group. Alternatively, monobromobimane (mBBr) has been employed to form a fluorescent derivative for glutathione determination by HPLC-fluorescence detection [31]. mBBr selectively reacts with thiols and the total time for preparation and analysis of a sample is reduced to 1-2 h. However, this method cannot be used to detect disulfides like GSSG. Winters *et al.* then combined N-(1-Pyrenyl) maleimide (NPM) derivatization, 2-vinylpyridine (2-VP) masking, and reduction of GSSG with glutathione reductase to analyze both GSH and GSSG by HPLC-fluorescence detection at an excitation and emission wavelength of 330 nm and 380 nm, respectively [32]. In this method, similar to the recycling assay, 2-VP was used to block the -SH group of GSH. GSSG was then reduced to GSH by GR and NADPH. The resulting GSH was measured as a fluorescent derivative after derivatization with NPM. The lower detection limit of the method was reported at 58 fmol load on the column.

In all the above methods, sample pretreatment such as the derivatization of an amino or thiol group is required to make the GSH detectable by HPLC-UV or HPLC-fluorescence detection. HPLC-MS, on the other hand, can achieve direct detection of GSH with high sensitivity and specificity. Combined with reduction to obtain total glutathione or derivatization to measure both GSH and GSSG, HPLC-MS has been employed frequently to determine glutathione in various specimens such as blood [26, 33], tissue [34], and cultured cell [3].

Of note, over the years, results have varied greatly from study to study regarding GSSG and GSH concentrations in biological samples, even in control groups. The main reason is thought to be autooxidation of GSH during sample collection and preparation. Roberts et al. [35] have pointed out the importance of appropriate tissue sample preparation in glutathione analysis. They compared two methods of sample preparation of various mouse organs to test the effect of sample preparation on resulting GSH values: tissue homogenization in sulfosalicylic acid, an acid used for protein precipitation in sample preparation, and tissue homogenization in 5,5’-dithio-bis (2-nitrobenzoic acid) (DTNB), an agent used to block the thiol group [35]. GSH levels were significantly underestimated when using DTNB to prepare tissue samples like kidney, liver, and pancreas. The author reasoned that DTNB only masked the thiol group but failed to protect against the

degradation of GSH by gamma-glutamyl transpeptidase (γ-GT). Inhibition of γ-GT with AT-125 (L-(αS, 5S)-α-amino-3-chloro-4,5-dihydro-5-isoxazole acetic acid), an irreversible inhibitor of γ-GT, restored GSH values to those seen with acid homogenization.

Protein precipitation with acids such as trichloroacetic acid and perchloric acid, is a common step in biological sample preparation for glutathione analysis. Russi *et al.* [36] discussed possible reasons that can cause artifact GSSG formation and erroneous GSH determination in blood during sample preparation, including oxidation of thiols in acidified sample or during acid deproteinization, GSSG reduction by GR and NADPH, and the reaction of electrophiles (-SH blocking reagent) with amino groups. Thus, blockade of the -SH group prior to protein precipitation and acidification was strongly recommended by the authors. *Nature Protocols* published a modified procedure in 2006 based on the recycling assay for quantitative analysis of glutathione in various specimens [15]. This protocol uses sulfosalicylic acid to precipitate proteins, as it can also inhibits γ-GT, thus, avoiding the degradation of GSH. In 2016, Giustarini *et al.* [13] reported a variant of the protocol that uses NEM to block the -SH group [15]. This protocol is believed to better prevent GSH autooxidation during sample collection and preparation.

Overall, the improved sample preparation and detection methods together with the increasing awareness to prevent GSH autoxidation or degradation during sample preparation will provide more reliable results and better understanding of the role of glutathione in metabolism and disease.

4.3 Isocitrate dehydrogenase mutation

Mutations in isocitrate dehydrogenases 1/2 (IDH1/2) have been frequently discovered in multiple types of human cancers, but mostly in acute myeloid leukaemia (AML) [37] and gliomas [4]. IDHs catalyze the oxidative decarboxylation of isocitrate to α-ketoglutarate (α-KG) coupled with the generation of NADPH (or NADH in the case of IDH3). There are three isoforms of this enzyme with same function, however, localized in different parts of cell, the cytosolic IDH1 and the mitochondrial IDH2 and IDH3 [38]. To date, all mutations observed in *IDH1* affected codon 132 (Arg132) and IDH2 mutations were identified at the

Arg172 and Arg140 codons [37]. In gliomas IDH1-R132H was found to be the most frequent mutant type (> 90%) where arginine is replaced with histidine [39] while the identified *IDH2* mutations in gliomas often results in the replacement of arginine with lysine at codon R172K [4]. In AML, in contrast, IDH2-R140Q accounts for the majority of the mutations observed [40]. Great efforts have been made to elucidate the mechanism of tumorigenesis in these cancers. Among those, metabolomics studies have revealed important aspects of tumor metabolism at different levels (cell or tissue) [7, 41-45]. A shift of the mutated enzyme's ability from catalyzing the conversion of isocitrate to α-KG to the production of D-2-hydroxyglutarate (D-2-HG) from α-KG in *IDH1/2* mutant cells was observed (see Figure 5) [4, 46, 47]. As a result, elevated levels of D-2-HG were found in tumor cells with *IDH1/2* mutation [48]. Tumor cells containing IDH1-R132H or IDH2-R172H mutations exhibit a more than 100-fold increase in D-2-HG amounts compared to tumors with wild-type IDH enzyme [47, 49, 50].

2-Hydroxyglutarate exists in two isoforms: L-2-HG and D-2-HG. Germline mutations in D-/ L-2-hydroxyglutarate dehydrogenase (*D2HGDH* / *L2HGDH*) can also cause the accumulation of 2-hydroxyglutarate (2-HG) [51]. D2HGDH / L2HGDH specifically oxide D-2-HG / L-2-HG back to α-KG, respectively. The deficiency in those two enzymes results in an elevated level of 2-HG, which have been observed in D-/L-2-hydroxyglutarate aciduria (D-/L-2-HGA) diseases [52]. Elevated level of 2-HG was also identified in renal cell carcinoma, however, more than 90% of it was the L-enantiomer due to the reduced expression of L2HGDH [53].

D-2-HG is considered as an oncometabolite and the accumulation of D-2-HG may promote tumorigenesis in cancers. In the past few years, researchers have focused on the role of D-2-HG in regulating the phenotype of *IDH1/2* mutant cancer cells. It was found that D-2-HG can act as an antagonist of α-KG as they are similar in structure, therefore inhibiting α-KG-dependent enzymes activity [46, 54]. These enzymes catalyze a variety of functions, including various metabolic reactions. Therapies to treat cancers harboring an *IDH1/2* mutation are being developed, targeting either the mutant IDH enzyme directly or 2-HG sensitizing pathways [46, 55, 56].

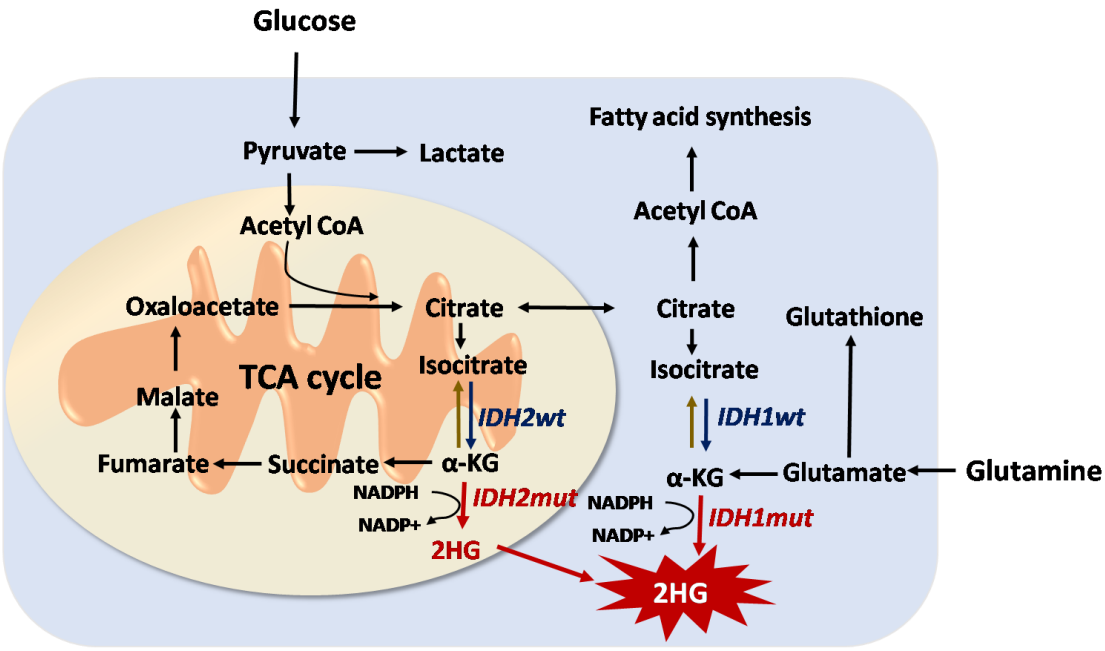

Figure 5. *Scheme depicting the intracellular metabolism associated with IDH mutation. The figure was drawn and modified referred to a previous report [57].*

Dysregulation of metabolism commonly occurs in cancer cells. Since IDH enzymes function at metabolic crossroads, mutations in *IDHs* influence other metabolic pathways [58-63]. Glutathione, as one of most important endogenous anti-oxidant, is generally maintained in its reduced form (GSH) in cells by glutathione reductase (GR) to protect cells against oxidative damage. Glutathione reductase specifically requires NADPH for the reduction of glutathione. Although NADPH can be supplied by several enzymes involved in different metabolic pathways, e.g., glucose-6-phosphate dehydrogenase in pentose phosphate pathway, IDH enzymes are considered as a major source of NADPH [38, 64]. Wild-type IDH enzymes reduce $NADP^+$ to NADPH while converting isocitrate to α-KG in cytosolic and mitochondrial compartments. Since NADPH does not permeate the mitochondrial membrane, wild-type IDH2 is essential to replenish this reducing equivalent to protect cells against local oxidative stress [38]. In contrast, mutant IDH1/2 consume NADPH to form D-2-HG (see Figure 5). Indeed, Shi *et al*. reported a decreased NADPH level in clonally generated mutant IDH1 glioma cells compared to the control cells [65]. More recently, it was argued that mutant IDHs sensitize cells to oxidative stress by

consumption of NADPH for D-2-HG synthesis, which may serve as a metabolic weakness for radiation anti-cancer therapy [66].

Additionally, mutant IDH cells show an increased dependence on glutaminase (GLS) for glutamate biosynthesis [8]. In fact, Seltzer et al. found that mutIDH1 glioma cells were particularly sensitive to GLS inhibition [67]. This phenomenon was then further proven in IDH1/2 mutant AML cells [45] and may provide a potential target for cancer therapy if IDH mutations are present. Furthermore, intracellular amino acids, choline derivatives, fatty acids, and TCA intermediates levels were also found to be altered in mutant IDHs expressing cells [63, 66]. Not surprisingly, exogenous 2-HG treatment can replicate most of the metabolic changes [68]. However, glutamate decrease is an exception which is a direct result of the mutation occurring in IDH enzymes and cannot be replicated by exogenous 2-HG treatment. All in all, a clear understanding of metabolic changes caused by *IDH* mutation, leading to a better understanding of the tumorigenesis, may provide exciting novel targets for cancer therapy.

4.4 Metabolomics

4.4.1 Basic principles and concepts

Metabolomics as one of the ‘omic’ sciences is used to investigate endogenous metabolites within a biologic system to determine metabolites levels or follow the fate of metabolites along metabolic pathways. Metabolites here are usually defined as small molecule with <1500 Da molecular-weight that are required for metabolism or are products of metabolic reactions [69]. Metabolomics covers the identification and quantification of all intra- and extracellular metabolites using different analytical techniques. Metabolic profiling and metabolic fingerprinting are the two complementary approaches used in metabolomics study [70]. Metabolic profiling aims at developing specific analytical tools to analyze known groups of metabolites that are involved in one or more pathways of interest, yielding absolute quantification of the studied metabolites [71]. It is also often called targeted metabolomics. This approach generally needs a prior knowledge of the pathways associated with the study. Thus, it is a hypothesis-driven approach [72]. Metabolic fingerprinting, also called ‘non-targeted metabolomics’, on the

other hand, aims at investigating the global metabolite profile and comparing patterns or ‘fingerprints’ of metabolites that change in response to internal or external perturbations under specific conditions [73, 74]. Thus, it is a hypothesis-free approach. Combined with statistical analysis, non-targeted metabolomics can be used to quickly identify small molecule biomarkers and affected pathways related to specific disease and provide a prior knowledge for targeted metabolomics. Combination of targeted and non-targeted metabolomics serves an extremely important role in metabolic research. Moreover, metabolic flux / tracer analysis which can be used to study the fate and origin of the metabolites in biological systems is also being increasingly applied in biomedical research.

4.4.2 Flux / tracer analysis

In the past decade, metabolic flux and stable-isotope tracing analyses have become powerful tools for uncovering cellular metabolic pathways. Metabolic flux analysis (MFA) aims to detect the rate of consumption / production of metabolites in biological systems. In general, the labeled substrates are used to feed the cells and incorporated into the metabolites of the metabolic network, and the incorporation can be used to resolve the fluxes [75-77]. By combining isotopic labeling data, nutrient uptake, and product excretion rates, the flux of the pathway can be determined with a computational model of the metabolic network [78-80]. Metabolic flux analysis can be used to reconstruct a comprehensive flux map that describes cellular metabolism. Comparisons of flux maps obtained under different experimental conditions provide a functional readout of the overall effect of the disturbance on cellular metabolism.

Tracer analysis can also be a powerful tool to investigate the metabolism of cells. It may be less informative, but it is easier to perform because mathematical model fitting with the obtained isotope labeling data is not necessary. Tracer analysis provides immediate insight into isotope labeling patterns of metabolites resulting from the labeled nutrient [81]. In many cases, tracer analysis can provide sufficient information to elucidate the nutrient / metabolic pathway contribution to the production of specific metabolites.

Mass spectrometry (MS) is the most frequently used technique to obtain isotope labeling data, while nuclear magnetic resonance (NMR), though well suited, is less often

employed. Of note, the obtained isotopic labeling data need to be corrected for the presence of naturally occurring heavy isotopes which can be performed with tools like IsocorrectoR [82].

The most frequently used tracer is ^{13}C, but other tracers such as ^{15}N, ^{2}H can also be employed [83]. Taking ^{13}C-tracer analysis as an example, by feeding cells with ^{13}C-labeled glucose, over time, the metabolites will become more and more enriched in ^{13}C until the point where ^{13}C enrichment in metabolites is stable. This state is called isotopic steady state during which the isotopologue distribution does not change with time [84]. The time that the cells need to reach isotopic steady state differs among metabolites and the tracer substrate employed. Besides, for some metabolites under certain cell culture condition, isotopic steady state might never be reached due to the constant and fast intracellular and extracellular exchange [81]. Alternatively, isotopically non-stationary metabolic flux analysis (INST-MFA), in which the metabolic network is regarded as a dynamic system, can be used to study local, relative fluxes when cells are not under isotopic steady state [85].

Metabolic flux analysis as well as tracer analysis, combined with advanced analytical techniques to obtain isotope labeling data, enables us to better understand cellular metabolism and enhances our knowledge to elucidate disease mechanism.

4.4.3 Analytical techniques

Metabolomics has experienced exponential growth in the past decade. This is largely attributed to the rapid development of increasingly sensitive and reproducible analytical platforms [86]. Mass spectrometry (MS) in combination with various separation techniques and nuclear magnetic resonance (NMR) spectroscopy are the two primary analytical techniques employed in metabolomics [87-89].

Proton NMR spectroscopy (^{1}H NMR) offers robust, high-throughput, unbiased metabolite detection [90-92]. It is characterized by high reproducibility, and requires only minimal sample preparation. Depending on the sample matrix, it can deliver data for a relatively large set of metabolites in a single analysis [93-95]. Nearly 70 blood metabolites have

been quantitatively determined in pooled human serum by combining ^{1}H NMR measurements, database searches, and spiking with authentic compounds [96]. Furthermore, chemical structure information can be obtained. In practice, NMR databases and search tools are commercially available and customizable, allowing fast and accurate identification of the compounds. However, NMR suffers from comparatively poor sensitivity. A concentration > 1 µM of the metabolite is typically needed for NMR-based analysis [97]. Underestimation of the metabolites due to their binding to proteins present in samples such as blood or urine, as well as signal overlaps from multiple detected metabolites are also issues that need to be taken into account when carrying out NMR-based metabolomics [94, 98].

Mass spectrometry, on the other hand, is a more sensitive technique. The high sensitivity enables the quantitative measurement of a broad spectrum of metabolites. Mass spectrometry coupled with a separation technique, such as liquid chromatography, gas chromatography, or capillary electrophoresis, has played an essential role in generating metabolomics data [99-104]. Hyphenation of MS with a separation technique tremendously expands the capability of MS for the analysis of complex biological samples. Due to separation of the metabolites in a time dimension, the complexity of the samples is tackled and cleaner mass spectra are obtained. However, MS-based methods generally require a more complex sample preparation. Ion suppression might also contribute a problem with complex samples, particularly when electrospray ionization (ESI) is employed [105].

Additionally, the combination of NMR and MS is advantageous for metabolite identification in complex samples. A fully automated workflow was introduced by Bingol and Brüschweiler as “NMR/MS Translator” [106]. It was applied to the metabolite identification in human urine and 98 metabolites in total were identified. With this strategy, metabolite candidates are firstly identified by 1D or 2D NMR, followed by the determination of their possible ions, adducts, fragments, and characteristic isotope patterns by MS. Together with NMR spectra, the mass spectrum generated by MS can be assigned with high confidence.

Metabolites are present over a wide concentration range. Moreover, they differ tremendously in their chemical structure and therefore also in their chemical and physical properties, making it virtually impossible to simultaneously determine the whole metabolome. Besides, there are still a lot of ‘unknowns’ that cannot be identified by MS or NMR alone [107]. To obtain as much information as possible in metabolomics studies, proper sample preparation and a combination of different analytical techniques are extremely advisable.

4.5 Mass spectrometry-based metabolomics

4.5.1 Mass spectrometry

Mass spectrometry is an analytical technique to determine molecules in gas-phase through the detection and characterization of their mass-to-charge ratios *(m/z)*. By comparing the identified *m/z* with the known compound mass, their fragmentation, and isotope patterns, unknown compounds can be identified. Currently, there are several types of commercially available MS analyzers that are used in metabolomics.

4.5.1.1 Single quadrupole mass spectrometer

A single quadrupole mass spectrometer is composed of four circular or hyperbolic parallel rods. A direct current (DC) voltage and a radiofrequency (RF) voltage are applied to the rods and the pairs of opposite rods have the same charge applied [108]. Ions are separated based on their trajectory stability in the electric field applied to the rods. Only ions with a certain *m/z*, depending on the applied voltage, can pass through the quadrupole and reach the detector [108-111]. By changing the applied voltage, ions are successively selected and scanned. This mass spectrometer can be operated in either full scan mode or selected ion monitoring (SIM) mode. In full scan mode, the transmitting ions are scanned in sequence. In SIM mode, only selected mass is allowed to pass the quadrupole. Thereby, longer scan time per mass can be realized. Thus, a better limit of detection (LOD) and lower limit of quantification (LLOQ) of the analyte can be achieved.

4.5.1.2 Time-of-flight mass spectrometer

Time-of-flight mass spectrometer (TOF) is a common mass spectrometer for gathering high resolution data. Using an electric field, ions are accelerated by a fixed voltage, traverse a field free flight tube, and the time required to reach the detector is measured [112]. The ions will have identical kinetic energies if they have the same charge and their velocities depend only on their masses. The lighter the ions are (lower *m/z*), the faster they will reach the detector. TOF mass spectrometry (TOFMS) can provide at least a mass resolution of 10,000 [113]. The resolution (or resolving power) is improved by using a reflectron (ion mirrors), which reduces the diffusion of the kinetic energy and, thus, a longer flight path is obtained [114]. A big advantage of TOFMS over the single quadrupole mass spectrometer is the high mass accuracy. That allows to generate a possible molecular formula for the detected ion, making it suitable for the identification of unknowns in metabolic fingerprinting.

4.5.1.3 Orbitrap

The Orbitrap mass spectrometer was invented in 1999 by Makarov [115]. It is an ion trap mass analyzer which consists of an outer barrel-like electrode and a central spindle electrode [116-118]. Ions enter the Orbitrap and oscillate around the central electrode. Ions are trapped because their electrostatic attraction to the central electrode is balanced by the centrifugal force created by their initial tangential velocity and the ions move in spiral patterns in the electrostatic field inside the trap [119, 120]. The axial oscillation of the trapped ions is detected as an image current and converted to a mass spectrum through Fourier transform of the frequency signal. Fairly high resolution (over 100,000) and mass accuracy (2 to 5 ppm) can be achieved by an Orbitrap mass spectrometer, as well as the detection of a wide range of compounds during both targeted and untargeted analyses without losing selectivity or sensitivity [116, 119, 121]. It has been increasingly applied in proteomics, metabolomics, as well as environmental, food and safety analysis [122-126]. However, compared to a TOF analyzer, Orbitrap analyzer suffers from a slow data acquisition. Fast acquisition rate is generally required to provide sufficient data points across a quantitatively chromatographic peak, especially when the mass spectrometry is

hyphenated with a UHPLC [121]. A comparison of the above introduced mass analyzers regarding their resolving power, mass accuracy, scan speed, as well as linear dynamic range is summarized in Table 1.

Table 1. Comparison of basic mass analyzers.

Mass analyzer	Resolving power (FWHM)	Mass accuracy	Scan speed	Linear dynamic range
Quadrupole	< 5,000	50-100 ppm	2 - 10 Hz	10^5
TOF	>10,000	3 ppm	5 - 40 Hz	10^4
Orbitrap	>100,000	2 ppm	1 - 5 Hz	5×10^3

Values shown in the table are considered when the mass analyzer is hyphenated with (U)HPLC and operated in full scan mode. This table was adapted from a previous report [127]. FWHM: full width at half maximum.

4.5.1.4 Tandem mass spectrometer

Triple quadrupole mass spectrometer (QqQ MS) is one of the most commonly used tandem mass spectrometers. It consists of three quadrupoles (see Figure 6) with the first and third quadrupole (Q1 and Q3) acting as a mass filter. The second quadrupole (q2), a non-mass resolving quadrupole, acts as a collision cell where the precursor ions selected in Q1 undergo collision-induced fragmentation. The resulting fragments are scanned or filtered by the third quadrupole (Q3) [128]. QqQ MS can be performed in various modes as shown in Table 2. QqQ MS contains double mass filtering, thus yields excellent LODs and LLOQs. It is highly suitable for selective and sensitive quantification of the analytes [129-134].

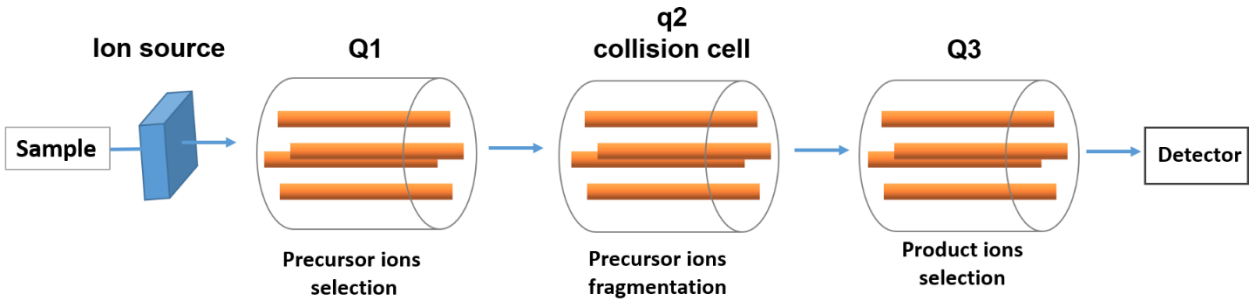

***Figure 6**. Schematic diagram of a Triple Quadrupole mass spectrometer.*

Table 2. Settings associated with each scan mode in QqQ MS.

Scan mode	Settings
Precursor ion scan	Q1: scan Q3: fixed *m/z*
Product ion scan	Q1: fixed *m/z* Q3: scan
Neutral loss scan	Q1: scan Q3: scan m/z_{Q1} - m/z_{Q3} = fixed *m/z (neutral loss)*
Selected reaction monitoring (SRM)	Q1: fixed *m/z (single ion)* Q3: fixed *m/z (single ion)*
Multiple reaction monitoring (MRM)	Q1: fixed *m/z (more than one)* Q3: fixed *m/z (more than one)*

4.5.1.5 Hybrid mass spectrometer

High resolution and sensitivity are desired for metabolite detection in metabolomics studies. However, in general, higher sensitivity leads to lower resolution and vice versa. Thus, with a single MS, it is challenging to achieve both. In addition, the increasing speed of chromatographic separation and the complexity of analyzed mixtures require faster and more intelligent and robust detectors [135]. Hybrid instruments are such mass spectrometric detectors, which combine different types of mass analyzers within a single

instrument. It typically consists of a low-resolution analyzer which is used to filter ions (e.g., quadrupole, linear trap) and a high resolution mass analyzer at the back end (e.g., TOF or Orbitrap) [120, 136]. When performing a full scan acquisition, it is similar to a standalone high-resolution mass analyzer, while in MS/MS mode ions can be selected and fragmented in the front analyzer and the fragments can be analyzed by the high-resolution mass analyzer.

Quadrupole-time-of-flight mass spectrometer (QTOFMS) is a common hybrid mass spectrometer. It is constructed like a QqQ MS except the Q3 is replaced by a TOF mass analyzer (see Figure 7). When performing full scan acquisition, the quadrupole serves only as a transmission unit while the TOF analyzer is used to record the mass spectra. TOF analyzers record all ions without scanning and can be operated in high acquisition speed which allows the acquisition of more data points per time unit, dramatically increasing sensitivity compared to a triple quadrupole mass spectrometer performed in full scan mode [137]. In MS/MS mode [138], Q1 serves as a mass filter. The selected precursor ions in Q1 are transferred to the collision cell (q2) where the ions undergo collision-induced dissociation (CID). The product ions are then analyzed by TOF mass spectrometer with high resolution. Hybrid QTOFMS such as Bruker Maxis Impact series can also perform broadband collision-induced dissociation (bbCID) acquisition whereby all precursor ions observed in the MS scan are simultaneously fragmented. It is similar to data independent acquisition (DIA) methods, which are now commercialized as SWATH and SONAR platforms by AB Sciex and Waters, respectively [139]. DIA and bbCID are able to capture both all MS and MS/MS data scans in a single run, enabling the acquisition of full information for all compounds and their fragments. They overcome the disadvantage of the traditional data dependent acquisition (DDA) method in which only the most abundant ions are fragmented, resulting in the information loss of low-abundance compounds [139]. Additionally, the Q1 on a QTOFMS platform can also be operated to allow ions over a given *m/z* range to pass through. Thus, only ions within the given *m/z* range will be transferred to collision cell and fragmented. The fragments can then be analyzed in parallel by the TOF analyzer with high resolution. In this thesis, we applied the wide Q1 isolation window strategy to ^{13}C-tracer analysis of glutathione (see Chapter 8). QTOFMS provides the exact masses of the quasi-molecular ions, the

fragments information, as well as the structural information of the detected ions. Hybrid QTOF mass spectrometers have been widely used in the field of proteomics and metabolomics for metabolic fingerprinting and identification of unknowns [140-144].

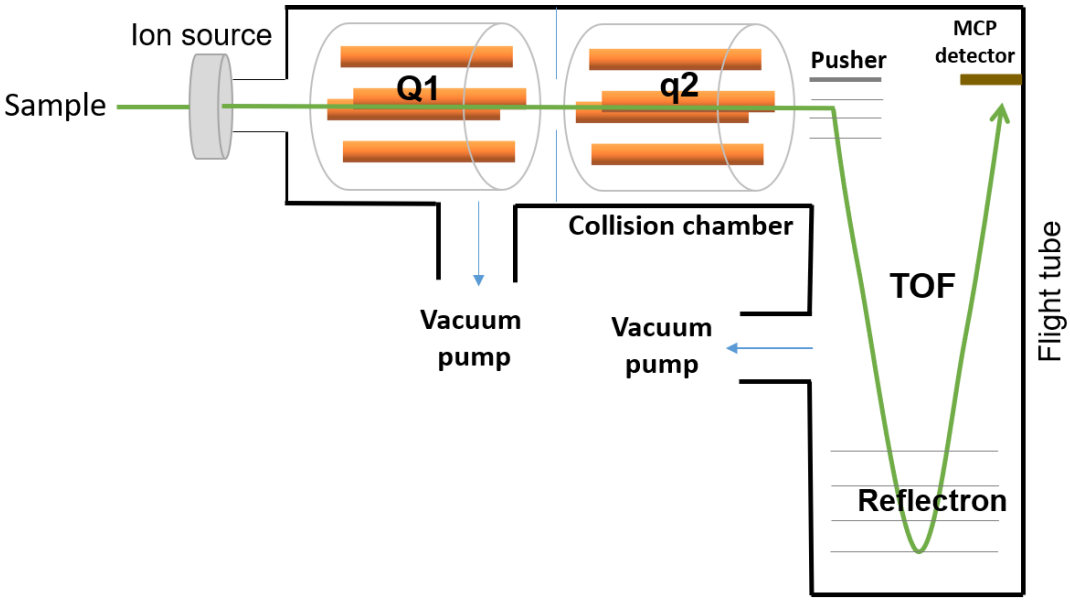

Figure 7. *Schematic diagram of a Quadrupole Time-of-Flight mass spectrometer.*

Other hybrid mass spectrometers such triple quadrupole MS where the third quadrupole can be used as linear ion trap (Q-Trap) [145-152] and a linear ion trap combined with a Fourier transform ion cyclotron resonance mass analyzer (LTQ-FTICR) [153-156] or an Orbitrap mass analyzer (LTQ-Orbitrap) [120, 157, 158] also play an increasingly role in proteomics as well as metabolomics studies.

4.5.1.6 Ion source

Techniques based on mass spectrometry require an ionization step (ion source) through which gas-phase ions are generated. Electron ionization (EI) and chemical ionization (CI) are typical ionization techniques used with GC [159]. For both EI and CI, samples much be introduced as a gas, thus are used exclusively for GC applications. EI is a hard ionization technique [160]. It generates many fragments and the fragmentation patterns

are unique and reproducible. By employing databases or reference libraries containing electron ionization mass spectra under the same operating conditions, it facilitates the identification of unknown compounds [161]. With CI, ions are generated through the collision of the analytes with a reagent gas ions (usually ammonia or methane) [162]. CI is a low energy process, being considered a much softer ionization technique compared to EI. It was originally used to produce quasi-molecular ions for GC-MS. However, CI requires additional maintenance in practice and it is not as sensitive as EI [159].

Electrospray ionization (ESI) has increasingly become one of the most important ionization techniques in mass spectrometry since its introduction in 1989 [163]. It is a soft ionization method and generates intact, multiply charged (typically for large molecules) gas-phase ions, and can be applied to a wide range of chemical and biological applications [164-167]. ESI generates gas-phase ions of the analytes directly from a liquid solution by applying a strong electric field to the droplets, creating a spray in an electric field [168]. Polar molecules are ionized especially well by ESI. To note, ESI could result in underestimation of the analyte concentrations due to the competitive ion formation (so-called ion suppression) [169]. This problem could be solved by using isotope labeled internal standard, which will experience identical ion suppression to the analyte of interest. Serial dilution of the sample could also be an alternative, especially when isotopic standards are not available. A linear response suggests the absence of ion suppression, while a strongly nonlinear one points to a problem.

Atmospheric pressure chemical ionization (APCI) is a form of chemical ionization that uses solvent spray at atmospheric pressure. It can be coupled to both liquid chromatography [170] and gas chromatography [171]. APCI is an ESI variant, however, is not as soft an ionization technique as ESI. With APCI, sample solution is nebulized by the nitrogen nebulizer gas to form a spray as it enters the heater and both sample and solvent molecules are vaporized to a gaseous state and ionized by a corona discharge [168]. The corona discharge is created at atmospheric pressures by applying a voltage on the needle. Nonpolar and slightly polar molecules can be ionized by APCI. In addition, compared to ESI, APCI has lower ion suppression effect. However, APCI is typically used for small molecules (<1000 u) [168]. Large proteins remain inaccessible to APCI.

Matrix-assisted laser desorption ionization (MALDI) is an ionization technique which can ionize solid-phase molecules. It is first introduced in 1987 by Karas et al [172]. Although the exact mechanism of MALDI ionization technique is not well known, it is generally believed that MALDI produces ions through laser excitation and ablation of the sample matrix [173, 174]. MALDI can produce high ionization yields of the intact analyte with a charge of 1. The generated ions are mostly detected by a TOF mass analyzer. This technique favors polar compounds.

Desorption electrospray ionization (DESI) is a very new ionization technique compared to others which was proposed by Cooks et al in 2004 [175]. DESI ionization technique relies on solvent extraction directly on the surface of the sample for localized information. It is a combination of ESI and desorption ionization technique. However, not like in ESI in which the sample is in the solution, sample of interest in DESI is in the solid phase. On the other hand, it is not like in MALDI since the sample is not under vacuum. Instead, DESI is performed under ambient environmental conditions [176]. Applications of DESI in metabolomics studies, especially in imaging mass spectrometry, have been frequently reported recently [177-181].

4.5.2 Liquid chromatography-mass spectrometry (LC-MS)

High performance liquid chromatography (HPLC) with its advanced form ultra-high performance liquid chromatography (UPLC) is an analytical technique used to separate each component in a mixture [182]. Liquid chromatography coupled to mass spectrometry (LC-MS) is a powerful tool for the identification and quantification of metabolites from complex samples in metabolomics studies [100, 183-186]. By combing HPLC separation of compounds with high resolution MS analysis, the detection limits and data quality can be dramatically improved, as the separation of the metabolites in a time dimension reduces the complexity of the samples and cleaner mass spectra are obtained.

Reversed-phase liquid chromatography (RP-LC) is the most frequently used liquid chromatography in HPLC practice. It utilizes a non-polar stationary phase, usually an alkyl- bonded silica phase, and an aqueous, moderately polar mobile phase. With RP-LC,

less polar molecules will show a stronger retention while polar molecules are less strongly retained on the column and elute earlier [182]. Normal-phase liquid chromatography (NP-LC), on the other hand, utilizes a polar stationary phase column and non-polar, non-aqueous mobile phase [187-190]. Thus, it is only suitable for the analysis of compounds that are readily soluble in non-polar solvents. NP-LC possesses its own advantages in specific studies. William et al [183] reported the determination of lipopolysaccharide (LPS) biosynthetic intermediate with normal phase liquid chromatography mass spectrometry (NPLC-MS/MS) and pointed out the more sensitive detection, low carry-over, smaller sample volumes, and extended column lifetimes of NP-LC achieved compared to RP-LC.

In addition, hydrophilic interaction liquid chromatography (HILIC) is another valuable alternative. “Hydrophilic” here refers to the affinity to water. It can be used to separate polar, weakly acidic or basic samples [191-194]. In HILIC, the separation of the samples is performed with a polar column and aqueous-organic mobile phase, typically acetonitrile with a small amount of water. The water in the mobile phase is attracted by polar groups of the stationary phase and an aqueous layer is formed over the surface of the stationary phase. Present theories of separation mechanism in HILIC include partitioning between the mobile phase and the water layer, hydrogen bonding, dipole-dipole interactions, and electrostatic interactions [195]. In a specific study, a combination of different separation mechanisms is most probably involved, depending on the column and buffer conditions employed i.e., the type of organic solvent, salt, and the pH [196]. HILIC can provide sufficient retention for strongly polar compounds with highly organic mobile phase and is well suitable for coupling to mass spectrometry, making it complementary to RP-LC [186, 197-199]. However, HILIC is not suitable for the analysis of compounds with low solubility in high proportion of organic solvent. Besides, relatively long equilibration time will be necessary to form stable water layer on the surface of stationary phase and achieve reproducible measurement in HILIC.

Furthermore, mixed-mode liquid chromatography (MM-HPLC) is also an alternative in HPLC practice. MM-HPLC is a type of chromatography in which the separation of the analytes is achieved based on more than one interaction form of the analytes with the chromatographic stationary phase in one single column [200]. The advantages of MM-

HPLC over a conventional single-mode stationary phase include high separation efficiency and selectivity, high loading capacity, as well as its possible replacement of two conventional corresponding columns under certain conditions [201]. MM-HPLC has been increasingly employed in the study of metabolomics [202-205].

4.5.3 Gas chromatography-mass spectrometry (GC-MS)

Gas chromatography (GC) is another type of chromatography used for analyzing compounds which can be vaporized without thermal decomposition. In modern GC, capillary columns are used, where the stationary phase is coated as layer of liquid (wall coated open tubular column) or particles (porous layer open tubular column) on the inner surface of a thin fused silica or metal tube. GC uses carrier gas (Helium, hydrogen, or nitrogen) to transport the analytes through the column. In contrast to liquid chromatography, carrier gas in GC will not interact with the stationary phase and the gas type has no influence on the retention of the analyte. Gas chromatography coupled to mass spectrometry (GC-MS) has been frequently used in metabolomics studies for both targeted and untargeted analysis [101, 102, 206-211].

Gas chromatography is restricted to analytes that can be vaporized without decomposition. However, most of the metabolites, such as organic acids and sugars, possess polar functional groups and have poor volatility and thermal stability. Derivatization is thus necessary to make those compounds suitable for GC analysis. Derivatization not only increases the volatility and thermal stability of the analytes, but often also improves the chromatographic properties of the analytes [212]. Silylation, alkylation, acylation, oximation, and cyclization are the commonly used derivatization reactions [212]. Sometimes, even more than one derivatization reaction is used within a protocol. Mu et al. has employed oximation and silylation reactions combined GC-MS analyss to carry out metabolomics study of non-small cell lung cancer (NSCLC) patients serum, providing a biomarker panel for the auxiliary diagnosis of NSCLC in nonsmoking females [206]. Combination of methoximation and silylation of organic acids e.g., TCA cycle intermediates, and subsequent GC-MS analysis has been frequently used in metabolomics studies [213, 214]. Besides, fatty acids are usually analyzed by GC-MS

after derivatization to form respective fatty acids methyl esters (FAMEs), especially for the fatty acids containing more than 10 carbon numbers [215]. Nowadays, due to the progress of the instrument development, automated derivatization can be performed on GC-MS coupled with a sample-preparation device which can not only improve the speed, efficiency, and reproducibility of the analysis, but also the safety of the operators.

Investigation of volatile organic compounds (VOCs) is also an important application of GC-MS in metabolomics studies. VOCs are a diverse group of carbon-based compounds such as alkanes, alcohols, aldehydes, and ketones that exist in exhaled breath and biofluids e.g., blood, urine, feces, and sweat [216]. VOCs patterns have been linked to a variety of diseases like cancers [207, 216-218] and diabetes [219]. Coupled with extraction device such as solid phase microextraction (SPME) [101, 218, 220], GC-MS has been frequently used for VOCs detection and analysis, especially in the investigation of potential cancer biomarkers.

4.5.4 Ion mobility spectrometry-mass spectrometry (IMS-MS)

Ion mobility spectrometry (IMS) is another analytical technique used to separate gas-phase ions. With IMS, ions are separated based on their size, shape, and charge, which is also defined as their ‘mobility’, in an electric field [221]. IMS provides an additional selectivity dimension, increasing the ability to separate and analyze compounds even when they have the same molecular weight and chromatographic retention time. Numerous ion mobility technologies have been introduced including drift tubes, traveling wave, trapped IMS, and differential mobility analyzers, among others [222]. Drift tube IMS (DTIMS) is the most established form of IMS. In DTIMS, ions are propelled by an electric field against a counter current flow of a drift gas (mostly nitrogen, helium or argon). In the drift tube, ions collide with the drift gas multiple times, which slows them down. The ions are accelerated again by the applied field and they move at a constant velocity which depends on their charge, size, shape, and collision cross section, allowing them to be identified by the time they arrive at the detector [223]. Traveling wave IMS (TWIMS) is another widespread IMS technology. TWIMS works along similar lines to DTIMS. However, instead of having a constant electric field, in TWIMS, the ions are propelled by

a set of continuously symmetric potential waves in the tube [224]. Although different mobility dispersive fields were employed in those IMS technologies to generate ion mobility spectra, all of them work on the common basis that the analytes are separated based on their different ion mobility behavior in the gas phase.

IMS can be hyphenated with MS, referred to as ion mobility spectrometry-mass spectrometry (IMS-MS). IMS-MS provides multidimensional characterization of detected analytes, making it a powerful analytical tool in the studies of proteomics [225], lipidomics [226, 227], and metabolomics [228-230]. It offers advantages in isomer separation and structural characterization [231, 232]. IMS-MS has become an increasingly popular technique in metabolomics [233-235]. In a metabolic profiling study of human blood with IM-TOF-MS, simultaneous separation of 300 isomeric / isobaric metabolites, along with the detection of ~ 1,100 metabolite ions, was accomplished [234]. Six-fold of peak capacity increase of the MS was also achieved by coupling IMS prior to MS analysis as introduced in the study. Moreover, using DTIMS-QTOF-MS, more than 500 small molecules including metabolites involved in TCA cycle, glycolysis, pentose phosphate pathway, secondary metabolites such as terpenes and flavonoids, and the xenobiotics such as antibiotics and pesticides were characterized [236]. Database developed based on that study is freely available at *http://panomics.pnnl.gov/metabolites/*. Additionally, combination of IMS with imaging mass spectrometry has also been increasingly explored to improve the performance of biological tissue imaging [237].

5 Experimental section

5.1 Materials and chemicals

Ammonium hydrogen carbonate (NH_4HCO_3) was purchased from AppliChem GmbH (Darmstadt, Germany), and DL-dithiothreitol (DTT) from Sigma-Aldrich (Taufkirchen, Germany). Stable isotope labeled glutathione (glutathione-(glycine-$^{13}C_2$,$^{15}N_1$)), stable isotope labeled glutathione disulfide (glutathione-(glycine-$^{13}C_4$,$^{15}N_2$)) as internal standard, unlabeled GSH, and unlabeled GSSG were purchased from Toronto Research Chemicals (Toronto, Canada). *N*-ethylmaleimide (NEM) was purchased from Sigma Aldrich (Taufkirchen, Germany). U-$^{13}C_6$-glucose and U-$^{13}C_5$-glutamine were purchased from Cambridge Isotope Laboratory, Inc. (Andover, MA, USA). Buthionine sulfoximine (BSO, Sigma-Aldrich) was kindly provided by Dr. Raquel Blazquez from the University Hospital Regensburg. 2-Propanol (LC-MS grade), acetylchloride, methyl chloroformate, methoxylamine hydrochloride, and pyridine were from Sigma-Aldrich (Taufkirchen, Germany). Chloroform (HPLC grade) was from Fisher (Fisher Scientific GmbH, Ulm, Germany). *N*-Methyl-*N*-(trimethylsilyl) trifluoroacetamide (MSTFA) was purchased from Macherey-Nagel (Dueren, Germany). L-glutamine was from Sigma-Aldrich (Taufkirchen, Germany). Solvents for sample preparation and LC-MS analysis were HPLC grade and purchased from VWR (Vienna, Austria). Purified water used in this thesis was from a PURELAB Plus system (ELGA LabWater, Celle, Germany).

5.2 Instrumentation

5.2.1 Glutathione determination and ^{13}C tracer analysis by HPLC-ESI-QTOF MS

Glutathione determination and ^{13}C-tracer analysis in chapter 7 and chapter 8 were performed as our previous report [3]. “The measurements employ a Maxis Impact QTOFMS (Bruker Daltonics, Bremen, Germany) with an ESI source coupled to a Dionex Ultimate 3000 UHPLC system (Thermo Scientific, Idstein, Germany) consisting of the HPG3400 RS pumping system, the WPS3000TFC autosampler, and the Dionex Diode Array Detector (shown in Figure 8). A Waters Atlantis T3 reversed-phase column (2.1×150 mm, 3 µm) with a 2.0 × 4 mm C18 pre-column (Phenomenex) was used with

mobile phase A (0.1% formic acid in H_2O, *v/v*) and B (0.1% formic acid in acetonitrile, *v/v*) gradient elution. The column was kept at 35 °C and a flow rate of 0.3 mL/min was employed in all studies. For full MS analysis the mass range was set from 50 to 1000 *m/z*. The optimized MS parameters are as follows: end plate offset 500 V; capillary voltage 4500 V; nebulizer pressure 2.6 bar; dry gas flow rate 10.0 L/min; dry temperature 220 °C. Before measurements, an external mass calibration was carried out using sodium formate clusters (10 mM sodium formate in 50 / 50 water / isopropanol, *v/v*). Moreover, each run was started with an injection of the sodium formate solution for internal recalibration using a six-port valve." [3]

Figure 8. *Instrument used for glutathione determination and ^{13}C-tracer analysis: Maxis Impact QTOF mass spectrometer coupled to a Dionex Ultimate 3000 UHPLC system.*

Analysis of the ratio of GSH (determined as GS-NEM) to GSSG (see chapter 6) was performed by HPLC-UV-ESI-QTOF-MS with a gradient chromatographic separation as shown in Table 3. For GS-NEM determination, the diode-array detector was operated over a range of 200 to 400 nm. The GS-NEM absorption peak was extracted at 210 nm. The eluent is then transferred into the QTOF mass spectrometer through an ESI source for GSSG monitoring in positive MRM mode with a 10 Da Q1 selection window.

Table 3. Gradient used for GSSG and GS-NEM analysis with HPLC-UV-ESI-QTOF-MS/MS.

Total time (min)	Flow rate (µL/min)	A %	B %
0.00	300	95	5
15.00	300	95	5
17.00	300	0	100
20.00	300	0	100
20.10	300	95	5
25.10	300	95	5

Quantification and ^{13}C-tracer analysis of total reduced glutathione (tGSH) in chapters 7 and 8 are performed with HPLC-ESI-QTOF-MS/MS. A gradient chromatographic separation was used (shown in Table 4). “Absolute quantification of tGSH was performed in positive ion MRM mode with a 0.7 Da Q1-isolation window (centering on 308 *m/z* for unlabeled GSH and 311 *m/z* for labeled GSH), while isotope labeling analysis was performed in positive ion MRM mode with a 20 Da window (centering on 313 *m/z*). A collision energy of 15 eV was used for both. For full MS and broadband collision-induced dissociation (bbCID) analysis the mass range was set from 50 to 1000 *m/z* in Chapter 8. When performing bbCID acquisition, collision energy of MS was 5 eV and collision energy of MS/MS (bbCID) was 15 eV” [3]

Table 4. Gradient used for quantification and ^{13}C-tracer analysis of total reduced glutathione with HPLC-ESI-QTOF MS/MS.

Total time (min)	Flow rate (µL/min)	A %	B %
0.00	300	100	0
10.00	300	40	60
12.00	300	0	100
17.00	300	0	100
17.10	300	100	0
22.10	300	100	0

5.2.2 Amino acids tracer analysis by HPLC-ESI-QqQ-MS

Amino acids tracer analysis in chapter 9 was performed after propyl chloroformate/propanol derivatization (see section 5.4.4) as described in a previous report [238] using an Agilent 1200 Series HPLC system (Boeblingen, Germany)

containing a binary pump, a temperature-controlled autosampler, and a column oven. The HPLC was coupled to an AB SCIEX 4000 QTRAP mass spectrometer (Darmstadt, Germany), equipped with a TurboV electrospray ion source (see Figure 9). A reversed-phase column Phenomenex EZ: faast AAA-MS (250×3 mm i.d., 4 µm) with mobile phase A: 10 mM ammonium formate and 0.1% (*v/v*) heptafluorobutyric acid in water and B: 10 mM ammonium formate and 0.1% (*v/v*) heptafluorobutyric acid in methanol was used. The column was kept at 30 °C. Gradient used for chromatographic separation is shown in Table 5. A 10 µL of solution was subjected to the analysis for each sample. The MS was performed in multiple reaction monitoring (MRM) after ESI ionization in positive mode using the parameters and transitions for different isotopologues listed in Table S1 (see supplementary information in chapter 11).

Figure 9. *Instrument used for amino acids isotope labeling analysis: AB SCIEX 4000 QTRAP mass spectrometer coupled to an Agilent 1200 Series HPLC system.*

Table 5. Gradient used for amino acids chromatographic separation on HPLC-ESI-QqQ MS.

Total time (min)	Flow rate (µL/min)	A %	B %
0.00	350	38	62
12.00	350	21	79
12.01	350	2	98
15.00	350	2	98
15.10	350	38	62
23.00	350	38	62

5.2.3 Organic acids tracer analysis by GC-EI-MS

Tracer analysis of organic acids in chapter 9 was carried out with an Agilent model 6890 GC (Agilent, Palo Alto, CA, USA) equipped with a mass selective detector (MSD) model 5975 Inert XL using an EI source, and an MPS-2 Prepstation sample robot (Gerstel, Muehlheim, Germany) (see Figure 10). Analytes were derivatized (see section 5.4.2) and separated on an RXI-5MS column, 30 m × 0.25 mm ID × 0.25 µm film thickness (Restek, Bad Homburg, Germany) equipped with a deactivated precolumn (2 m × 0.25 mm ID). Splitless injection was employed with an injection volume of 1 µL at 280 °C. The initial oven temperature was set at 50 °C, equilibrated for 0.5 min, ramped at 5 °C / min to 120 °C, and then to 300 °C at 8 °C / min, and held for 5 min. Total runtime is 42.5 min. A flow rate of 0.7 mL/min of the carrier gas (Helium) was employed. The transfer line to the mass spectrometer was kept at 310 °C. A full scan acquisition ranged from 50 to 550 *m/z* was performed.

Figure 10. *Instrument used for organic acids isotope labeling analysis: Agilent model 6890 GC-EI-MS equipped with a mass selective detector and an MPS-2 Prepstation sample robot.*

5.2.4 Fatty acid (C16:0) tracer analysis by GC-EI-MS

Tracer analysis of C16:0 as FAME in chapter 9 was carried out with a Agilent model 6890 GC (Agilent, CA, USA) equipped with a Mass Selective Detector (MSD) model 5975 using

an EI source and an Auto Liquid Injector model 7683 with a 10-µL syringe (see Figure 11). Analytes were derivatized (see section 5.4.3) and separated on a DB-Wax UI column, 32 m × 0.25 mm ID × 0.25 µm film thickness (Restek, Bad Homburg, Germany) equipped with a deactivated precolumn (2 m × 0.25 mm ID). Splitless injection was employed with an injection volume of 1 µL at 250 °C. The initial oven temperature was set at 50 °C, equilibrated for 1 min, ramped at 10 °C /min to 245 °C and held for 10 min. A flow rate of 1 mL/min of the carrier gas (Helium) in constant flow mode was employed. Total run time is 30.5 min. A full scan acquisition ranged from 60 to 550 *m/z* was performed.

Figure 11. *Instrument used for fatty acids isotope labeling analysis: Agilent model 6890 GC-EI-MS equipped with a Mass Selective Detector (MSD) model 5975 and an Auto Liquid Injector model 7683 with a 10 µL syringe.*

5.3 Cell culture

The colon carcinoma HCT116 panel (Horizon Discovery Ltd, Water beach, UK), parental cell line (WT-IDH1/2) and three mutant cell lines carrying *IDH1/2* mutations (IDH1-R132H, IDH2-R172K, IDH2-R140Q), and the colon adenocarcinoma LS174T cell panel (kindly provided by J. Pouyssegur, University Côte d'Azur, Nice, France and M. Kreutz, Regensburg) were cultivated in RPMI (PAN, Aidenbach, Germany), supplemented with

10 % FCS (Biochrom), 1 % Pen/Strep and 2 mM L-glutamine, incubated at 37 °C with 5% CO_2. For experiments, cells were seeded in 6-well plates in triplicate and incubated at 37 °C with 5 % CO_2.

For GSH and GSSG determination in chapter 6 and 7, 350,000 cells of LS174T cell lines were seeded per well in 6-well plates and 300,000 cells of HCT116 cell line were seeded per well in 6-well plates. For GSH isotope labeling analysis in chapter 8, 250,000 cells of HCT116 cell line were seeded per well in 6-well plates. Cell density used in chapter 9 is shown in Table S2 (see supplementary information in chapter 11).

“To harvest the cells for GSSG and GSH analysis, the medium was discarded and the cells were washed twice with 1 mL PBS (PAN) containing 1 mM NEM. Each PBS washing step lasted 1 min. After the second PBS/NEM wash solution was removed, 10 µL of 25 µM glutathione disulfide internal standard (glutathione-(glycine-$^{13}C_4$,$^{15}N_2$)) was added into each well before cells were scrapped in 600 µL 80% methanol. The extract was transferred to a 1.5 mL-cup and the wells were washed with 400 µL of cold 80% methanol twice and collected into the same cup.” *(Sun et al., in submission)*

“For absolute GSH quantification, parental and IDH1-R132H mutant cells were pre-cultured on plates overnight, then incubated with or without 5 µM BSO for another 24 h. All media were sterile filtered using a 25-mm syringe filter with a 0.2-µm cellulose acetate membrane (VWR, USA) before treating the cells. To harvest the cells for further analysis, the medium was discarded and the cells were washed twice with 1 mL PBS (PAN). Then, 20 µL of 500 µM glutathione internal standard (glutathione-(glycine-$^{13}C_2$,$^{15}N_1$)) was added into each well before cells were scrapped in 600 µL cold 80 % methanol. The extract was transferred to a 1.5-mL cup and the wells were washed with 400 µL of cold 80 % methanol and collected into the same cup.” [3]

“For stable isotope tracing analysis, cells were pre-cultured in standard RPMI medium for 24 h. Then the supernatant was removed and the cells were washed once with 2 mL of PBS. RPMI medium supplemented with 2 g/L $^{13}C_6$-glucose or 2 mM $^{13}C_5$-glutamine, respectively, but devoid of the respective unlabeled compound, was added. Cells were then cultured with the labeled nutrient for different time periods depending on the

experiment design before being harvested. Samples were collected as described above, but without the addition of labeled internal standard.” [3]

5.4 Sample preparation

5.4.1 Cell extraction

Cell extracts in 80 % methanol (*v/v*) were centrifuged at 4 °C and 10,000 xg for 5 min. The supernatant was then collected and the pellets were washed twice with 200 µL of 80 % methanol (*v/v*). The combined supernatants were evaporated to dryness (CombiDancer, Hettich AG, Bach, Switzerland) and then re-dissolved either with 100 µL or 50 µL water. The extracts contain the hydrophilic metabolites.

To measure fatty acids in the samples, pellets after 80% methanol extraction were subjected to chloroform extraction. Pellets were extracted with 600 µL of chloroform, centrifuged at 4 °C and 10,000 xg for 5 min, the chloroform phase was collected and the pellets were washed twice with 200 µL of chloroform. The combined chloroform fraction was evaporated to dryness and stored at -20 °C for further sample preparation.

5.4.2 Derivatization for organic acids analysis by GC-MS

For GC-MS analysis, 35 µL of the aqueous cell extracts were taken from each sample and evaporate to dryness in flat bottom insert. The dried residue was subjected to methoximation and silylation and the derivatives were analyzed by GC-MS analysis. The derivatization protocol and instrumental setup referred to previous reports [239]. Briefly, 50 µL of 20 mg/mL methoxylamine hydrochloride (MeOX, Sigma-Aldrich, Taufkirchen, Germany) in pyridine were added to the sample residue and incubated at 60 °C for 60 min. Then, 10 µL of an undecanoic acid solution(C11:0) with a concentration of 1 mM were added to each sample as a quality control as well as for retention time shifts normalization, followed by the addition of 50 µL of *N*-methyl-*N*-trifluoroacetamide (MSTFA, Macherey-Nagel, Dueren, Germany) and incubation for 60 min at 60 °C. Derivatization steps were automated using a GC-MS with a robot (MPS prepstation)**.**

5.4.3 Derivatization for fatty acids analysis by GC-MS

Fatty acids were transformed into the respective methyl esters prior to the GC-MS analysis according to a standard protocol adopted from Masood et al. [240] in the lab at the Institute of Functional Genomics. As internal standard, 10 µL of a heptadecanoic acid solution at a concentration of 1 mM was added to the dried chloroform extracts and evaporated to dryness. Then, 100 µL of 0.5 mg/mL BHT (3,5-di-tert-butyl-4-hydroxytoluene in methanol) was added to each sample and vortex. For derivatization, a reaction mix was freshly prepared containing acetylchloride and methanol at a ratio of 83 to 1417. 1500 µL of reaction mix were added to each sample, followed by 1 h incubation at 100 °C after thorough vortexing. After samples had cooled down to room temperature, 750 µL of hexane were added to extract the fatty acid methyl esters, followed by vortexing for 4 s. The upper fraction was collected in a glass vial and the extraction step was repeated one more time. The combined upper fractions were evaporated to dryness and re-dissolved in 100 µL of hexane.

5.4.4 Derivatization for amino acids analysis by LC-MS

Propyl chloroformate/propanol derivatization of amino acids was performed prior to LC-MS analysis according to a published protocol [238]. Ten µL of aqueous cell extracts were diluted with water to a final volume of 200 µL. Then, 80 µL of derivatizing reagent (A) containing 77% of n-propanol and 25% of 3-picoline (*v/v*) were added to the samples followed by the addition of 50 µL of derivatizing reagent (B) containing 17.4% of propyl chloroformate, 11% of isooctane, and 71.6% of chloroform (*v/v*) and through vortexing. The derivatives were extracted by the addition of 250 µL of ethylacetate. 200 µL of the upper organic phase were taken after thoroughly mixing and dried with N_2 gas. The residue was re-dissolved in 100 µL water/methanol (38% / 62%, *v/v*).

5.5 Protein determination

Total protein content of cell pellets was determined using the FluoroProfile® Protein Quantification Kit (Sigma-Aldrich) according to manufacturer's instructions. Alternatively, the fluorescent dye SERVA Purple (SERVA, Heidelberg, Germany) was used in an

analogous manner. Protein precipitates were lysed in a 20 mM solution of NaH_2PO_4 containing 1.2% SDS (*w/v*) and followed by fluorometric analysis. The excitation and emission maxima for the SERVA Purple dye were ~ 518 nm and ~ 610 nm, respectively. Prior to analysis, samples were diluted with water if necessary. Intracellular metabolites determined in Chapter 6 and 7 were normalized to total protein content.

5.6 GC-MS analysis of lactate, pyruvate, glucose and glucose 6-phosphate

“Uptake of glucose and release of lactate and pyruvate in section 6.5 were determined by GC-MS analysis cell culture supernatants of LS174T parental and MCT1/4 knockout clones grown for 24 hours. 10 µL of cell culture supernatant were spiked with 10 µL internal standard solution containing $^{13}C_3$-lactate, $^{13}C_3$-pyruvate, $^{13}C_6$-glucose, $^{13}C_6$-glucose-6-phosphate (each 1 mM) and dried directly in a flat bottom insert in 1.5- mL vial for subsequent GC-MS analysis. The measured concentrations were converted to uptake/release data (molar amounts per mg cellular protein per unit time) by subtracting the fresh medium concentration of each respective metabolite, and normalizing to the area under the growth curve according to Jain et al. [241].” *(Sun et al., in submission)*

“For determination of the intracellular concentrations of glucose and glucose 6-phosphate in section 6.5 by GC-MS, the cell culture medium was removed and cells were washed with 1 mL PBS twice before cell-scraping with 600 µL cold 80% methanol. During scraping, 10 µL of an internal standard solution (see above) was added to each sample. The sample suspension was collected in a 1.5-mL cup. The wells were further rinsed with 400 µL cold 80% methanol and the wash was added to the sample extract. Samples were then stored at -80 °C. Further sample extraction was performed as described above. The dried sample extract was subjected to GC-MS analysis employing the derivatization protocol and instrumental setup previously described [239]. Splitless injection with an injection volume of 1 µL was performed. Quantification was achieved based on calibration curves using the corresponding stable isotope labeled analog as internal standard.” *(Sun et al., in submission)*

5.7 DTT reduction to obtain total reduced glutathione

The optimized procedure of DTT reduction to obtain total glutathione in cell extracts in Chapter 7 was performed as our previous report. “33 µL of 100 mM NH_4HCO_3 were pipetted into a vial, before the addition of 10 µL cell extract. After mixing, 5 µL of DTT (100 mM in water) were added, followed by thorough mixing and incubation at room temperature for 20 min. In a final step, 2 µL of 25% formic acid are added. The final volume of the mixture is 50 µL, containing 10 mM DTT and 1% formic acid.” [3]

5.8 Data analysis and statistics

Mass spectra obtained by HPLC-ESI-QTOFMS were internally recalibrated based on the sodium formate clusters analyzed prior to each run using Bruker Data Analysis V4.1 (Bruker Daltonics). Data were then imported into Bruker Quant Analysis 2.2 (Bruker Daltonics) for retention time checking and peak integration. For quantification, calibration curves as well as the concentration of specific metabolites in real samples can be obtained from Quant Analysis software. Data obtained by HPLC-ESI-QqQ-MS were processed in MultiQuant analysis software 3.0.2 (AB Sciex) while data obtained by GC-MS were processed using the Agilent Mass Hunter Quantitative Analysis Workstation Software Version B.07.01.

All isotopologues from tracer analysis were corrected for natural isotope abundance and isotopic tracer purity using the IsoCorrectoR package [82], which can be downloaded from http://bioconductor.org/packages/release/bioc/html/IsoCorrectoR.html.

Group comparisons were conducted using either a two-sided Student’s *t* test or ANOVA, depending on the group number and size. Basic statistics were performed with MS Excel 2013. Analysis of variance (ANOVA) was performed using the R/Bioconductor software package (version 3.5.1). Pairwise comparisons between cell lines or groups were performed with Tukey’s post hoc test. Differences were considered significant with a p value <0.05. Figures were prepared with GraphPad Prism 6. In figures, asterisks denote statistical significance (* $p< 0.05$; ** $p<0.01$; *** $p<0.001$).

6 Simultaneous determination of GSH and GSSG in cultured cells by LC-UV-QTOFMS after in situ derivatization with N-ethylmaleimide

Over the years, a wide variety of methods have been introduced for the determination of glutathione in biomedical specimens, including spectrophotometric [13, 15, 242], fluorometric [21, 22, 243], and the more recently developed HPLC-MS techniques [25, 26, 244, 245]. However, large differences in the reported values have been observed, particularly for GSSG [36, 246]. The main cause of this variation is the non-enzymatic autoxidation of GSH during sample preparation and, therefore, the overestimation of GSSG [13, 33, 247]. Hence, for reliable determination of GSSG, it is critical to prevent artefactual GSH oxidation. 2- Vinylpyridine (2-VP) is one of the most widely used agents to block the -SH group in GSH and, thus, to prevent autooxidation. Drawbacks of 2-VP include poor cell membrane permeability and slow reactivity with GSH [13]. N-Ethylmaleimide (NEM) is another commonly used agent, which rapidly permeates cell membranes and quickly blocks the -SH group by alkylation [17]. In addition, NEM can also prevent the reduction of GSSG in biological samples through inhibition of the corresponding enzyme glutathione disulfide reductase (GR) [2, 13]. Thus, in GR involved enzymatic assay of GSH and GSSG, NEM is not recommended.

We developed an HPLC-UV-QTOF-MS method for the simultaneous determination of GSH and GSSG in cultured cells using NEM derivatization. This protocol is based on the publication by Giustarini *et al.* [2] but differs in the determination of GSSG. Instead of tedious DTT reduction of GSSG into GSH and subsequent fluorescent labeling of the -SH group to make the compound detectable by HPLC-UV, GSSG is directly detected by mass spectrometry with high sensitivity. The method presented here is more straightforward, rapid, and suitable for high-throughput analysis of GSH and GSSG in cultured cells with possible extension to other types of biological samples. Detailed instrumental setup and conditions used for the analysis of GSH (GS-NEM) and GSSG are introduced in chapter 5. A manuscript regarding the study presented in this Chapter is in submission, titled “*Simultaneous determination of GSH and GSSG in cultured cells*

by LC-UV-QTOFMS after in situ derivatization with N-ethylmaleimide". Of note, determination of pyruvate secretion, lactate secretion, glucose uptake, cell growth, and intracellular glucose and glucose 6-phosphate discussed in section 6.6 (data shown in Figure 26) were performed by Dr. Raffaela Berger. Paragraphs taken directly from the manuscript are marked with quotation marks.

6.1 Derivatization of GSH standard with NEM

GSH standard solutions were prepared and used to test NEM derivatization efficiency. NEM at a final concentration of 1 mM was added to 200 µM solution of solution prepared either in water or in 80% methanol and incubated for different time spans from 5 min to 1 hour, followed by LC-MS analysis. 80% methanol is routinely used to extract aqueous metabolites from cultured cells at Institute of Functional Genomics. Hence, combined extraction and derivatization in a single step would be preferred. However, more than 40 min of incubation time were necessary when the reaction was performed in 80% methanol until GS-NEM was completely formed and no free GSH was detectable. In contrast, the reaction is complete within minutes in aqueous solution by monitoring free GSH in the reaction solution.

6.2 Chromatography and mass spectrometry

An extracted ion chromatogram of a GSSG standard measured by LC-QTOFMS is shown in Figure 12A. Figure 12B displays the respective spectrum. On a QTOFMS, GSSG is detected as $[M+H]^+$ ion at *m/z* 613.1598 as well as its doubly charged ion at *m/z* 307.0850. The doubly charged ion yielded the higher intensity and was used for quantification in the present study.

"To improve the sensitivity of GSSG determination by mass spectrometry, a 10 Da Q1 selection window was employed so that only a limited *m/z* range covering the unlabeled and stable isotope-labeled GSSG was transmitted and detected. Compared to full scan detection, this led to a highly significant increase in the signal-to-noise ratio of the GSSG peak (Figure 13)." *(Sun et al., in submission)*

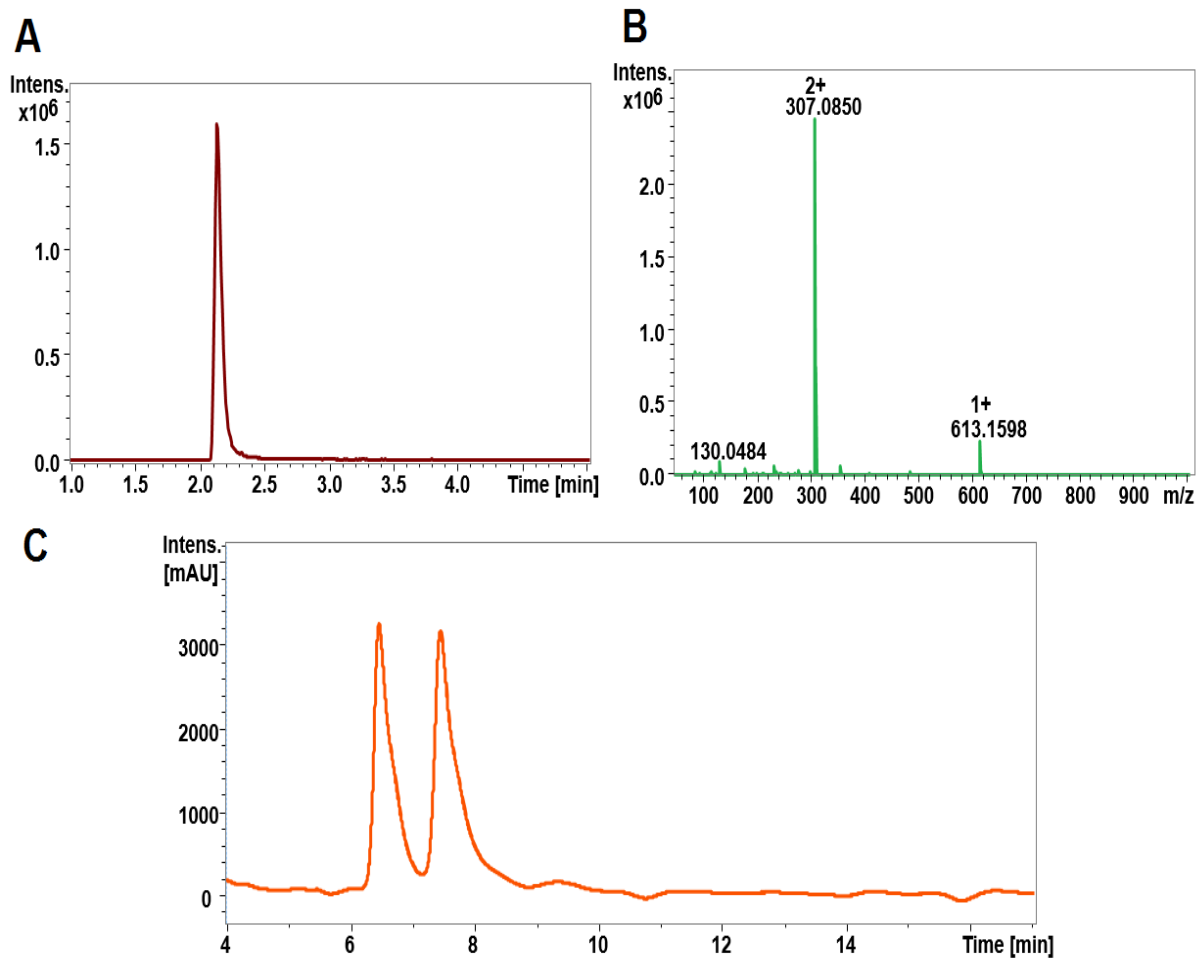

Figure 12. *"Chromatographic separation and detection of GSSG and GS-NEM. (A) Extracted ion chromatogram (XIC) and (B) mass spectrum of GSSG standard measured by LC-ESI-TOFMS. (C) GS-NEM was measured by LC-UV and the trace at 210 nm is shown. The doubly charged ion of GSSG at m/z 307 in Figure 1B was used for GSSG determination throughout the study. In Figure 1C, two separate GS-NEM peaks at 6.7 min and 7.8 min, respectively, were observed due to the generation of diastereomers. The peak at 6.7 min was chosen for GS-NEM determination." (Sun et al. in submission)*

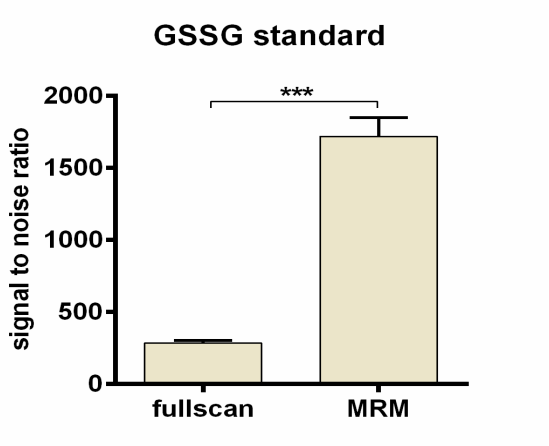

Figure 13*. "Comparison of signal-to-noise ratio for 2.5 µM solution of GSSG measured by mass spectrometry in full scan or MRM mode (n=3)." (Sun et al., in submission)*

"GS-NEM yielded two separate peaks of equal peak area ratio with an RSD of 3.13% at 6.7 min and 7.8 min due to the generation of diastereomers that are separated under the given chromatographic conditions (Figure 12C and Figure 14). Here, the peak eluting at 6.7 min was used for GS-NEM quantification. GS-NEM was also detected by QTOFMS. No other biomolecules existing in the samples coeluted with GS-NEM as evidenced by Figure 15 demonstrating that a pooled cell sample and a GS-NEM standard share the same MS spectrum at 6.7 min. Intracellular GSH/GSSG ratios are typically too high to be determined accurately by mass spectrometers with a linear dynamic range of less than four orders of magnitude. Hence, GSSG and GSH would have to be determined separately after appropriate dilution of the samples. Thus, here MS detection was only used to monitor the potential influences arising from the complex cell samples and UV absorbance was used to determine GS-NEM." *(Sun et al., in submission)*

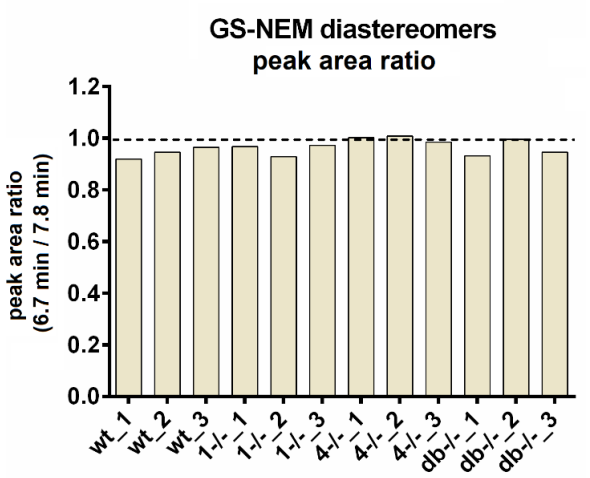

Figure 14. *"GS-NEM diastereomers peak area comparison detected by LC-UV eluted at 6.7 min and 7.8 min, respectively. Peak area ratios of the GS-NEM diastereomers in cultured cell samples detected by LC-UV are all stably around 1 with an RSD of 3.13%." (Sun et al., in submission)*

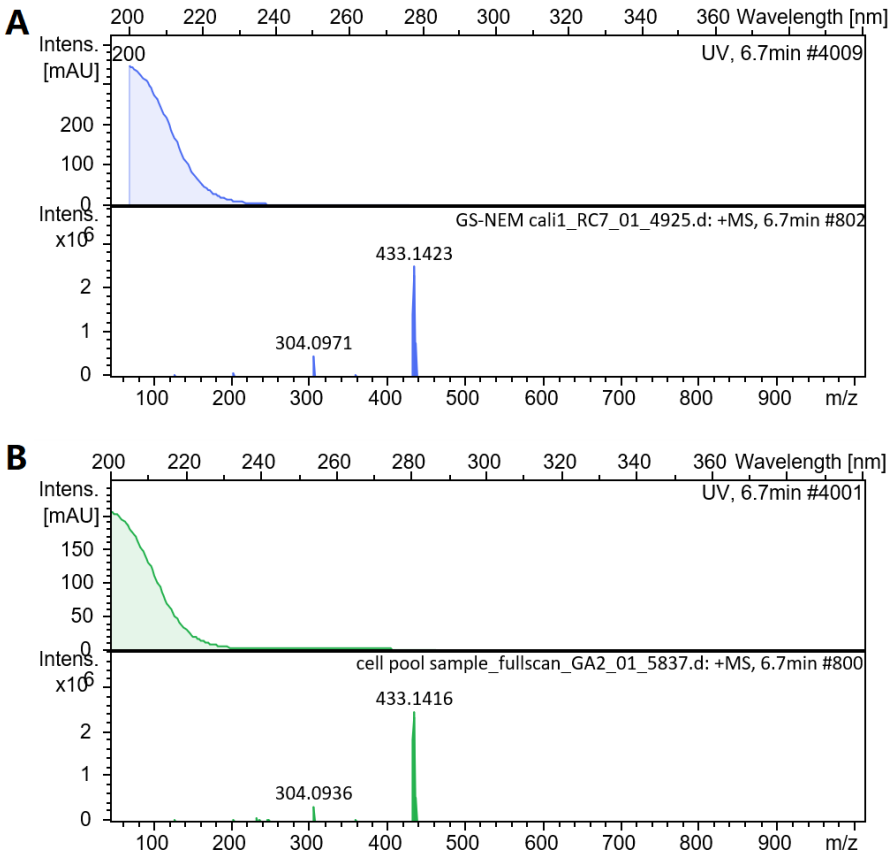

Figure 15. "*Exemplary MS spectra of GS-NEM detected by QTOFMS in (A) standard sample and (B) a pooled cell sample. GS-NEM shows a $[M+H]^+$ ion at m/z 433 and a fragment ion at m/z 304 due to the loss of Glu." (Sun et al., in submission)*

6.3 Method validation

“The linear range for GSSG quantification was determined based on a serial dilution of a GSSG standard (10 µM to 0.0024 µM) with a constant concentration of the internal standard (5 µM). The calibration curve was built based on the peak area ratio of analyte to internal standard versus the corresponding nominal concentration ratio. Lower limit of quantification (LLOQ) and limit of detection (LOD) were defined according to the FDA Guide for Bioanalytical Method Validation [248] with LLOQ as the lowest concentration of calibration curve, for which the analyte can be quantitatively determined with an accuracy of 80% - 120%, and the LOD as the lowest analyte concentration that yields a peak with S/N ≥ 3.” *(Sun et al., in submission)*

“Linearity of GS-NEM quantification was evaluated in a concentration range of 15.63 µM to 1000 µM. A GS-NEM standard solution was produced by reaction of fresh GSH standard with NEM. Calibration samples were diluted from this standard GS-NEM solution.” *(Sun et al., in submission)*

“For GSSG determination, the limits of detection and quantification were 0.001 µM and 0.0098 µM, respectively. Compared to previously reported methods as shown in Table 6, the here presented method features better detection sensitivity for GSSG. A twelve-point calibration covering a concentration range of 0.0098 µM to 10 µM yielded excellent linearity (R^2 = 0.9994). For GS-NEM determination, a nine-point calibration curve was generated that was linear from 15.63 µM to 1000 µM (R2 = 0.9997). The LOD for GS-NEM was 7.81 µM. Representative calibration curves for both GSSG and GS-NEM are shown in Figure 16.” *(Sun et al., in submission)*

“It should be noted that high amounts of GSSG were observed in GSH standard stock solutions after storage for 1 month at -20 °C (data not shown). To generate a reliable GS-NEM calibration curve, GSH stock solutions should be either freshly prepared from powder or the concentration must be recalculated through the quantification of GSSG in the stock solution.” *(Sun et al., in submission)*

Table 6. "Comparison of methods reported for the determination of GSH and GSSG." *(Sun et al., in submission)*

Method	Sample	GSH LOD *	GSH LOQ*	GSSG LOD*	GSSG LOQ*	Derivatization	Ref.
Enzymatic recycling	Rat liver/bile	--	6.25 pmol	--	2.17 pmol	M4VP	[249]
HPLC-UV	Erythrocytes	820 pmol (0.041 mM)	2700 pmol (0.135 mM)	--	--	DTNB	[19]
HPLC	Plasma	0.6 pmol (0.03 µM)	2 pmol (0.10 µM)	--	--	NBD-F	[21]
LC-MS/MS	Whole blood	4 pmol (0.4 µM)	15 pmol (1.5 µM)	1.5 pmol (0.1 µM)	1.5 pmol (0.1 µM)	NEM	[26]
HPLC	Cultured cells	--	--	--	--	NEM/DTT/ mBrB	[2]
LC-UV-MS	**Cultured cells**	**78.1 pmol (7.81 µM)**	**156.5 pmol (15.65 µM)**	**0.01 pmol**	**0.1 pmol**	**NEM**	**This study**

M4VP: 1-methyl-4-vinyl-pyridinium; **DTNB**: 5,5'-dithio-bis-(2-nitrobenzoic acid); **NBD-F**: 7-flouro-4-nitrobenzo-2-oxa-1,3-diazole; **NEM**: N-ethylmaleimide; **mBrB**: monobromobimane; **DTT**: dithiothreitol; ***** Amount of substance loaded on column.

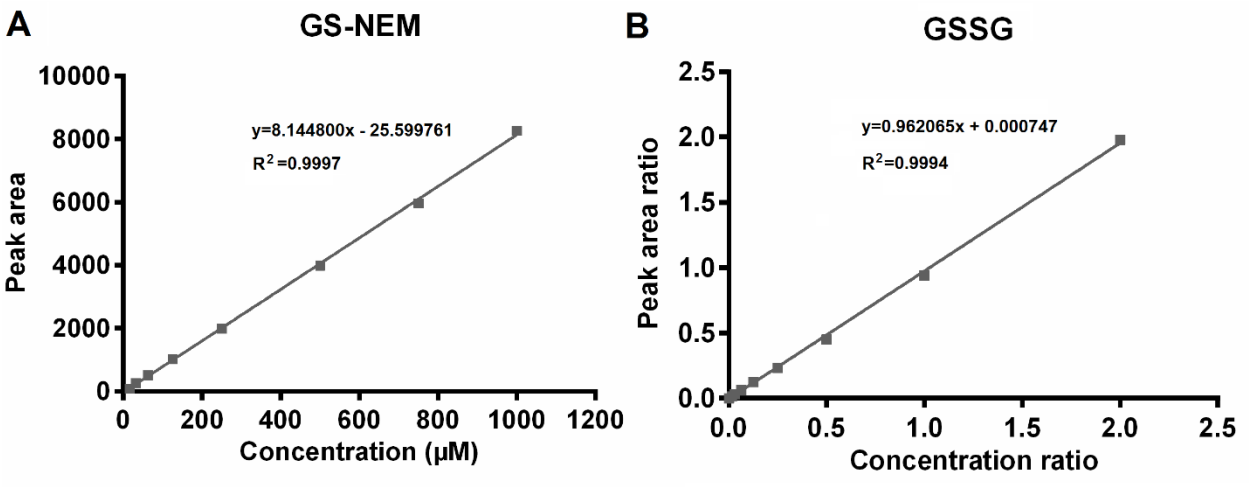

Figure 16. *"Calibration curves for GS-NEM and GSSG. (A) A nine-point GS-NEM calibration curve was generated over a concentration range of 15.63 µM to 1000 µM by plotting the peak area versus the corresponding nominal concentration. (B) A twelve-point GSSG calibration curve was constructed over a concentration range of 0.0098 µM to 10 µM based on the peak area ratios and concentration ratios of unlabeled to stable isotope-labeled GSSG (GSSG-(glycine-$^{13}C_4$,$^{15}N_2$))." (Sun et al. in submission)*

"Within-run precision was evaluated by ten successive injections of a pooled cell culture sample. The obtained peak areas of GS-NEM and the peak area ratios of GSSG to GSSG internal standard are shown in Figure 17. The corresponding coefficients of variation (CV)

for within-run repeatability of GS-NEM and GSSG were 3.48% and 3.11%, respectively. Inter-run repeatability was determined by injecting aliquots of the same pooled cell culture sample on five successive days in triplicate each day (see Figure 18). A CV of 2.51% and 3.66% was obtained for GS-NEM and GSSG, respectively." *(Sun et al., in submission)*

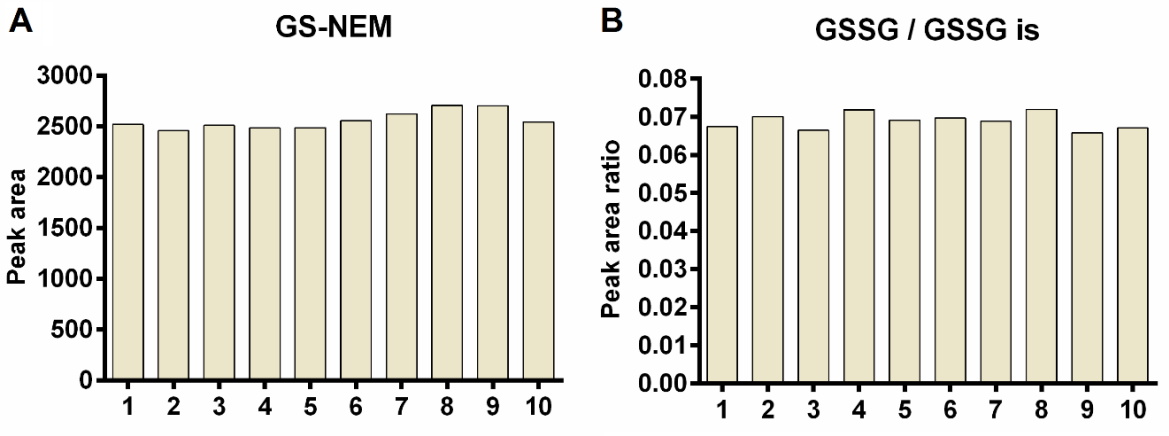

Figure 17. "*(A) Peak areas of GS-NEM and (B) peak area ratios of GSSG to GSSG internal standard for ten successive injections of a pooled cell culture sample measured by LC-UV-QTOFMS." (Sun et al., in submission)*

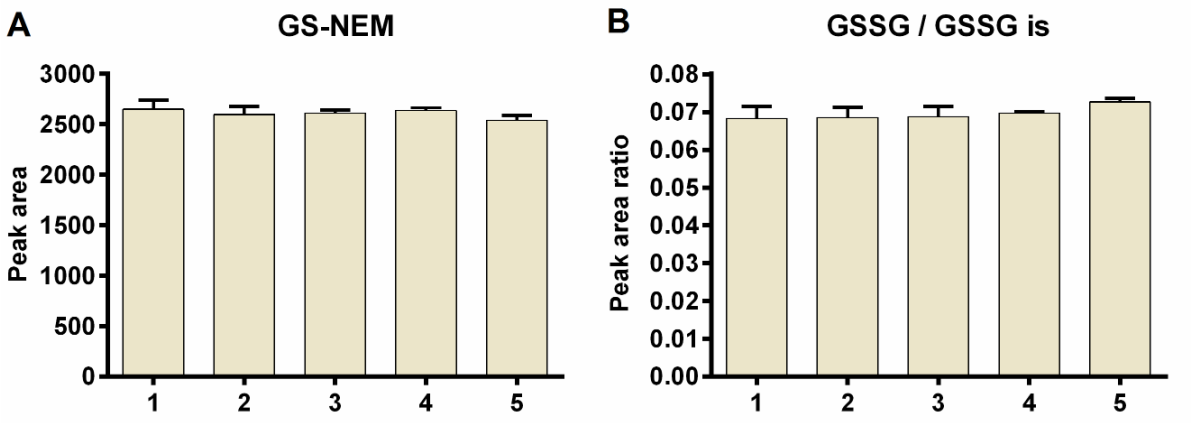

Figure 18. "*(A) Peak areas of GS-NEM and (B) peak area ratios of GSSG to GSSG internal standard for a pooled cell culture sample measured on 5 successive days by LC-UV-QTOFMS (n=3 for each day)." (Sun et al., in submission)*

“Quality control samples (QCs) of GSSG and GS-NEM were prepared from stock solutions on five different days over a period of five months prior to analysis. Results are shown in Figure 19. All QC samples showed an accuracy in the range of 80% - 120%. For GSSG, the respective accuracies were 96.74 ± 4.54% (calcheck1), 96.16 ± 5.16% (calcheck2), 99.27 ± 5.34% (calcheck3), 102.46 ± 6.60% (calcheck4), and 106.47 ± 16.00% (calcheck5). The corresponding accuracies for GS-NEM were 101.20 ± 3.40% (calcheck1), 104.29 ± 5.40% (calcheck2), 107.46 ± 6.68% (calcheck3), 105.32 ± 6.58% (calcheck4), and 103.79 ± 19.83% (calcheck5). Calcheck5, the closest to the LLOQ, featured the highest standard deviations of 16.00% and 19.83%, respectively, for GSSG and GS-NEM. However, mean accuracies of 106.47% and 103.79% for GSSG and GS-NEM, respectively, were still acceptable.” *(Sun et al., in submission)*

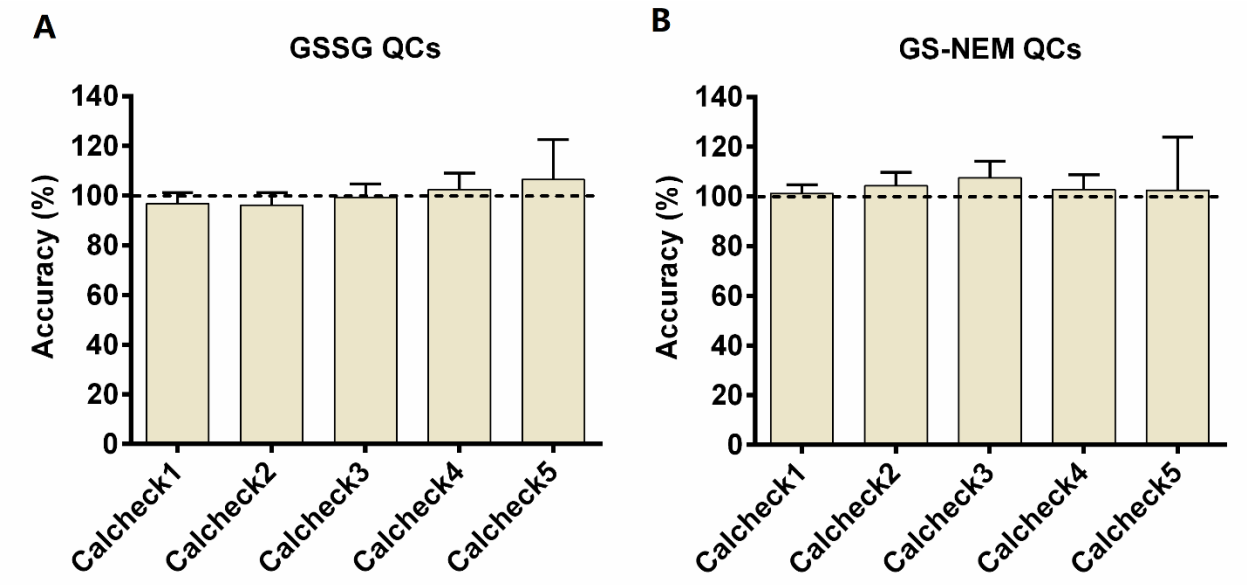

Figure 19. *“Accuracies of five quality control samples measured on different days. QCs were standard samples prepared from different stock solutions (n=3) on different days (n=5) within five months. (A) The concentrations of calcheck1 to calcheck5 for GSSG were 3 µM, 1.5 µM, 0.15 µM, 0.05 µM, and 0.02 µM, respectively. (B) The corresponding concentrations for calcheck1 to calcheck5 for GS-NEM were 500 µM, 200 µM, 100 µM, 50 µM, and 20 µM.” (Sun et al., in submission)*

“Furthermore, we investigated the stability of GS-NEM solutions under different storage conditions. A standard GS-NEM sample was stored at 4 °C, -20 °C, and -80 °C, respectively, for the periods of time indicated in Figure 20. The CVs of average peak area over all injections (15 injections in total) were 3.10% (4 °C), 5.66% (-20 °C), and 2.47% (-80 °C), respectively, thus attesting to adequate sample stability over at least one month.” *(Sun et al., in submission)*

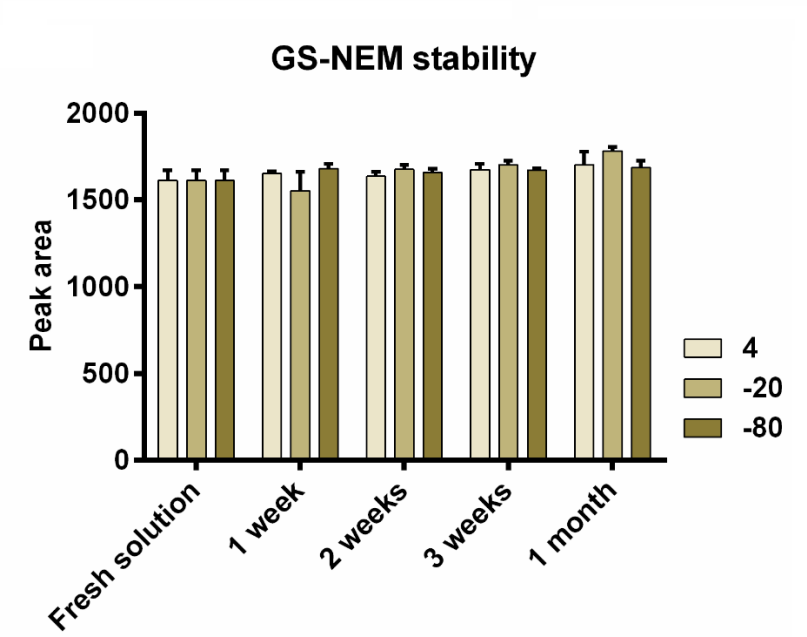

Figure 20. *“GS-NEM stability was investigated by comparing GS-NEM peak areas after storage at different temperature for up to one month (n=3).” (Sun et al., in submission)*

6.4 Cell harvesting

“The timing of the addition of NEM to cultured cells is critical for the accurate determination of GSH as is evident from Figure 21. The amount of GSSG determined decreased dramatically by adding NEM already during cell harvesting instead of adding it later to the methanolic cell extract. This impressively shows the importance of immediately trapping GSH to prevent autooxidation when analyzing GSSG in cultured cells.” *(Sun et al., in submission)*

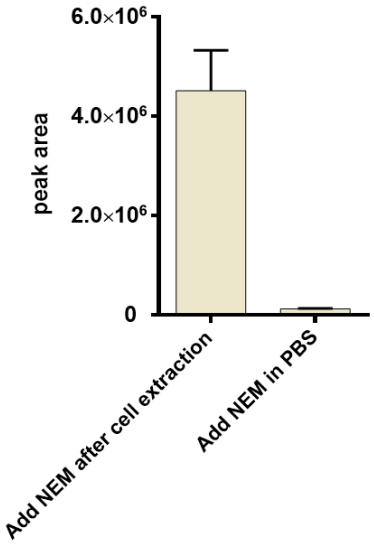

***Figure 21**. "Peak area of GSSG detected in cell culture samples after derivatization of GSH with NEM either in the final extract or during cell harvesting by adding NEM to the PBS wash (n=3)." (Sun et al., in submission)*

"To further optimize the protocol, we tested four different cell harvesting procedures:

1) As described above, the cell culture medium was removed and the cells were washed twice for 1 min with PBS containing 1 mM NEM prior to cell harvesting in cold 80% methanol.
2) Cells were washed twice with 1 mL of PBS prior to addition of 400 µL of 1 mM NEM solution for 5 min, followed by cell harvesting in cold 80% methanol.
3) Cells were washed twice with 1 mL of PBS and then scrapped with 1 mL of cold 80% methanol containing 0.5 mM NEM.
4) NEM was added directly to the cell culture medium at a final concentration of ~1 mM for 2 min (add 10 µL of 310 mM NEM) prior to discarding the medium and washing the cells with PBS." *(Sun et al., in submission)*

"Cells were seeded at the same density and each procedure was performed in triplicate. Results are shown in Figure 22. No significant difference between the four procedures was observed for GS-NEM (ANOVA p=0.59). However, a significant lower GSSG amount was detected when cells were washed with PBS containing 1 mM NEM (procedure 1), indicating that autooxidation was kept to a minimum. In procedure 4, NEM was directly

added into cell culture medium prior to PBS washing. Components present in the medium may interfere with NEM and influence the reaction efficiency. Consequently, procedure 1 became the standard protocol. Besides, no free GSH was detected in cell culture samples after NEM derivatization, indicating sufficient derivatization of GSH with NEM." *(Sun et al., in submission)*

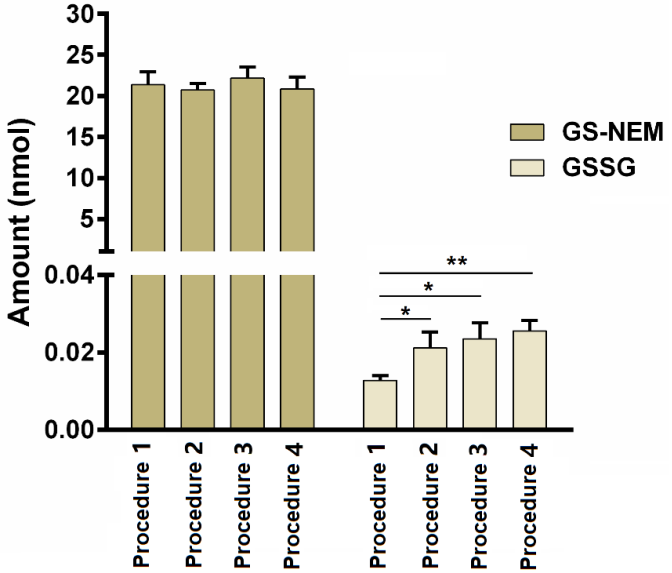

***Figure 22**. "Optimization of the NEM derivatization procedure. **Procedure 1**, cell medium was discarded, followed by two 1-min washing steps with PBS containing 1 mM NEM. **Procedure 2**, cell medium was discarded, followed by PBS washing twice. Then, 400 µL of 1 mM NEM was added to the cells and incubated at room temperature for 5 min before harvesting the cells in 80% methanol. **Procedure 3**, cells were harvested with 1 mL of 80% methanol containing 0.5 mM NEM after PBS washing twice. **Procedure 4**, 10 µL of 310 mM NEM were added directly to the cells and incubated for 2 min before discarding the medium and PBS washing. No significant difference in GS-NEM amount was observed between groups (ANOVA, p=0.59). For GSSG, significant differences were found between groups (ANOVA, p=0.0068): 1 versus 2: p=0.0364; 1 versus 3: p=0.0171; 1 versus 4: p=0.0064. One-way ANOVA and post hoc analysis with Tukey's test were performed in R (version 3.5.1)." (Sun et al., in submission)*

"We also compared the quantification of GSH as GS-NEM with the determination of total reduced GSH (tGSH) in the colorectal adenocarcinoma cell line LS174T to validate the GS-NEM method. Quantification of tGSH employing DTT reduction was performed according to our previously reported method [3]. The results are shown in Figure 23.

There is no significant difference between GS-NEM and tGSH amount after normalization to protein amount. This indicates correct analysis of GSH by LC-UV after NEM derivatization, as the very low intracellular amounts of GSSG will not contribute significantly to tGSH." *(Sun et al., in submission)*

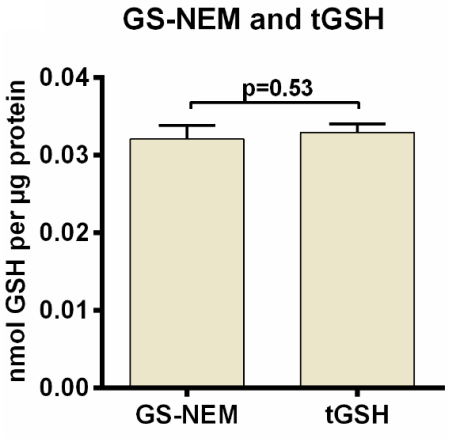

Figure 23. *"Total GSH was assessed with DTT reduction and both tGSH and GS-NEM were normalized to protein amount. No significant difference was observed between GS-NEM and tGSH (p=0.53, n=3)." (Sun et al., in submission)*

"Furthermore, spike-in experiments were performed with LS174T wild type cells to assess GSH (GS-NEM) and GSSG recovery. To minimize autooxidation artefacts, GS-NEM rather than GSH was used for the spike-in experiments. Recovery of GS-NEM and GSSG was assessed separately. Three different GS-NEM or GSSG standard solutions of known concentration (low, medium, and high) were added to the culture dishes and cell extraction was performed as described above. The spike-in amounts were selected according to the endogenous levels of GSH (GS-NEM) and GSSG measured previously in LS174T wild type cells, which were about 20 nmol absolute for GSH and 0.02 nmol absolute for GSSG. Based on the endogenous levels, spike-in amounts of 10, 20, and 40 nmol for GS-NEM, and 0.02, 0.06, and 0.2 nmol for GSSG were selected. For each experiment, three replicates were generated. Recovery of GS-NEM and GSSG were calculated as follows:" *(Sun et al., in submission)*

$$"Recovery = \frac{{amount\ in\ spike-in\ sample}/{protein\ amount} - {amount\ in\ control\ sample}/{protein\ amount}}{{theoretical\ amount\ of\ standard\ spiked}/{protein\ amount}} \times$$

100%" *(Sun et al., in submission)*

"Absolute amounts were normalized to protein amount in the sample to correct for differences in cell number. As shown in Figure 24, recovery of GS-NEM and GSSG was satisfactory for all three spike levels. Mean recovery of GS-NEM ranged between 92.2 and 101 % (101.01 ± 7.96%, 94.25 ± 2.00%, and 92.15 ± 1.06%) while the mean recovery and standard deviation for GSSG was 104.28 ± 11.18%, 98.70 ± 1.99%, and 97.49 ± 9.60%, respectively." *(Sun et al., in submission)*

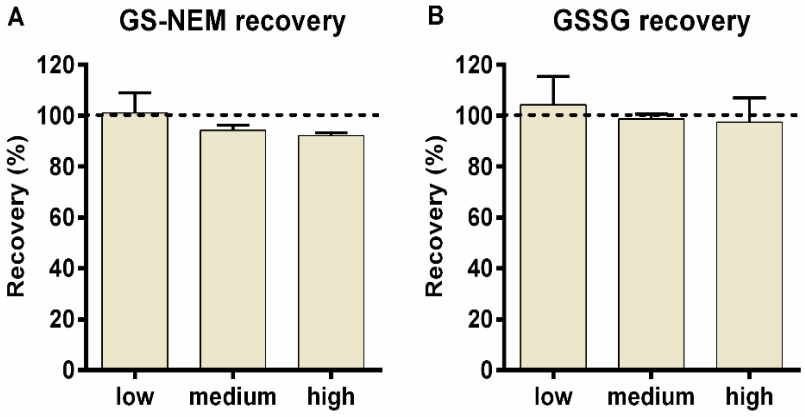

***Figure 24**. "(A) GS-NEM and (B) GSSG spike-in experiments. Recovery was determined by adding defined amounts of GS-NEM or GSSG at low (10 nmol of GS-NEM, 0.02 nmol of GSSG), medium (20 nmol of GS-NEM, 0.06 nmol of GSSG), and high (40 nmol of GS-NEM, 0.2 nmol of GSSG) concentration into LS174T wild type cell cultures before 80% methanol cell extraction. GS-NEM and GSSG recovery experiments were performed separately (n=3 for each)." (Sun et al. in submission)*

6.5 GSH and GSSG determination in monocarboxylate transporter deficient cells

"To demonstrate the applicability of the developed LC-UV-QTOFMS method, we measured the intracellular concentrations of GSH and GSSG in parental LS174T cells as well as derived single (SKO) and double knockout (DKO) clones of the monocarboxylate transporters *MCT1* and *MCT4*. As is evident from Figure 25A, under normal cell culture

conditions, parental and SKO cells exhibited similar GSH/GSSG ratios with a more than 2,000-fold molar excess of GSH, while the GSH/GSSG ratio of the DKO cells was significantly lower but still in excess of 1,500:1. This can be readily explained by the observation [250], that complete disruption of MCT activity in LS174T cells by a combination of genetic and pharmacological means results in a more than 6-fold increase in oxidative phosphorylation, which leads in turn to the increased generation of mitochondrial reactive oxygen species (ROS) and, consequently, an increase in cellular content of GSSG. As expected, when cells were challenged with 0.2 mM H_2O_2 for 10 min, all four cell lines showed a dramatic decrease in the GSH:GSSG ratio compared to the corresponding unstressed condition due to a collapsing NADP+/NADPH ratio ($p<0.001$ for all cell lines, normal condition versus H_2O_2 treatment) (Figure 25B). But rather unexpectedly, the decrease in GSH/GSSG ratio upon H_2O_2 treatment was by far the most pronounced in the *MCT4-/-* SKO cells (for statistics see Supplementary Table S3 in Chapter 11)." *(Sun et al. in submission)*

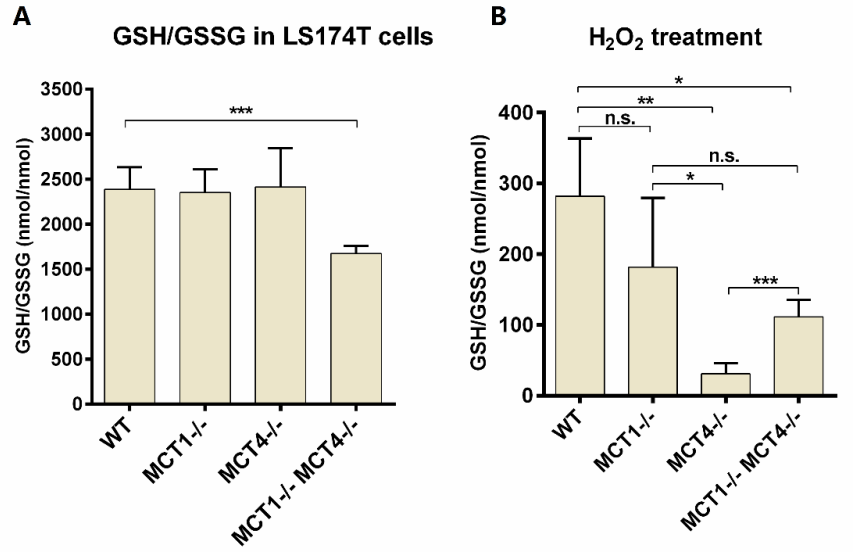

Figure 25. *"GSH/GSSG ratio in MCT-competent and MCT-deficient LS174T cells, respectively, in response to oxidative stress. Cells were not treated (Figure 6A, n=6) or treated (Figure 6B, n=6) with 0.2 mM H_2O_2 for 10 min, before they were washed with PBS containing 1 mM NEM. Treatment with H_2O_2 decreases the ratio of GSH to GSSG in all cell lines. However, MCT4-/- and double knockout cells are more sensitive to oxidative stress than MCT-competent and MCT1-deficient cells. * p< 0.05, ** p< 0.01, *** p< 0.001, n.s., not significant." (Sun et al. in submission) For further statistics see Supplementary Table S3 in Chapter 11.*

“Any attempt to interpret the above finding needs to account for the fact that both, differences in the expression of *MCT1* and *MCT4* as well as the choice of methodology to knock them out or down or to inhibit them pharmacologically may exert different effects on cell metabolism. In cells that express little, if any, MCT4, knockdown or pharmacological inhibition of MCT1 has been reported to result, amongst others, in increased levels of glucose- and fructose-6-phosphate, as was observed here, as well as in marked reductions in the intracellular levels of pyruvate and GSH and in reduced glucose uptake and lactate efflux, all of which were not detected in the present study [251]. In contrast, knockdown or pharmacological inhibition of MCT1 in cells expressing considerable amounts of MCT4 resulted in reduced pyruvate export and increased oxygen consumption, accompanied by increased expression of genes involved in oxidative phosphorylation, while the expression of glycolytic genes such as hexokinase 1, phosphofructokinase M, and enolase 1 was decreased. Moreover, continued glucose uptake and lactate export were sustained by MCT4 [252]. Increased mitochondrial respiration and the consequently enhanced generation of ROS are known to inactivate the M2 isozyme of pyruvate kinase (PKM2) through oxidation of Cys^{358} [253]. The resulting accumulation of phosphoenolpyruvate, in turn, results in direct catalytic inhibition of triosephosphate isomerase. This mediates a protective diversion of glucose flux into the oxidative branch of the pentose phosphate pathway (PPP) to generate NADPH required for the reduction of the antioxidants glutathione, thioredoxin and peroxiredoxin [254]. MCT1 facilitates the proton-linked bi-directional transport of both lactate and pyruvate, while MCT4 is considered primarily a high-affinity exporter of lactate with a significantly lower affinity for pyruvate [255]. Indeed, under unstressed conditions, growth rate adjusted export of pyruvate was lower in *MCT1*$^{-/-}$ than *MCT4*$^{-/-}$ SKO cells, while they did not differ in glucose uptake and lactate release from the parental clone (Figure 26A-C). Given that LS174T cells express only MCT1 and MCT4 [250], genetic ablation of both *MCT1* and *MCT4* resulted in an almost complete inhibition of pyruvate and lactate export and very little glucose uptake, as DKO cells meet their energy requirements mostly by oxidative phosphorylation [250]. The present observation, that both the *MCT1*$^{-/-}$ SKO and the *MCT1*$^{-/-}$*/ MCT4*$^{-/-}$ DKO clone exhibit a higher abundance of glucose and glucose 6-phpsphate than the MCT4$^{-/-}$ SKO clone under unstressed conditions, may provide an

important clue toward understanding the pronounced drop of GSH:GSSG ratio in the *MCT4*$^{-/-}$ SKO clone upon H_2O_2 treatment (Figure 26D). As shown previously, MCT1 blockade leads to increased mitochondrial respiration and generation of ROS, which redirect via inhibition of triosephosphate isomerase glucose flux to the PPP [250, 252]. *MCT4*$^{-/-}$ null cells, in contrast, show under unstressed conditions neither a significant increase in extracellular acidification rate (ECAR) nor a significant decrease in intracellular pH [250]. The roughly two-fold increase in oxygen consumption rate (OCR) is also very modest. As cells experience an oxidative burst upon exposure to H_2O_2, they inactivate glycolysis within seconds via oxidation of not only pyruvate kinase but also glyceraldehyde 3-phosphate dehydrogenase, while glucose flux through the PPP continues to generate NADPH [256]. Given that glucose flux through the PPP is already increased in MCT1 deficient cells, these cells can stage most likely a faster response to H_2O_2 exposure, which should be reflected in lower intracellular GSSG levels. Indeed, as evident from Figure 27, intracellular levels of GSSG in *MCT1*$^{-/-}$ *SKO* cells are similar to those found in wild type cells under both unstressed and stressed conditions, with only the level of GSH being somewhat lower in the former under oxidative stress. Both *MCT4*$^{-/-}$ SKO and *MCT1*$^{-/-}$*/MCT4*$^{-/-}$ DKO cells show highly significant increases in GSSG content compared to parental and *MCT1*$^{-/-}$ SKO cells. Interestingly, the increase in GSSG content in DKO cells as compared to MCT competent cells is lower than in *MCT4*$^{-/-}$ *SKO* cells and further compensated by a higher GSH content in the DKO cells. In conclusion, it appears that *MCT4*$^{-/-}$ null cells are poorly adapted to sudden bursts of oxidative stress.” *(Sun et al. in submission)*

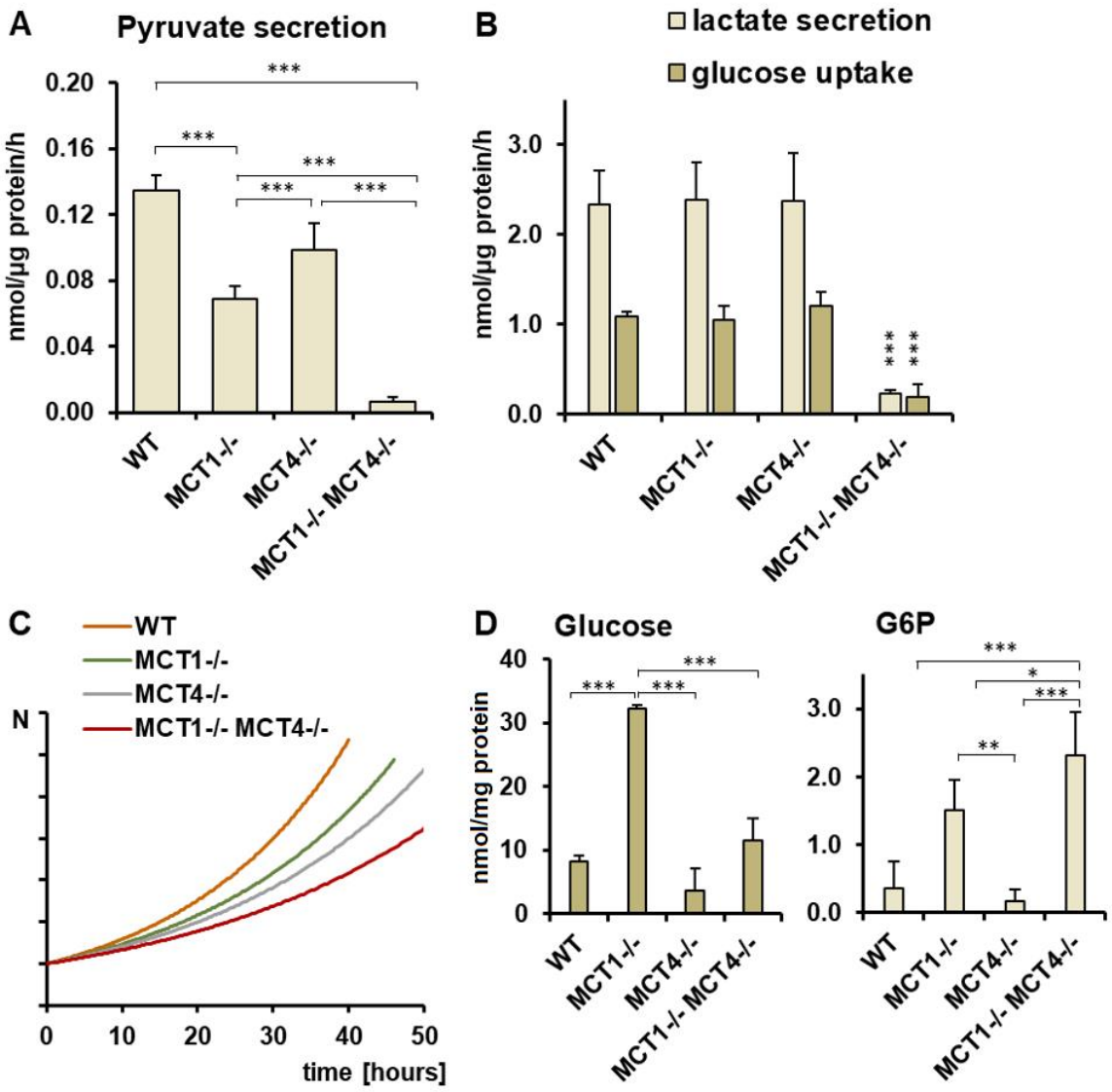

Figure 26. *"Release of **(A)** pyruvate and **(B)** lactate as well as uptake of glucose normalized to **(C)** area under the growth curve, and **(D)** intracellular content of glucose and glucose 6-phosphate (G6P) in unstressed LS174T parental and MCT1/4 single and double knockout clones cultured for 24 h. Metabolites in methanolic extracts of both cell culture supernatants (A, B) and cell pellets (D) were analyzed by GC-MS. Two independent experiments, each in triplicate, were performed. (ANOVA for pyruvate $p = 5.1\times10^{-4}$, for lactate secretion $p = 9.7\times10^{-9}$, for glucose uptake $p = 1.3\times10^{-9}$, for intracellular glucose $p = 2.4\times10^{-6}$ and intracellular G6P $p = 2.8\times10^{-5}$, * $p< 0.05$, ** $p< 0.01$, *** $p< 0.001$, n.s., not significant)." (Sun et al. in submission) For further statistics see Table S4 in Chapter 11. Note: This figure was kindly provided by Dr. Raffaela Berger. Dr. Raffaela Berger performed all experiments involved in this figure (for detailed method, see section 5.6).*

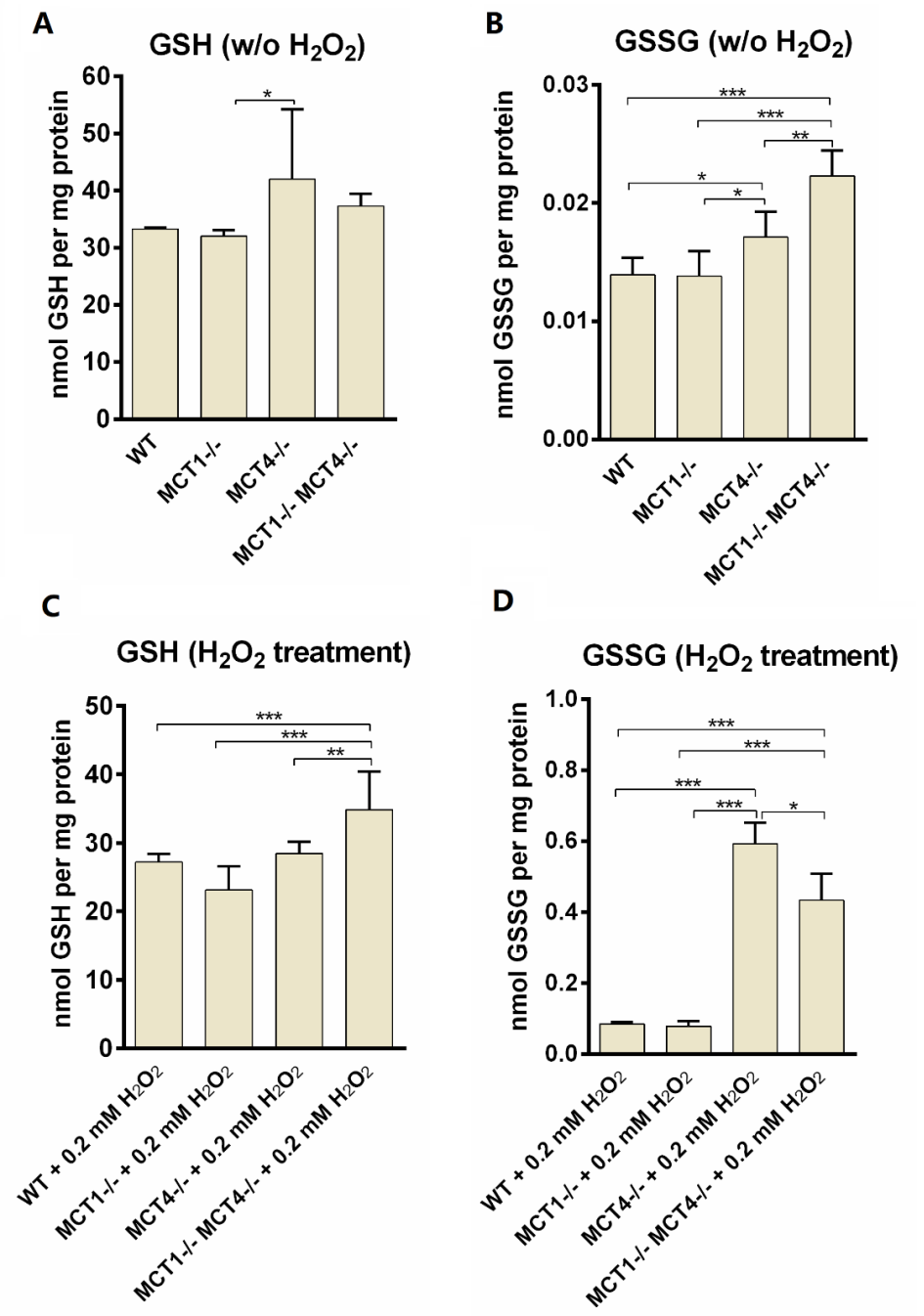

Figure 27. *"Intracellular levels of GSH and GSSH in LS174T parental and MCT1/4 single and double knockout clones before (unstressed, n=6 each) and after treatment with 0.2 mM H_2O_2 for 10 min (n=3 each). One-way ANOVA (p=0.0473 for GSH, unstressed; $p=7.44\times10^{-7}$ for GSSG, unstressed; $p=1.65\times10^{-4}$ for GSH, H_2O_2 treated; $p=2.04\times10^{-6}$ for GSH, H_2O_2 treated) and post hoc analysis with Tukey's test were performed in R (version 3.5.1). * p< 0.05, ** p< 0.01, *** p< 0.001." (Sun et al. in submission)*

6.6 GSH and GSSG determination in isocitrate dehydrogenase wild type and mutant cells

“Next, we applied the developed method to the determination of the intracellular levels of GSH and GSSG in the colon cancer cell line HCT116, in which we had already determined previously total GSH content [3]. The wild type and isocitrate dehydrogenase 1/2 (*IDH1/2*) mutant cell clones IDH1-R132H, IDH2-R172K, and IDH2-R140Q, respectively, were used to study the effect on the GSH/GSSG ratio in cells carrying neomorphic *IDH1/2* mutations, which enable cells to catalyze the NADPH consuming reduction of α-KG to D-2-HG (see Figure 28A) [4, 46, 47]. As shown in Figure 28B, all *mutIDH* cell lines show a significant lower GSH/GSSG ratio compared to the wild type cell line (for statistics see Supplementary Table S5 in Chapter 11), supporting the notion that increased consumption of NADPH by *IDH1/2* mutant cells will impair their ability to reduce GSSG to GSH. Interestingly, the GSH/GSSG ratios observed in the three mutant cell lines appear to correlate indirectly with the amounts of D-2-hydroxyglutarate detected in these cells [257]. Furthermore, it *mutIDH1* cells seem to be less capable of regenerating GSH than *mutIDH2* (mitochondrial isoform) cells. IDH1 is the cytosolic isoform and, therefore, increased consumption of NADPH by the mutated enzyme has a more direct effect on the reduction of GSSG, which also takes place in the cytosol.” *(Sun et al., in submission)*

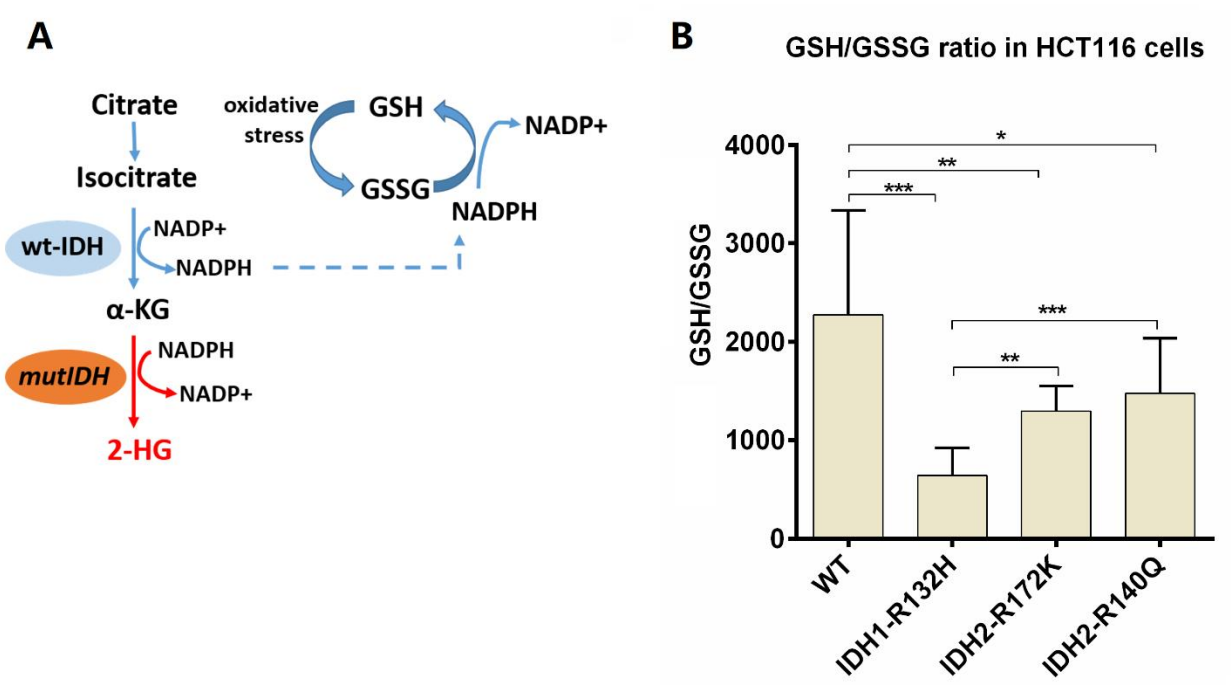

Figure 28. *"**(A)** Scheme depicting the reactions catalyzed by wild type and mutant IDH enzymes and their respective effects on the provision of NADPH for the reduction of GSSG to GSH by glutathione reductase. **(B)** Effect of different IDH1/2 mutations on the GSH/GSSG ratio in HCT116 cells compared to IDH1/2 wild type cells. * p< 0.05, ** p< 0.01, *** p< 0.001, n=3." (Sun et al., in submission) For statistics see Supplementary Table S5 in Chapter 11.*

7 Quantification of total reduced glutathione by HPLC-QTOFMS/MS

Derivatization or tailored sample preparation is generally necessary to determine the ratio of GSH and GSSG in cell cultures as described above. In studies only interested in the total size of the glutathione pool, separate determination of GSH and GSSG is not necessary. In this chapter, an optimized HPLC-MS/MS method is described for the absolute quantification of total reduced glutathione.

Dithiothreitol (DTT) [20, 23] and tris-(2-carboxyethyl)-phosphine (TCEP) [22, 258] are two commonly used reductants. The mechanism of disulfide reduction by DTT is shown in Figure 29. To achieve effective reduction with DTT, alkaline pH is required as the negatively charged thiolate group (S^-) is more reactive than the thiol group (–SH) to reduce disulfide bonds.

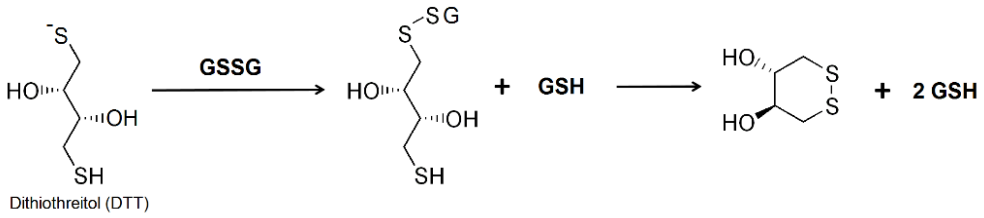

***Figure 29**. "Mechanism of disulfide reduction by DTT." [3]*

TCEP, is commercially available since 1992 [259, 260]. The reaction of disulfide reduction by TCEP of GSSG proceeds as follows [259]:

$(CH_2CH_2COOH)_3P + GSSG + H_2O \rightarrow (CH_2CH_2COOH)_3P{=}O + 2\ GSH.$

In preliminary experiments performed by Paul Heinrich, the reduction efficiency of DTT and TCEP with a standard mixture of GSH and GSSG was assessed. DTT proved to be a better choice for the reduction of the disulfide bond in GSSG, as TCEP gave rise to significant ion suppression if used at a concentration needed for complete reduction of GSSG. Based on an optimized DTT reduction protocol developed by Paul Heinrich (see

section 5.7), an LC-MS/MS method for the direct determination of total intracellular glutathione in cultured cells was developed and adapted for ^{13}C tracer analysis.

The study introduced in this chapter was published in *Analytica Chimica Acta (Sun et al., Quantification and ^{13}C-Tracer Analysis of Total Reduced Glutathione by HPLC-QTOFMS/MS*, *2019, 1080, 127-137).* Paragraphs taken directly from the publication are marked with quotation marks.

7.1 Chromatography and mass spectrometry

“GSH is a tripeptide, which contains both basic and acidic sites that undergo protonation or deprotonation depending on pH [29]. We selected 0.1 % formic acid in water / 0.1 % formic acid in acetonitrile as the mobile phase A / B, respectively. Figure 30 shows an exemplary extracted ion chromatogram (XIC) and spectrum of the $[M+H]^+$ ion of GSH standard measured by LC-ESI-MS after DTT reduction. To improve selectivity and specificity, as well as peak intensity, GSH was measured by tandem mass spectrometry. Figure 31 displays the ESI- MS/MS spectrum of the GSH standard. GSH forms a quasi-molecular ion at *m/z* 308.0966 ($[M+H]^+$ion) and two product ions at *m/z* 179.0497 and *m/z* 233.0613, respectively, which occur due to the loss of glutamate and glycine. The fragment at *m/z* 179 (Gly-Cys) shows the highest intensity, while fragment *m/z* 233 (Glu-Cys) shows only 25 % - 30 % of the *m/z* 179 intensity (see Figure 31). Preliminary experiments were performed to evaluate both fragments for quantification, with fragment *m/z* 179 showing the better performance. Hence, this fragment ion was used to build the calibration curves.” [3]

“In addition, the settings of the mass spectrometer were tuned with direct infusion of a GSH standard solution in order to yield maximum intensity for the *m/z* 179 fragment. An increase in collision energy from 10 to 15 led to an increased intensity of the *m/z* 179 signal and a decreased precursor signal (*m/z* 308). A further increase in collision energy caused a decrease in the *m/z* 179 signal due to enhanced fragmentation.” [3]

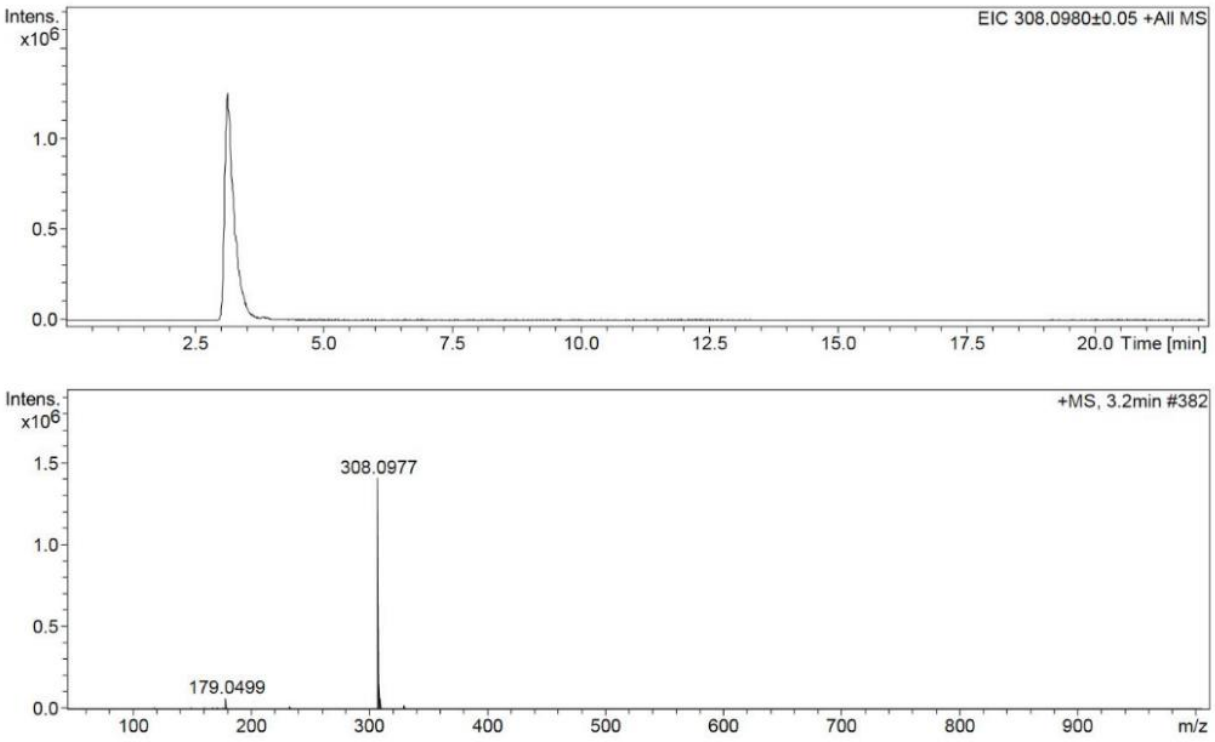

***Figure 30**. "Exemplary extracted ion chromatogram and spectrum of a GSH standard as measured by LC-QTOFMS in positive ion mode." [3]*

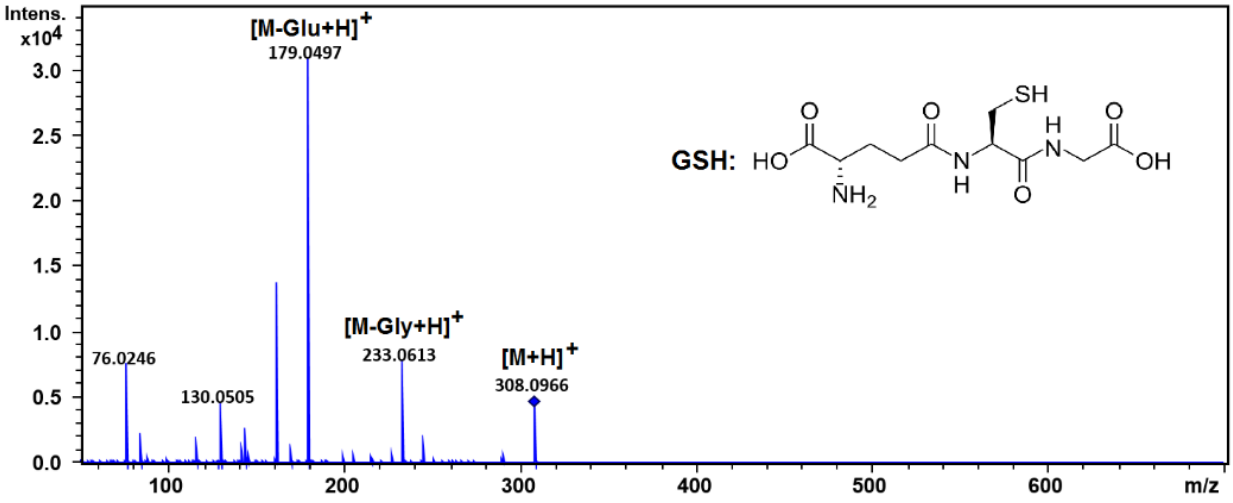

***Figure 31**. "Exemplary mass spectrum of GSH acquired in positive ion multiple reaction monitoring mode with a 0.7 Da window, in which the parent ion m/z 308 was selected in Q1 and a collision energy of 15 eV was employed." [3]*

7.2 Method validation

The developed LC-MS/MS method was systematically validated by assessing the LOD, LLOQ, linear range, intra/inter-day precision, as well as recovery.

“The limit of detection for tGSH was 0.01 µM. The lower limit of quantification (LLOQ) of the analytical procedure was 0.78 µM, *i.e.*, the lowest point of the calibration curve with a signal-to-noise ratio > 10 and 80 % - 120 % accuracy. Within-run precision was evaluated by ten consecutive injections of the same reduced sample (20 µM GSH standard solution) and comparing targeted peak areas of *m/z* 179. The coefficient of variation (CV) for intra-run repeatability was 2.49 %. The corresponding CV for inter-run repeatability, which was determined by reducing and injecting the same aliquoted sample on five consecutive days, was 2.04 %.” [3]

“Eight-point calibration curves were acquired over the concentration range of 0.78 µM to 100 µM GSH after DTT reduction. Figure 32 shows the accuracy of each concentration point from 5 replicates measured over 9 months. Mean accuracy per calibration point ranged from 98.85 % to 105.56 %. Repeatability was calculated from the 5 replicates of each concentration point. CVs of the accuracy for all studied concentration points were lower than 10 %. The calibration curve was linear over the studied concentration range with a squared correlation coefficient R of 0.9997 and an equation of y=1.2314 x + 0.0069 as obtained by plotting the relative responses versus relative concentrations.” [3]

“To check the stability of GSH at 4 °C, we reanalyzed in triplicate a sample that had been kept in the autosampler for 24 h. The coefficient of variation of the peak areas is 2.13 %, thus indicating sufficient sample stability.” [3]

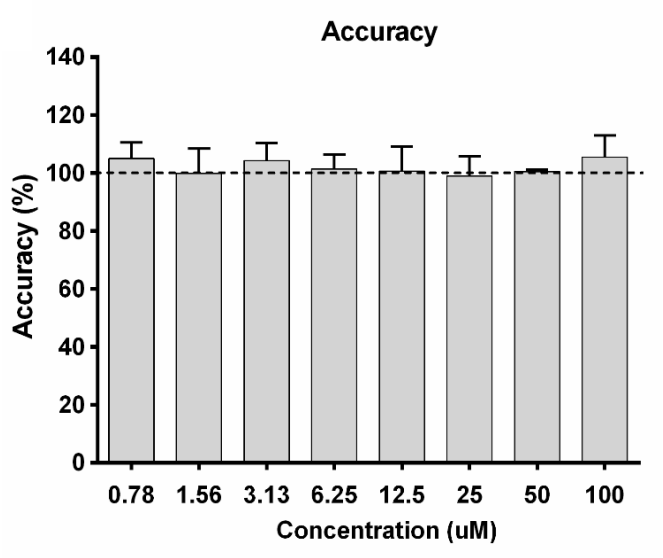

***Figure 32**. "Quantification of GSH. **A**: Accuracy of each concentration point from five calibration curves detected within 9 months. Results are shown as mean + SD (n=5)." [3]*

"Recovery of tGSH for the analysis of cell pellets was determined by adding standard working solutions of GSH at low, medium, and high concentrations (2, 10, 50 nmol) to cell pellets. Cell aliquots with the same cell count (~300,000 cells) were generated from a pool sample of HCT116 cells (parental cell line) and spiked with GSH standard and stable isotope-labeled internal standard (20 µL of 500 µM) before precipitation in 1 mL of 80% methanol. In addition, control samples were analyzed to determine endogenous tGSH levels. The recovery experiment workflow is displayed in Figure 33. The spike-in experiment was performed in triplicate for each group. The endogenous amount of GSH, determined from the analysis of the control samples was subtracted to obtain the spike-in amount of GSH. The recovery of each spike concentration was calculated as follows:" [3]

$$"Recovery = \frac{GSH\ amount\ in\ spike{-}in\ sample / cell\ number - GSH\ amount\ in\ control\ sample / cell\ number}{theoretical\ amount\ of\ GSH\ standard\ spiked / cell\ number} \times 100\%"$$

"The mean recovery and standard deviations for the three spike-in amounts of GSH were 108.9 ±2.1 %, 100.8 ± 8.3 %, 99.9 ± 7.1 %, respectively." [3]

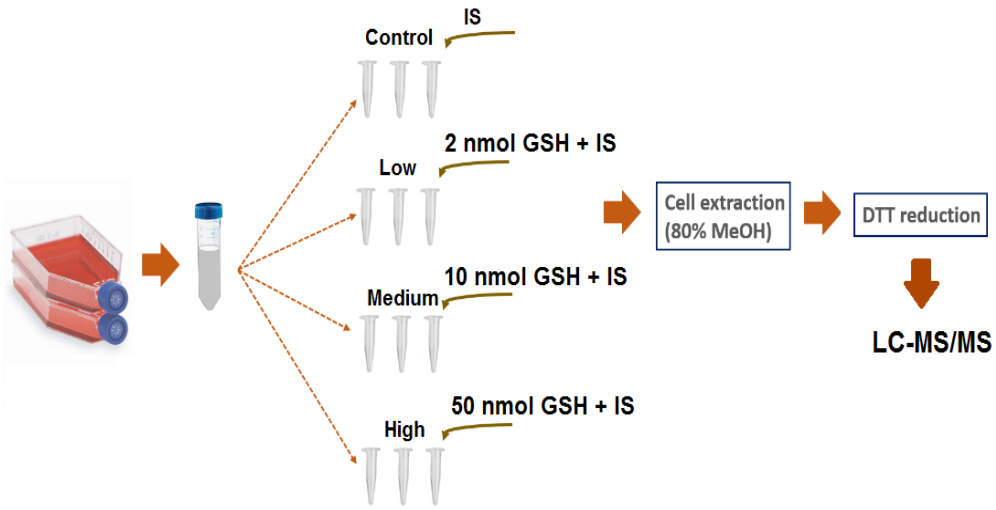

***Figure 33**. "Intracellular GSH recovery experimental workflow." [3]*

"A comparison of reported methods for GSH determination with our method in terms of LOD, LLOQ, recovery, and reductant or derivatization reagent used is given in Table 7. Compared to most of the methods listed, our method achieves similar or even better LOD and LLOQ. To measure GSH, one can – as reported in this study - use reduction to obtain tGSH. If the GSH/GSSG ratio is of interest, derivatization has to be employed to protect the –SH group of GSH from autooxidation. Then the quantity of the derivatized species can be determined, accompanied by either a measurement of sample GSSG or tGSH to obtain ratio information. However, if derivatization is employed to assess the GSH/GSSG ratio, the timing of addition of derivatizing reagent is very critical. Autooxidation of GSH may occur from the very beginning of sample collection and preparation. Since our method does not require derivatization at the point of cell sampling and only a sample aliquot is needed for the reduction step, the remaining sample can be used for further metabolic analyses. Most importantly, the present method can be extended easily to the comprehensive analysis of isotope labeling patterns of GSH in stable isotope tracing experiments, as shown in the discussion of our wide Q1 window method which we developed specifically for that purpose." [3]

***Table 7**. "Comparison of methods reported for the determination of reduced GSH." [3]*

Method	LOD *	LOQ	recovery	intra-day precision	inter-day precision	reductant	Derivatization	Ref.
HPLC-Fluorescence	0.05 pmol (50 fmol)	--	98.40%	4.9%	4.2%	DTT	OPA	[23]
LC-ESI-MS	0.10 pmol (0.01 µM)	0.05 µM	98.5 % - 100.6 %	1.6% - 1.9%	1.75%	--	NEM	[29]
LC-MS/MS	0.20 pmol	--	--	3.1% - 14.1%	4.2%-24.5%	--	--	[28]
HPLC-UV	0.20 pmol (0.02 µM)	--	99.4 % - 102.2 %	--	--	DTT	DTNB	[20]
HPLC-Fluorescence	--	1.56 µM	88.4 % - 97.5 %	1.7% - 4.1%	3.1%-4.9%	TCEP	SBD-F	[22]
HPLC-UV	820 pmol (0.041 mM)	135 µM (0.135 mM)	94.5% - 104.5%	6.64% - 9.65%	4.60%-7.67%	--	DTNB	[19]
HPLC-Fluorescence	0.60 pmol (0.03 µM)	0.1 µM	--	6.3%	6.90%	--	NBD-F	[21]
LC-MS/MS	4.00 pmol (0.4 µM)	1.5 µM	95% - 97%	3.3%	4.10%	--	NEM	[26]
LC-MS/MS	--	--	93.3% - 106.0%	--	--	DTT	NEM	[25]
LC-MS/MS	1000 pmol (50 µM)	75 µM	98.0% - 105.9%	2.0% - 4.3%	4.10%	--	NEM	[24]
LC-MS/MS	**0.05 pmol (0.01 µM)**	**0.78 µM**	**99.9% - 108.9%**	**2.49%**	**2.04%**	**DTT**	**--**	**This study**

OPA: ortho-phthalaldehyde; **NEM**: N-ethylmaleimide; ***DTNB***: 5,5'-dithio-bis-(2-nitrobenzoic acid);
SBD-F: 7-fluorobenzofurazan-4-sulfonic acid ammonium salt;
NBD-F: 4-flouro-7-nitrobenzofurazan; ***mBBr***: monobromobimane
***** Amount of substance loaded on column

7.3 Quantification of intracellular tGSH in HCT116 cells

"To further demonstrate the applicability of the developed LC-MS/MS method, we measured the total intracellular concentration of glutathione in HCT116 cells. Both parental HCT116 and IDH1-R132H mutant cell lines were employed to study the effect of a neomorphic mutation in isocitrate dehydrogenase 1. The mutated enzyme catalyzes the NADPH consuming conversion of α-ketoglutarate to 2-hydroxyglutarate, while wt-IDH1 catalyzes the oxidative decarboxylation of isocitrate to α-ketoglutarate producing NADPH. NADPH is used to reduce GSSG and, therefore, to maintain the reductive capacity of the cell. Cells carrying mutated IDH1 might compensate for changes in the redox system by upregulation of cellular biosynthesis of GSH. BSO, on the other hand, is a specific and competitive inhibitor of gamma-glutamylcysteine synthetase, the rate-limiting enzyme in GSH biosynthesis. Therefore, it can reduce the intracellular level of glutathione [261, 262]. To assess the method using biological samples, both parental HCT116 and IDH1-R132H mutant cells were cultured with/without BSO for 24h. As shown in Figure 34, intracellular tGSH was decreased significantly after 24h of BSO treatment in both parental and mutant

cells compared to the corresponding untreated controls ($p = 1.80\times10^{-7}$ and 1.47×10^{-8}, respectively, for parental and mutant cells) and BSO suppressed glutathione levels to a similar extent in both cell lines. However, no significant difference in tGSH was observed between parental and IDH1-R132H mutant cell lines. Maybe an alteration of NADPH levels by the IDH1 mutation only affects the GSH to GSSG ratio but not overall GSH biosynthesis (and thus tGSH) in HCT116 cells." [3]

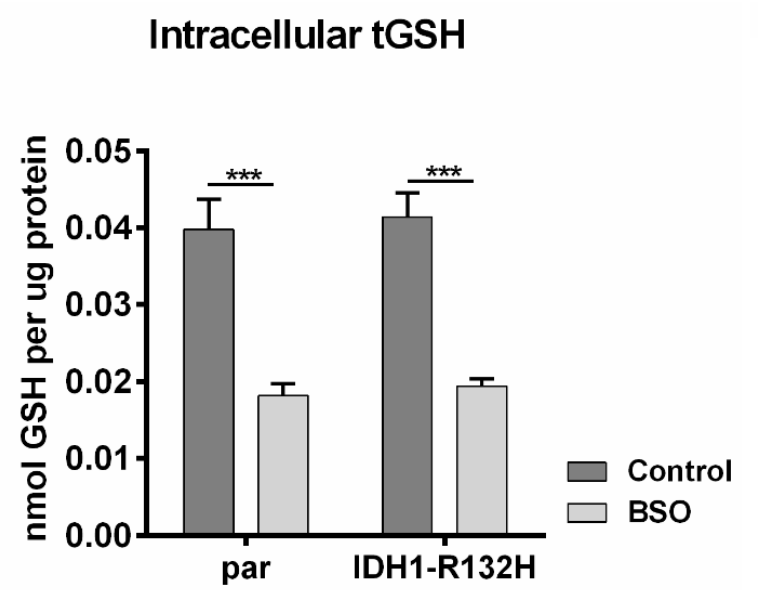

Figure 34. *"Total GSH amount in parental HCT116 and IDH1-R132H mutant cells after treatment with or without 5 µM BSO for 24 h, n=6, two independent experiments. Cell pellets were extracted using 80 % methanol and the extracts were reduced with DTT. Data is shown as mean + SD, p-values for parental and mutant cells are 1.80×10^{-7} and 1.47×10^{-8}, respectively." [3]*

8 Tracer analysis of glutathione by HPLC-QTOF-MS/MS

So far, studies regarding glutathione have focused on its quantification either in total or in oxidized and reduced form. However, the distribution of glutathione isotopologues in cells from tracer analysis experiments can also provide vital information on cell metabolic changes induced by internal/external stimuli. In this chapter, a wide Q1 isolation MRM window strategy on a QTOFMS instrument is presented for assessing the distribution of glutathione isotopologues from stable isotope labeling experiments. The developed method was applied to study the effect of a neomorphic mutation in isocitrate dehydrogenase gene (IDH1) on the biosynthesis of glutathione in the presence of fully ^{13}C labeled glucose or glutamine.

This chapter was published in *Analytica Chimica Acta (Sun et al., Quantification and ^{13}C-Tracer Analysis of Total Reduced Glutathione by HPLC-QTOFMS/MS, 2019, 1080, 127-137)*. Paragraphs taken directly from the publication are marked with quotation marks.

8.1 Method development and optimization

Tracer analysis using a triple quadrupole MS in multiple reaction monitoring mode requires the setup of individual transitions for each isotopologue. Moreover, if tracer atoms are lost in the neutral loss, this must be accounted for by separate transitions. As the number of tracer atoms (^{13}C) increases in a given compound, the number of transitions to be considered increases rapidly. Operation of a QTOFMS instrument for MS/MS experiments is not hampered by setting up transitions. In this study, the first quadrupole (Q1) is operated to allow ions over a given *m/z* range to pass through. That allows all of the GSH isotopologues that can originate from ^{13}C incorporation to enter the collision cell simultaneously. The resulting fragments can then be analyzed in parallel by the TOF analyzer with high resolution, yielding the full isotopologue distribution of both GSH precursor ion and its fragment ions. The window width was optimized and the performance of the wide Q1 window strategy was compared with full scan and all ion fragmentation acquisition mode on the same MS instrument with standard solutions of labeled (glutathione-(glycine-$^{13}C_2$,$^{15}N_1$)) and unlabeled GSH.

“We firstly assessed the performance of MRM methods with different Q1 isolation window widths (8, 10, 12, and 20 Da). The wide-window MRM strategy was then compared with full scan MS and bbCID performed in the *m/z* range of 50 to 1000 using mixtures of standard stable isotope labeled and unlabeled GSH. bbCID is an approach to achieve all ion fragmentation (AIF) whereby all ion precursor ions observed in the MS survey scan are fragmented [139]. GSH standard solutions containing equal amounts of labeled and unlabeled GSH were prepared at different concentrations (10, 20, 40 µM). Those solutions were then processed according to our reduction protocol (see section 5.7) and subjected to LC-MS/MS measurements with different MRM window widths (8, 10, 12, and 20 Da), bbCID, and LC-MS measurements in full scan mode. We compared the peak areas of the parent ions (*m/z* 308 from unlabeled GSH and *m/z* 311 from isotope labeled GSH) and the product ions (*m/z* 179 and *m/z* 182) of unlabeled and labeled GSH, respectively. Peak area ratios are shown in Figure 35 (different MRM window widths) and Figure 36 (20 Da-window MRM, bbCID and full scan). In Figure 35, peak area ratio increases with increasing window width from 8 Da to 20 Da. ANOVA statistics was run to test the difference between different window widths, the results are shown in Table S6 (see supplementary information in Chapter 11). In stable isotope tracer analysis, it is important to properly quantify isotopologues of a molecule relative to each other. Window width should be adjusted in a metabolite specific manner to achieve accurate labeling analysis. An insufficiently wide window may exclude some of the isotopologues from the measurement or reduce their measured intensity relative to isotopologues with an *m/z* more central in the window as we can see from Figure 35. Unlabeled GSH (*m/z* 308) was partly excluded from the measurement at smaller MRM window widths, resulting in a lower peak area ratio. In the case of GSH, we set up the central selection *m/z* at 313 as all possible isotopologues of GSH that can result from a ^{13}C-tracing experiment are in the *m/z* range of 308 to 318. To be sure that all GSH isotopologues ions will be included equally in the MRM selection window, we measured a GSH standard solution (unlabeled GSH) by MRM with an isolation window width from 12 Da to 24 Da. Of all isotopologues, unlabeled GSH (*m/z* 308) and GSH+10 (*m/z* 318) are farthest from the center of isolation, making unlabeled GSH a suitable choice for this analysis. Results are shown in Figure 36. Peak area increases with increasing MRM isolation window width and levels off at a

window width of 20 Da. This means that even the ions at the selection boundary are reliably included when using this window width. Therefore, a 20 Da window was finally set for the MRM-based isotope labeling analysis of GSH. We compared the performance of the wide-window MRM strategy with full scan MS and bbCID. No significant differences can be found with regard to the peak area ratios of unlabeled and labeled GSH measured by the three methods (see Figure 37). However, peaks measured by full scan MS show relatively low intensity. bbCID might be an alternative to isotope labeling pattern analysis of GSH. However, in our preliminary experiment, bbCID also showed very low peak intensities. We optimized it by adjusting the acquisition time factor (ATF) to try to achieve peak intensity comparable to the MRM measurements. ATF is the factor by which the sample time of the digitizer is multiplied. This parameter applies only to MS/MS spectra and is used to increase the intensity of small peaks in the MS/MS spectrum. Figure 38 shows the chromatograms of GSH standard measured under different bbCID conditions. Peak intensity improves upon increasing the acquisition time factor. However, it also dramatically decreases the number of data points taken across a peak. For good quantitative reproducibility, it is necessary to acquire enough data points to precisely define a chromatographic peak. We therefore finally set up the acquisition time factor at 15 for bbCID acquisition. However, still, the intensity of the peak obtained from bbCID mode is much lower than in wide-window MRM with the same mass spectrometer acquisition parameters as shown in Figure 39. Besides, since all ions will undergo fragmentation without any precursor ion selection in bbCID, interferences might be a substantial issue especially for complex samples. With a wide window strategy on the other hand, interfering ions must not only coelute with the analyte but have a precursor ion within the specified *m/z* window of e.g. 20 Da and fragment *m/z* that cannot be resolved from target product ion *m/z*. This makes the wide window approach more selective compared to bbCID under the conditions we employed in this study.” [3]

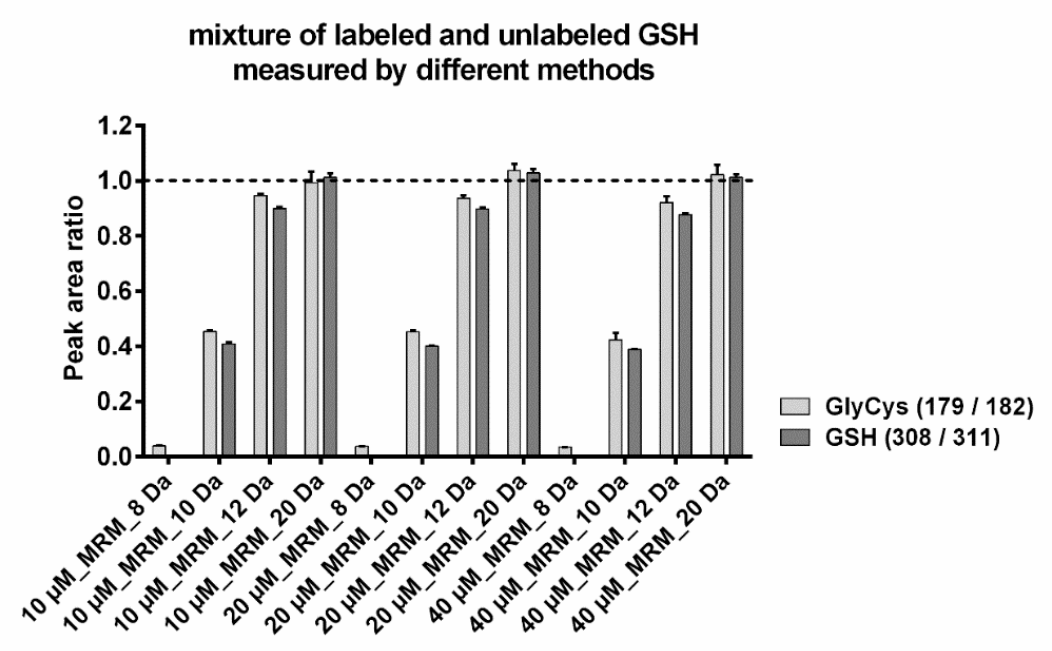

***Figure 35**. "Peak area ratios of labeled and unlabeled GSH measured by MRM with different window widths." [3]*

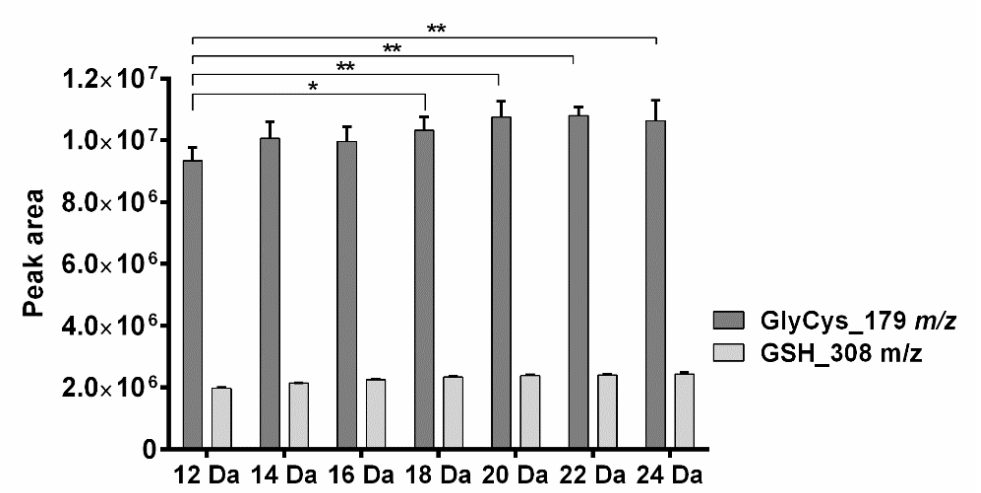

***Figure 36**. "Peak areas of GSH standard measured by MRM with different window widths." [3]*

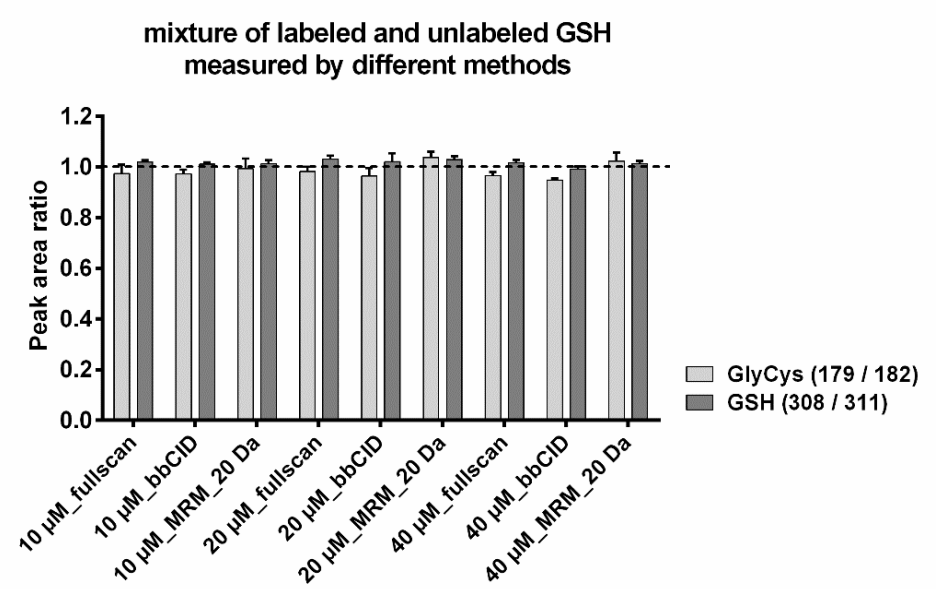

Figure 37. *"The unlabeled to labeled GSH peak area ratio was measured by different methods. Standard solutions containing unlabeled and labeled GSH at the same concentration (10 µM, 20 µM, 40 µM) were measured by LC-MS/MS in positive MRM mode with a 20 Da - Q1 selection window, by LC-MS in positive full scan mode, and by LC-MS/MS in bbCID mode. Data is shown as mean + SD (n=3)." [3]*

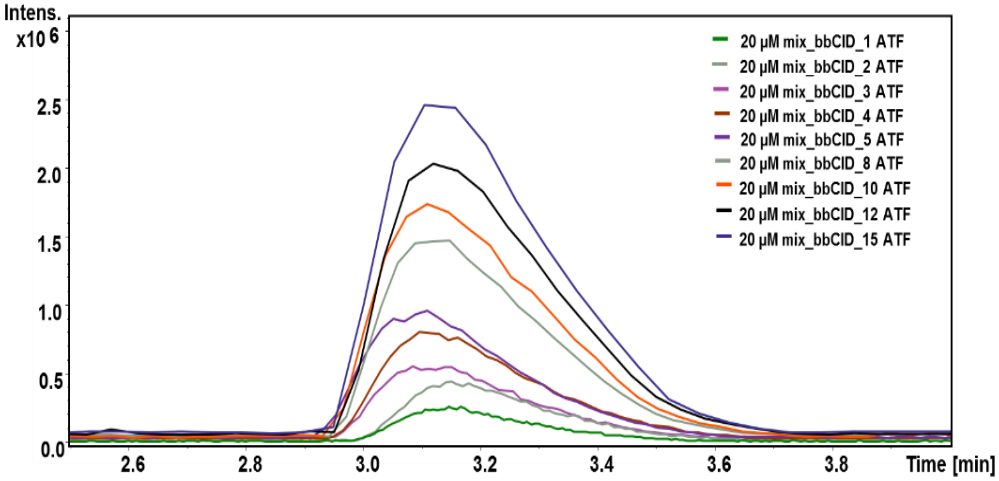

Figure 38. *"Chromatograms of a standard unlabeled and labeled GSH mixture as measured by bbCID mode with different acquisition time factors (ATF)." [3]*

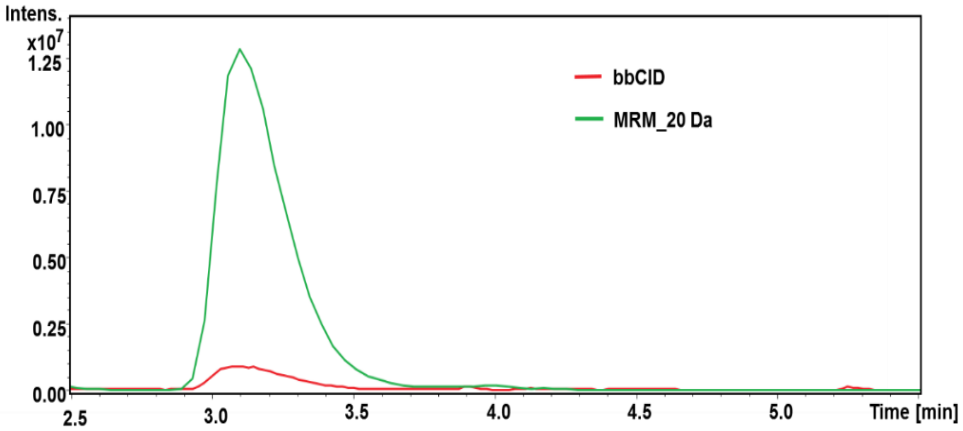

***Figure 39**. "Chromatograms of a mixture of unlabeled and labeled GSH (glutathione-(glycine-$^{13}C_2$,$^{15}N_1$)) as measured by bbCID mode and 20 Da-window MRM with the same mass spectrometer data acquisition parameters." [3]*

8.2 GSH tracer analysis in HCT116 cells

"To illustrate biological application, the developed wide Q1 isolation window HPLC-MS/MS method was applied to GSH stable isotope labeling analysis in HCT116 cells. Cells were cultured with fully ^{13}C-labeled glucose or glutamine to examine the fate of tracers in the glutathione synthetic pathway. To be able to see biologically induced changes in the GSH labeling patterns and/or GSH abundance, cells were pretreated with or without BSO for 24 h. Our wide-window HPLC-QTOF-MS/MS method in positive MRM mode with a 20 Da Q1-window was employed to analyze the GSH isotopologues. Cell samples were subjected to cell extraction and DTT reduction before LC-MS/MS measurement. Acquired data was transferred to Bruker QuantAnalysis 2.2 software for retention time and peak integration checking. Peak areas of all parent ions and fragment ions were then corrected for natural isotope abundance and purity of the tracer using the IsoCorrectoR R-package. Results are shown as mean enrichment in Figure 40A and 40B. Mean enrichment was calculated as follows:" [3]

$$"Mean\ enrichment = {\sum(fraction\ \times carbon\ number)}/{total\ carbon\ number}\ "$$ [3]

"Here, the fraction of the given isotopologue is multiplied with the carbon number of ^{13}C in that isotopologue and divided by the total carbon number of ^{13}C label the molecule in

question can contain. In ^{13}C-glucose tracing, the GluCys fragment showed a mean enrichment of 10-20 %, while for CysGly, only a mean enrichment of 0.5-1.5 % was observed. Thus, in the time period during which cells were given labeled glucose, glucose contributed to GSH synthesis mainly via its conversion to glutamate. Most likely, the majority of the glycine and cysteine required for GSH synthesis was taken directly from the cell culture medium and not synthesized from glucose via 3-phosphoglycerate/serine. When cells were cultured with ^{13}C-labeled glutamine, isotopic enrichment could only be observed in GluCys but not in CysGly. In addition, regarding the mean enrichment, contribution to GSH synthesis is higher for glutamine than for glucose as shown in Figure 40A and B. The total isotopic enrichment of GSH from labeled glucose and labeled glutamine is lower than 100 %, which is probably due to the existence of unlabeled amino acids and glutathione in cell culture RPMI medium as shown in Table S7 (see supplementary information in Chapter 11).” [3]

“We also observed a significant difference in isotopic enrichment of GSH between parental and mutant cells for both BSO treated ($p=1.55\times10^{-6}$) and untreated ($p=5.43\times10^{-6}$) cells when fed labeled glucose. A significantly higher GSH isotopic enrichment was observed in parental cells compared to (IDH1) mutant cells. It is known that mutIDH1 cells have to adapt their metabolism, such as TCA-cycle flux, to compensate for increased α-ketoglutarate consumption by mutant IDH1 for D-2- hydroxyglutarate production [58, 263, 264]. Besides, formation of glutamate from glucose has been shown to decrease due to the inhibition of branched-chain amino acid transaminase (BCAT transaminases) by D-2-HG [8]. This increases the dependence on glutaminase for the biosynthesis of glutamate from glutamine. This is corroborated by Figure 40B, which shows a higher isotopic enrichment of GSH in IDH1-mutant cells compared to parental cells when fed labeled glutamine.” [3]

“To further validate our LC-MS/MS method for stable isotope labeling analysis, we cultured the cells in the presence of equimolar amounts of both labeled and unlabeled glucose. Results are shown in Figure 40C and D. The mean enrichment values obtained for this experiment are fairly close to half of the enrichment values found in the cells cultured only with labeled glucose. This result further demonstrates the suitability and

accuracy of this wide-window LC-MS/MS method for GSH stable isotope labeling analysis." [3]

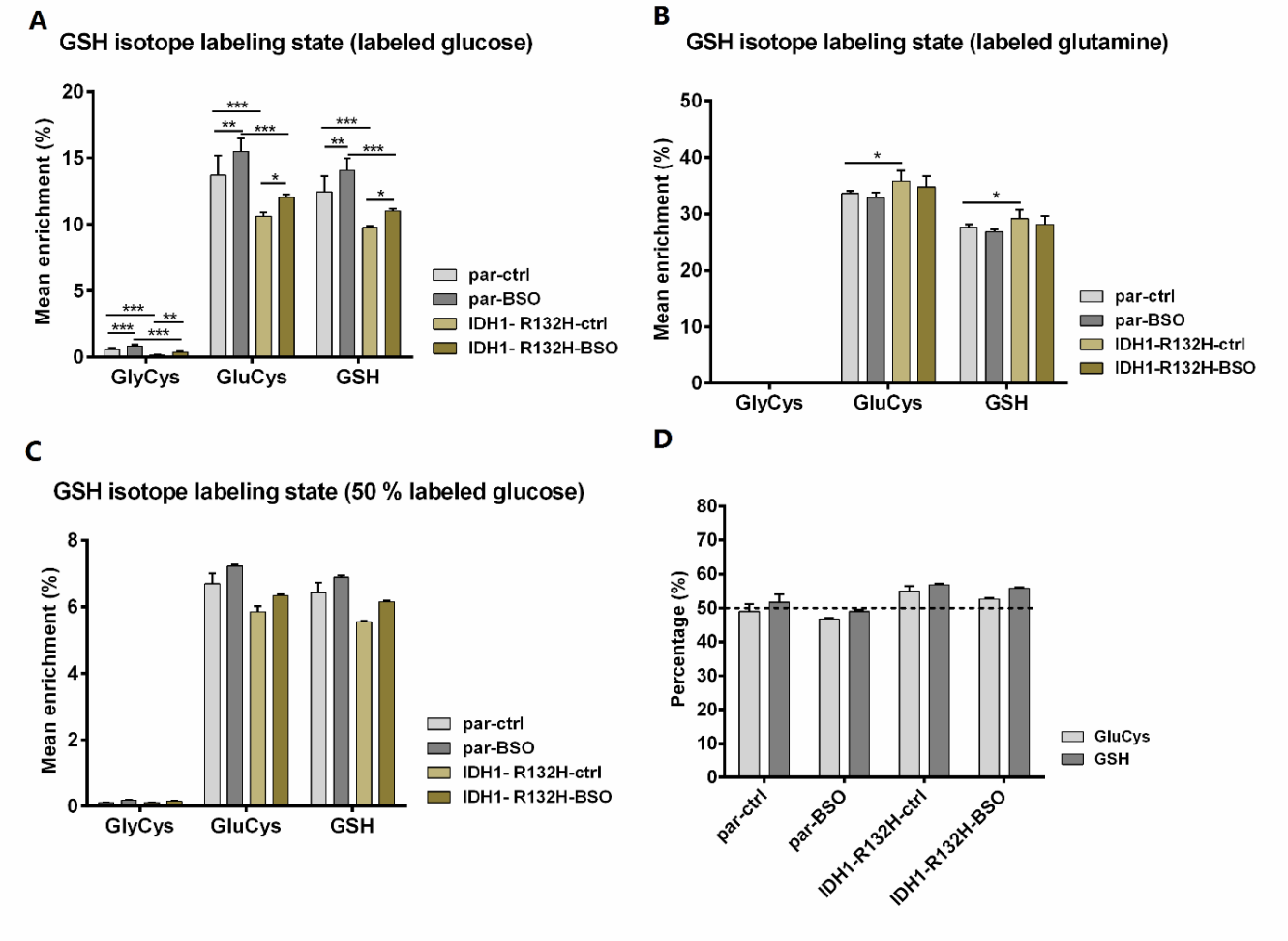

***Figure 40**. "GSH stable isotope labeling analysis results from tracing experiments with U-^{13}C-labeled glucose or glutamine. For BSO treated groups, cells were cultured and pretreated with BSO for 24 h before using labeled glucose/glutamine and then cultured with BSO and labeled nutrient for an additional 24 hours. **A**: Cells were cultured with fully-labeled glucose, two independent experiments, n=6; **B**: Cells were cultured with fully-labeled glutamine, two independent experiments, n=6; **C**: Cells were cultured with both labeled and unlabeled glucose (1:1), n=3; **D**: Mean enrichment ratio of A and C. Data is shown as mean + SD; p-values from the ANOVA are listed in Table S8 (see supplementary information in Chapter 11)." [3]*

9 ^{13}C-tracer analysis of metabolic changes induced by IDH mutation

The redirection of α-KG from normal reductive metabolism in citric acid cycle towards D-2-HG generation in cells harboring an IDH mutation has been suggested to dysregulate other metabolic fluxes [58, 265, 266]. Studies from chapter 6 to chapter 8 have demonstrated the changes in glutathione metabolism in IDH mutant cells. Glucose and glutamine metabolism were also found to be different in mutant IDH cells [38, 68]. To better understand the metabolic impact of different IDH mutations in vitro, we performed ^{13}C-tracer experiments with wild-type an IDH mutant (IDH1-R132H, IDH2-R172K, and IDH2-R140Q) HCT116 cell clones. The cells were incubated with fully ^{13}C labeled glucose or glutamine for different time periods. GC-MS and HPLC-MS were employed to analyze the isotope labeling pattern of various metabolites, *i.e.*, amino acids, TCA cycle intermediates, fatty acids, and GSH to identify important metabolic alterations associated with IDH1/2 mutations. Occurrence of metabolic alterations is evident from differences in isotopic mean enrichment, which reflects the overall tracer incorporation, and isotopologue fractions for a given metabolite. Details of sample preparation and instrumental analysis have been described in Chapter 5.

9.1 Study of isotopic steady state in various metabolites

^{13}C tracing experiments are commonly performed at isotopic steady state which describes a condition where ^{13}C enrichment into metabolites has reached an equilibrium and is stable over time. To determine the time needed to reach isotopic steady state for the metabolite examined, both HCT116 wild-type and IDH mutant cell lines (IDH1-R132H, IDH2-R172K, and IDH2-R140Q) were grown for different time periods (0h, 12h, 24h, 48h, 72h) in glucose or glutamine-free media supplemented with 2 g/L of U-^{13}C-glucose (11.1 mM) or 2 mM of U-^{13}C-glutamine. Mass spectrometry-based analytical tools were used to investigate the incorporation of ^{13}C atoms derived from labeled glucose and glutamine, respectively, into the studied metabolites.

Glucose contributes to the *de novo* biosynthesis of numerous amino acids such as alanine, glutamate, aspartate, proline, glycine, and serine. Incorporation of glucose-derived carbon into other amino acids such as ornithine, arginine, and asparagine can also be observed, albeit to a lesser degree (mean enrichment < 3%). From U-^{13}C- glucose tracer analysis it is evident, that all of the studied amino acids, with the exception of glycine (48 h vs 72 h, p=0.0359) and serine (48 h vs 72 h, p=0.0033) reached their isotopic steady state in IDH wild-type cells after 48 h, as indicated by stable isotopic mean enrichment (Figure 41A, statistics see Supplementary Table S9 in Chapter 11). In mutant IDH cells, in contrast, isotope labeling was still changing in most of the amino acids at 48 h (Figure 41B-D, 48 h vs 72 h, $p<0.05$ for alanine, glutamate, aspartate, proline and glycine). Only serine appeared to reach isotopic steady state at 48h in IDH2-R172K (48 h vs 72 h, p=0.6647) and IDH2-R140Q (48 h vs 72 h, p=0.0714) cells, as mean isotopic enrichment in serine did not differ significantly between 48 h and 72 h of incubation (detailed statistics see Supplementary Table S9 in Chapter 11). However, one should keep in mind that exchange reactions with extracellular pools of amino acids, e.g. amino acids in the growth medium, may prevent or disturb the establishment of isotopic steady state. Other factors that may contribute are autophagy. Autophagy is a self-degrading process, which is important to balance energy source and responses to nutrient stress at critical time [267]. Exogenous 2-HG treatment was found to be able to trigger autophagy in glioma U87MG cells and increased autophagosome was also observed in IDH1-R132H-expressing U87MG cells [268].

Glutamine, an important amino acid itself, has been recognized to play a nutrient role similar to glucose. It can be both used to generate ATP and provide precursors for biosynthetic reactions. Glutamate, aspartate, and proline are the main three glutamine-derived amino acids as indicated in Figure 42. Unlike glucose, carbons derived from glutamine are rapidly incorporated into glutamate, aspartate, and proline. When cells were fed with labeled glutamine, isotopic enrichment in glutamate and aspartate reached its maximum after 12 h of incubation (Figure 42). However, further incubation of the cells with labeled glutamine resulted in a gradual decrease in isotopic enrichment in glutamate and aspartate. This phenomenon can be seen in all cell lines, indicating that this effect is probably not related to the IDH mutation. We then hypothesized that this is caused by

glutamine deprivation in the cell culture medium after a certain time of incubation. To answer this question, we measured the extracellular U-^{13}C-glutamine level in cell culture medium by NMR after 0 h, 12 h, 24 h, 48 h, and 72 h of incubation. As shown in Figure 43A, about half of the labeled glutamine was consumed by the cells after 24 hours and after 72 h of incubation, only ~ 0.15 mM of labeled glutamine were left in the medium. Cell growth of the whole cell panel was also tested during 72h incubation. However, the quick consumption of the labeled glutamine seems not to affect cell growth as evidenced by Figure 43B. Both parental and IDH mutant cells show an exponential growth during the 72h of incubation. Cells may also take up unlabeled substrates *e.g.*, protein-derived glutamine to support growth. We therefore analyzed the unlabeled glutamine content in the supernatant. As shown in Figure 43C, a gradual increase of unlabeled glutamine was observed in the supernatant of all cell lines during the incubation, which may serve as an additional substrate in the medium. However, the concentration of unlabeled glutamine is more than an order of magnitude lower than the remaining labeled glutamine. We wondered whether the decrease in amino acid labeling can be rescued by supplying enough labeled glutamine in the medium during incubation. HCT116 wild-type cells were grown in the presence of U-^{13}C-glutamine for 48 h, while exchanging the medium every twelve hours. Cells were harvested at 12 h, 24 h, and 48 h and the corresponding supernatants were collected. Intracellular amino acids labeling was analyzed by LC-MS/MS (Figure 44A) and organic acids labeling was analyzed by GC-MS (Figure 44B). Both labeled and unlabeled glutamine in the supernatant were determined by NMR (Figure 44C). U-^{13}C-glutamine concentration determined at 0 h by NMR was lower than 2 mM (theoretical concentration of labeled glutamine at 0 h), which is probably due to the binding of glutamine to proteins present in the fetal calf serum added in the medium. Thus, the uptake values which were obtained by subtracting the U-^{13}C-glutamine concentration at each time point (12 h, 24 h, and 48 h) from the medium control (0 h) were calculated and shown in Figure 44D. By replenishing the medium every 12 hours, labeled glutamine concentrations above 1 mM were maintained, but still decreased over time due to the increasing number of cells in culture.

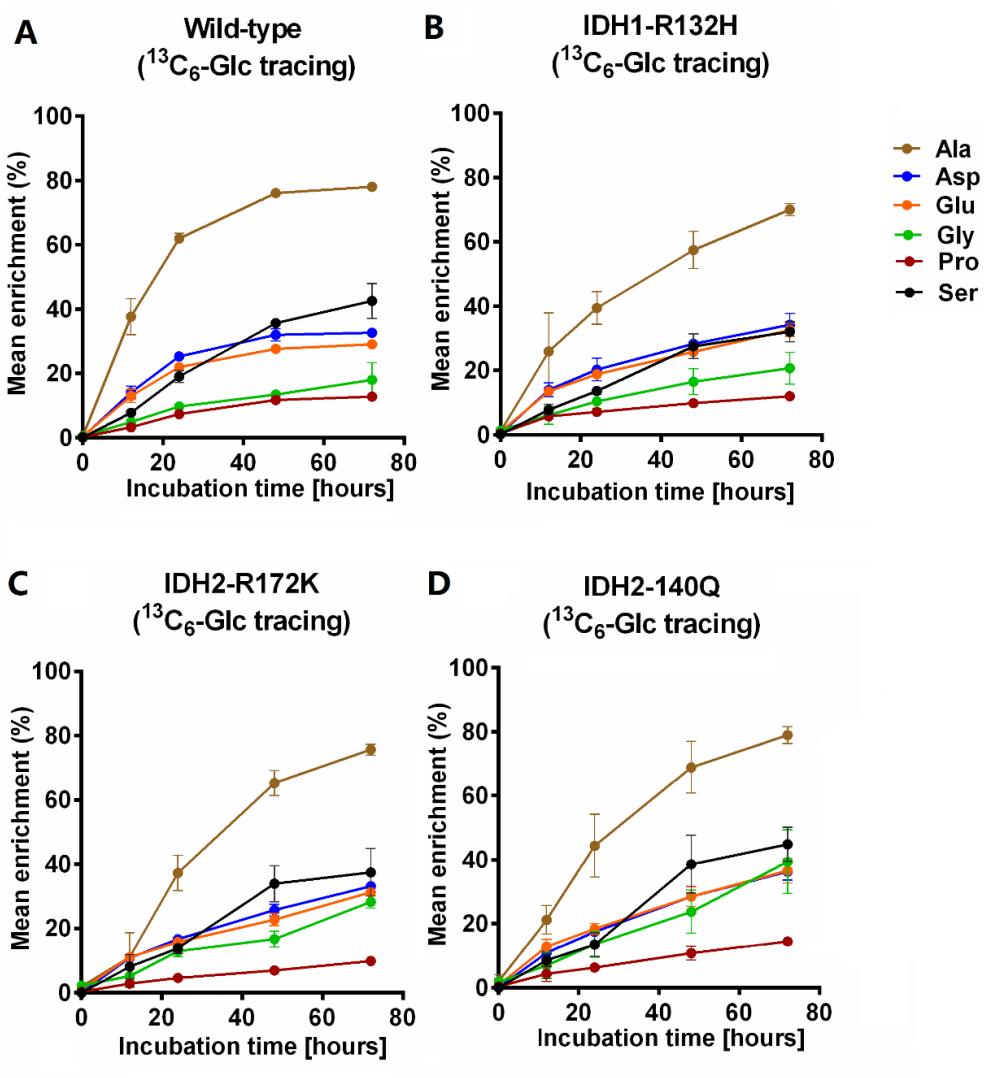

Figure 41. *Isotopic mean enrichment in amino acids at different incubation times (0 h, 12 h, 24 h, 48 h, 72 h) from U-^{13}C-glucose in HCT116 cells with wild-type IDH or mutant (IDH1-R132H, IDH2-R1172K, and IDH2-R140Q). Both IDH wild-type and mutant cells were cultivated in glucose free media supplemented with 2 g/L of U-^{13}C-glucose (11.1 mM) for different time periods. Data are shown as mean ± SD, n=6, two independent experiments. For statistics see Supplementary Table S9 in Chapter 11.*

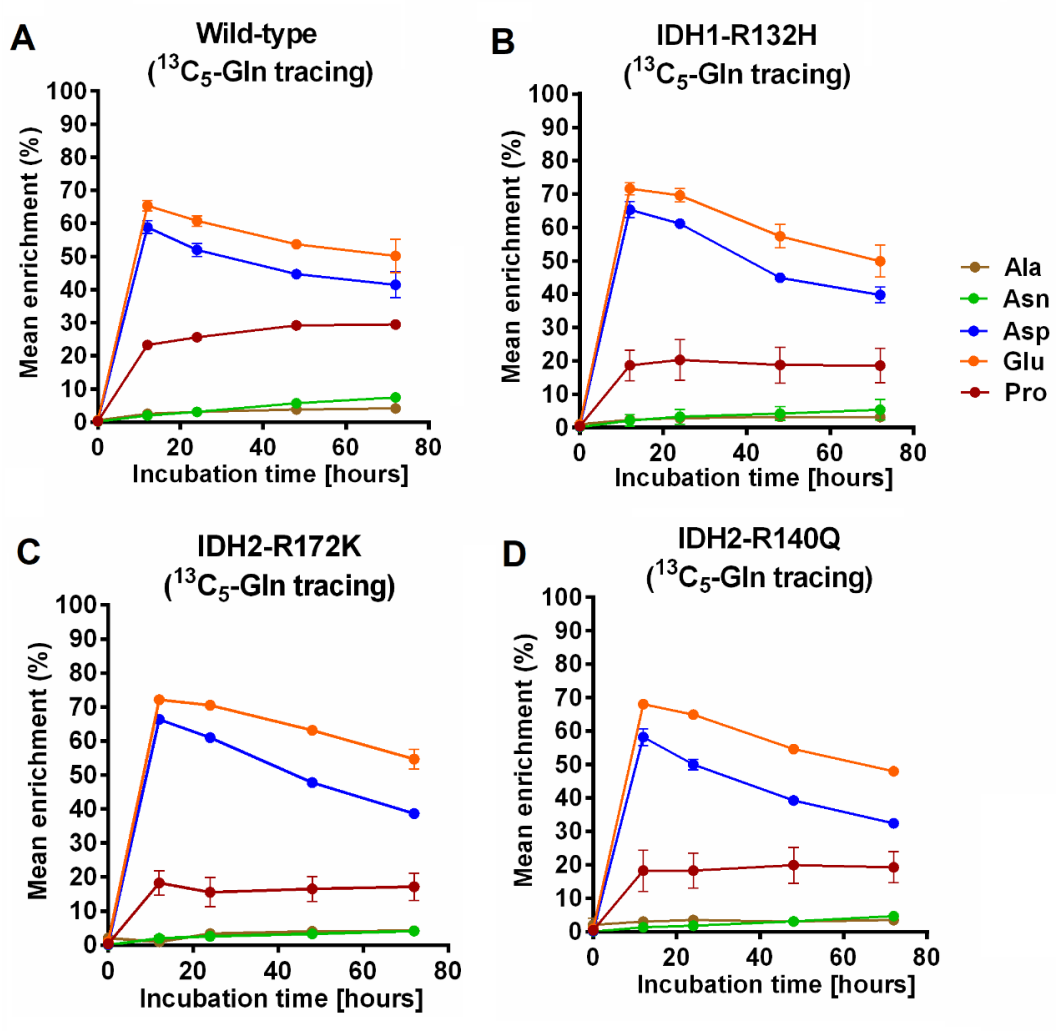

Figure 42. *Isotopic mean enrichment in amino acids at different incubation times (0 h, 12 h, 24 h, 48 h, 72 h) from U-^{13}C-glutamine in HCT116 cells with wild-type or mutant IDH (IDH1-R132H, IDH2-R1172K, and IDH2-R140Q). Both wild-type and IDH mutant cells were cultivated in glutamine free media supplemented with 2 mM of U-^{13}C-glutamine for different time periods. Data are shown as mean ± SD, n=6, two independent experiments. For statistics see Supplementary Table S9 in Chapter 11.*

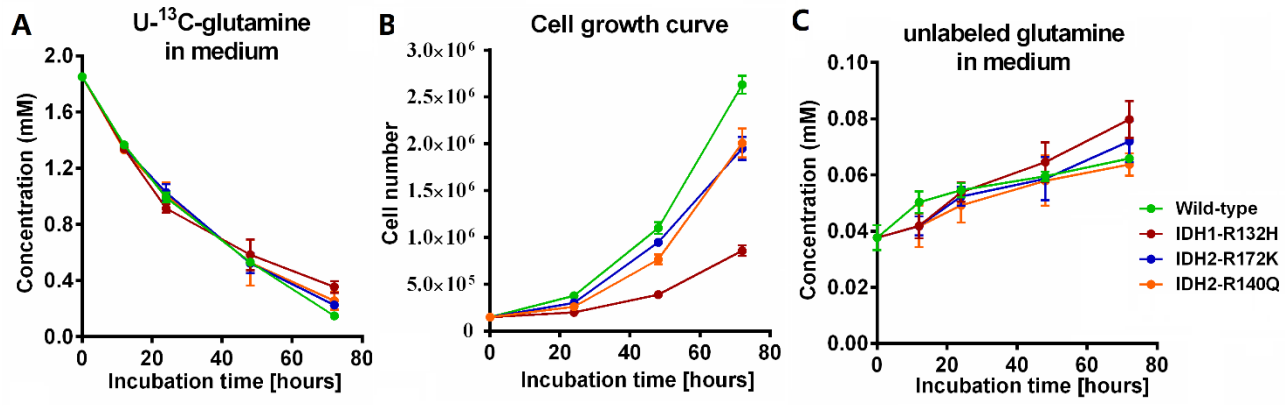

Figure 43. (A) *U-^{13}C-glutamine concentration in cell culture supernatants after incubation for different time periods (0 h, 12 h, 24 h, 48 h, 72 h). Concentrations were measured by NMR (n=6, two independent experiments).* ***(B)*** *Cell growth curve for each cell line over 72 h (n=3).* ***(C)*** *Unlabeled glutamine concentration in cell culture medium after incubation for different time periods (0 h, 12 h, 24 h, 48 h, 72 h) were measured by NMR (n=6, two independent experiments).*

As observed previously, isotopic steady state for the tested amino acids and TCA cycle intermediates was reached at 12 hours (Figure 44A-B) and the U-^{13}C-glutamine concentrations are sufficient to maintain a stable mean isotopic enrichment in those metabolites. Unlabeled glutamine in the supernatant was also kept at a relatively constant level which is quite equal to that in the blank medium (0h) (Figure 44C). Considering the increasing levels of unlabeled glutamine observed in Figure 43C, glutamine deficiency may drive protein degradation and release unlabeled glutamine into the medium. All in all, these experiments show that sufficient labeled nutrient supply by medium exchange every 12 hours can efficiently compensate for the decrease in amino acid labeling caused by the deficiency of labeled nutrient in the cell culture model under investigation.

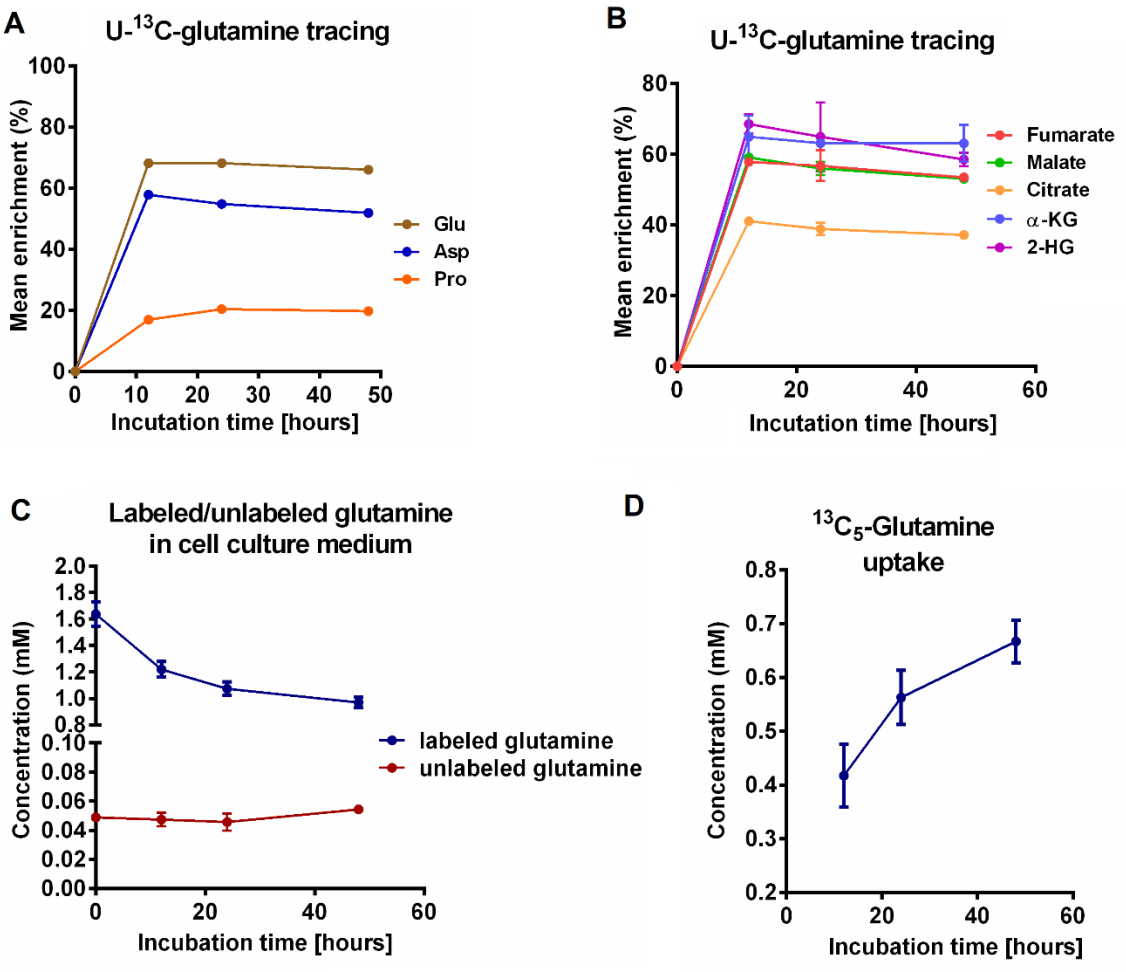

Figure 44. (A) *Isotopic mean enrichment of Glu, Asp, and Pro in parental HCT116 cells from U-^{13}C-glutamine at different incubation times (12 h, 24 h, 48 h, n=3 for each). Medium containing 2 mM of U-^{13}C-glutamine was exchanged every 12 hours.* ***(B)*** *Isotopic mean enrichment of TCA cycle intermediates in parental HCT116 cells from U-^{13}C-glutamine at different incubation times (12 h, 24 h, 48 h, n=3 for each). Medium containing 2 mM of U-^{13}C-glutamine was exchanged every 12 hours. In all figures, data are shown as mean ± SD.* ***(C)*** *Concentrations of unlabeled glutamine and U-^{13}C-glutamine in cell culture medium at different incubation times (12h, 24h, 48h, n=3 for each).* ***(D)*** *Glutamine uptake at each time point during 48 h of incubation (n=3). Medium containing 2 mM of U-^{13}C-glutamine was exchanged every 12 hours. U-^{13}C-glutamine concentration determined at 0 h by NMR was lower than 2 mM, which is probably due to the binding of glutamine to proteins present in the fetal calf serum added in the medium. Thus, the uptake values which obtained by subtracting U-^{13}C-glutamine concentration at each time point from the medium control (0 h) were calculated and shown in Figure 44D. Experiments in this figure were performed by Dr. Raffaela Berger. Sun, X analyzed the data and prepared the figures.*

Since IDHs are essential enzymes in the production of NADPH and α-KG, which is not only a key intermediate of the TCA cycle but also a (co-)substrate of transaminases and dioxygenases. Therefore, IDH mutations are expected to exert a significant impact on intermediary metabolism. The main metabolic change associated with IDH mutation is the gain of the new ability to convert α-KG to D-2-HG, resulting in elevated levels of D-2-HG in IDH mutant cells [48, 50]. However, in addition to D-2-HG accumulation, other TCA cycle intermediates are also markedly affected by mutations in IDH enzymes [63]. To better understand those mutant IDH-related metabolic changes during cell growth, we analyzed the isotopic steady state of glycolysis and TCA cycle intermediates with the HCT116 cell panel. As shown in Figure 45A, all of the studied TCA cycle intermediates, *i.e.*, citrate, α-KG, succinate, fumarate, and malate, reached isotopic steady state after 48 h of incubation with U-^{13}C-glucose in HCT116 wild-type cells (48 h vs 72 h, $p>0.05$ for citrate, α-KG, fumarate, and malate, detailed statistics see Supplementary Table S10 in Chapter 11), except succinate that showed a drop in isotopic mean enrichment at 72h. However, similar to the observation with amino acids, isotopic mean enrichment in those typical TCA intermediates is still changing from 48h to 72h in all IDH mutant cells (Figure 45B-D, 48 h vs 72 h, $p<0.05$ for citrate, α-KG, succinate, fumarate, and malate, detailed statistics see Supplementary Table S10 in Chapter 11).

Pyruvate and lactate, as important products from glycolysis were also investigated. Cells rapidly metabolize glucose into pyruvate and further into lactate in both wild-type and IDH mutant cells. At 24 h, both pyruvate and lactate reached isotopic steady state in wild type and IDH1-R132H mutant cells (Figure 45A-B, 24 h vs 48 h, $p>0.05$ for pyruvate and lactate in both cell lines). However, as shown in Figure 45C-D, IDH2 mutant cells needed more time to reach lactate isotopic steady state compared to wild-type and IDH1 mutant cells (24 h vs 48 h, $p<0.05$ for IDH2-R172K and IDH2-R140Q cells). Lactate reached isotopic steady state at 48h in IDH2-R172K and IDH2-R140Q mutant cells (48 h vs 72 h, $p=0.9310$ for IDH2-R172K cells and $p=0.7047$ for IDH2-R140Q cells). Glycerol-3-phosphate (glycerol-3-P) which is synthesized from the glycolysis intermediate dihydroxyacetone phosphate (DHAP), was also investigated. Interestingly, glycerol-3-P reached isotopic steady state at 48 h in all IDH mutant cells (48 h vs 72 h, $p>0.05$ for all IDH mutant cells), while the mean isotopic enrichment still differed significantly between

48 h and 72 h in wild-type cells (48 h vs 72 h, $p=4.50\times10^{-6}$). On the other hand, continuous labeling changes in 2-HG were observed in both IDH wild-type and mutant cells during the entire experimental time span. It should be noted that 2-HG analysis employed in this study did not distinguish between D- and L-2-HG.

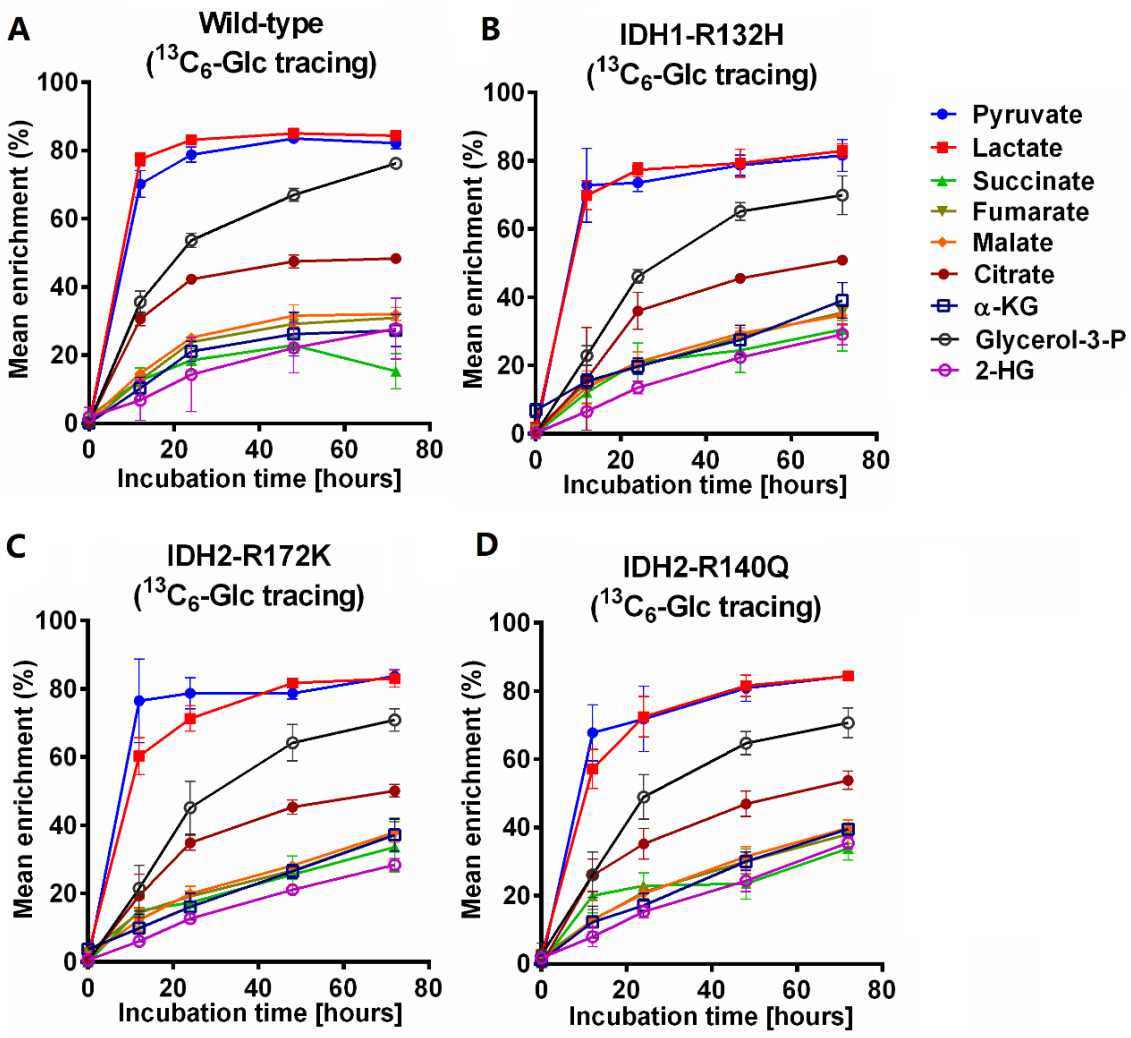

Figure 45. *Isotopic mean enrichment in glycolysis and TCA cycle intermediates at different incubation times (0 h, 12 h, 24 h, 48 h, 72 h) from U-^{13}C-glucose tracing experiments in HCT116 cells with wild-type and mutant IDH (IDH1-R132H, IDH2-R1172K, and IDH2-R140Q). Both IDH wild-type and mutant cells were cultivated in glucose-free medium supplemented with 2 g/L of U-^{13}C-glucose (11.1 mM) for different time periods. Data are shown as mean ± SD, n=5-6, two independent experiments. For statistics see Supplementary Table S10 in Chapter 11.*

When cells were fed with labeled glutamine (Figure 46A), all of the studied metabolites reached maximum isotopic mean enrichment in HCT116 wild-type cells after 12 h of incubation (12 h vs 24 h, $p>0.05$ for all tested TCA cycle intermediates and 2-HG). In IDH mutant cells, the highest mean isotopic enrichment of 2-HG appeared at 24h (12 h vs 24 h, $p<0.05$; 24 h vs 48 h, $p>0.05$ for all IDH mutant cells) while other tested metabolites showed the highest mean enrichment at 12 h (Figure 46B-D). Not surprisingly, decreased isotopic labeling also happened in organic acids after 24h incubation in all cell lines when U-^{13}C-glutamine was used as the labeled substrate (Figure 46). Glutamine anaplerosis is an important mechanism to replenish TCA cycle intermediates. Glutamine is deamidated by glutaminase (GLS) to form glutamate which is further metabolized to α-KG either by transaminases (alanine or aspartate transaminases) or by glutamate dehydrogenase (GDH) [269]. Since the carbon backbone does not change from glutamine to glutamate and α-KG, decreased availability of labeled glutamine directly influences the labeling of TCA intermediates. When the medium is supplied freshly every 12 h, the mean isotopic enrichment in TCA cycle intermediates is constant from 12 h to 48 h as shown in Figure 44B (ANOVA, $p>0.05$).

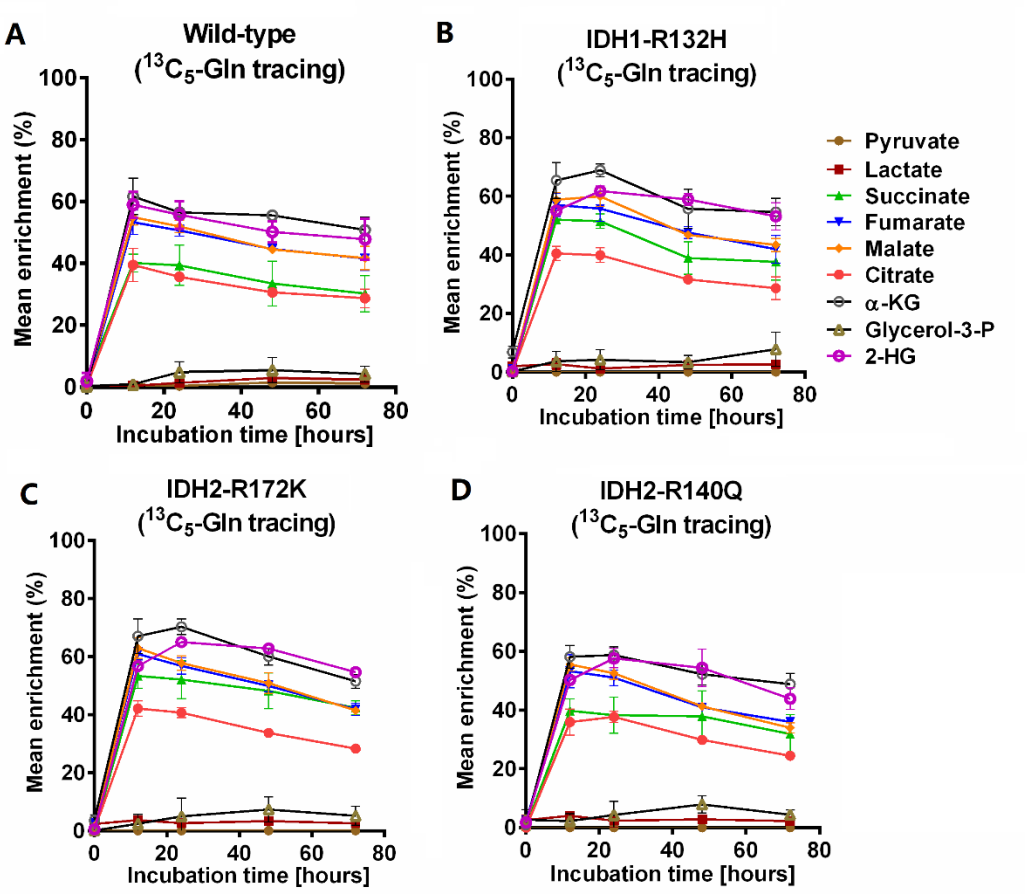

Figure 46. *Isotopic mean enrichment in glycolysis and TCA cycle intermediates at different incubation times (0 h, 12 h, 24 h, 48 h, 72 h) from U-^{13}C-glutamine in HCT116 cells with wild-type or mutant IDH (IDH1-R132H, IDH2-R1172K, and IDH2-R140Q). Both wild-type and IDH mutant cells were cultivated in glutamine-free media supplemented with 2 mM of U-^{13}C-glutamine for different time periods. Data are shown as mean ± SD, n=4-6, two independent experiments. For statistics see Supplementary Table S10 in Chapter 11.*

As previously discussed, glutathione (GSH) is an important cellular antioxidant to maintain redox homeostasis. The *de novo* synthesis of glutathione requires glycine, cysteine, and glutamate. Thus, its synthesis is highly determined by the availability of these amino acids. Recently, McBrayer et al have shown that mutant IDH affects GSH level in cells [8]. Both glucose and glutamine can contribute to GSH *de novo* synthesis by providing amino acid substrates. While glycine is mainly derived from glucose, glutamate can be produced from both precursors. Initial ^{13}C tracing experiments were performed

with two out of four cell lines (wt and IDH1-R132H). As already shown in Chapter 8, isotopic enrichment of GSH differed significantly between wild-type and IDH1-R132H cells in both U-^{13}C-glucose and U-^{13}C-glutamine tracing experiments [3]. However only one time point (24 h) was investigated in the initial experiments (Chapter 8). In the present study, we analyzed the isotopic labeling status of GSH during cell growth in both wild-type and all three IDH mutant HCT116 cell clones in the presence of U-^{13}C- glucose or U-^{13}C- glutamine. As shown in Figure 47A, if cells were grown in the presence of U-^{13}C-glucose, a gradual increase in GSH labeling was found in all cell lines (48 h vs 72 h, $p<0.05$ for all cell lines, detailed statistics see Supplementary Table S11 in Chapter 11). However, when U-^{13}C-glutamine was used as the tracer, isotopic steady state is reached at 24 h in all cell lines (Figure 47B, 24 h vs 48 h, $p>0.05$ for cell lines). The observable decrease at 48h can again be attributed to glutamine deficiency resulting in decreased glutamate labeling as discussed above.

Glucose and glutamine can also contribute to the *de novo* synthesis of fatty acids via conversion to acetyl-CoA. However, as the mean isotopic enrichment of palmitate (C16:0, 16 refers to the carbon number in the fatty acid, and 0 refers to the double bond number) shows in Figure 48, the whole HCT116 cell panel does not reach isotopic steady state in palmitate in the experimental time span no matter if U-^{13}C-glucose or U-^{13}C-glutamine tracing is performed. It has been reported that acetate also serves as a carbon source that provides acetyl-CoA for fatty acids synthesis [270]. Besides, cells will also continuously take up fatty acids from the microenvironment, in this case the cell culture medium. They may all influence the time required to reach isotopic steady state in fatty acids in cells.

Together, the data presented above point to difference between IDH mutant cells and the wild-type counterparts in terms of the contribution of glucose and glutamine to the *de novo* synthesis of amino acids, organic acids, fatty acids, as well as the endogenous antioxidant GSH.

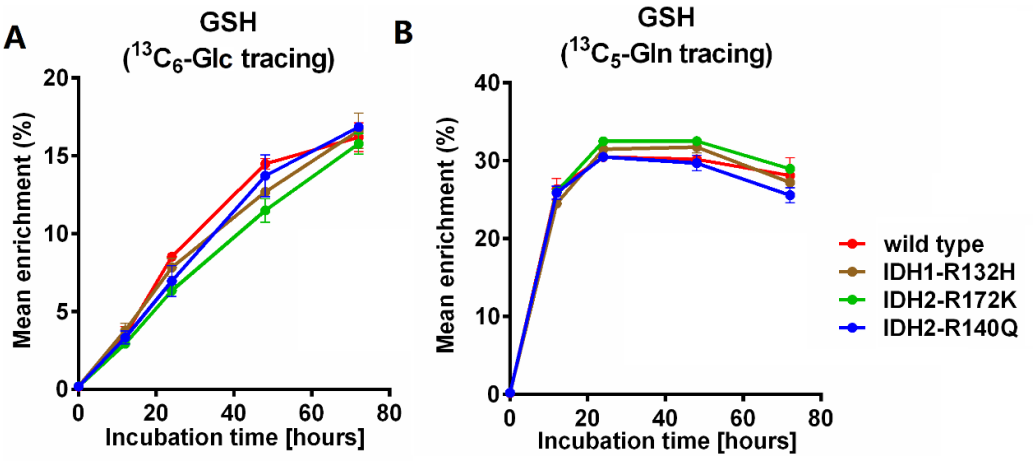

Figure 47. *Isotopic mean enrichment in glutathione at different incubation times (0h, 12h, 24h, 48h, 72h) from tracing experiments with U-^{13}C-glucose **(A)** and U-^{13}C-glutamine **(B)**, respectively, in HCT116 cells carrying wild-type or mutant IDH (IDH1-R132H, IDH2-R1172K, and IDH2-R140Q). Both IDH wild-type and mutant cells were cultivated in glucose/glutamine-free media supplemented with 2 g/L of U-^{13}C-glucose (11.1 mM) or 2 mM of U-^{13}C-glutamine, respectively, for different time periods. Data are shown as mean ± SD, n=6, two independent experiments. For statistics see Supplementary Table S11 in Chapter 11.*

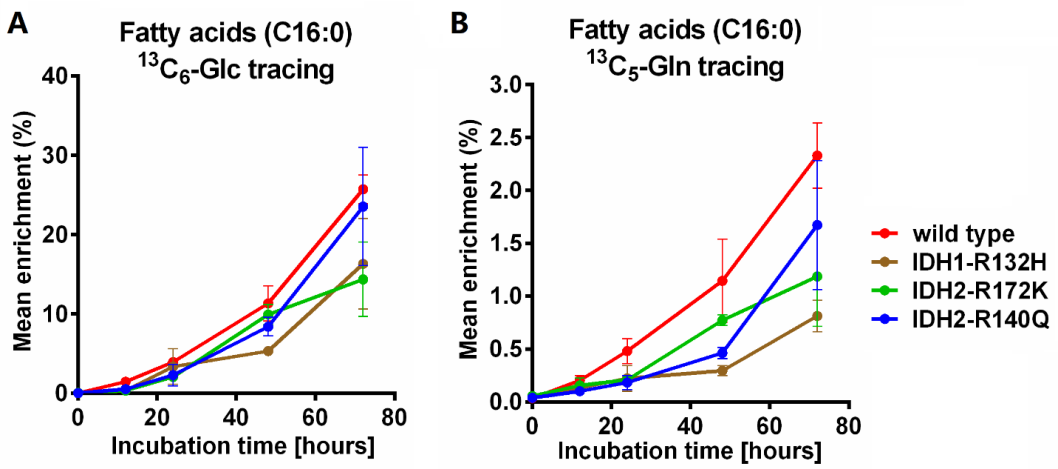

Figure 48. *Isotopic mean enrichment in palmitate (C16:0) at different incubation times (0 h, 12 h, 24 h, 48 h, 72 h) from tracing experiments with U-^{13}C-glucose **(A)** and U-^{13}C-glutamine **(B)**, respectively, in HCT116 cells carrying wild-type or mutant IDH (IDH1-R132H, IDH2-R1172K, and IDH2-R140Q). Both IDH wild-type and mutant cells were cultivated in glucose/glutamine-free media supplemented with 2 g/L of U-^{13}C-glucose (11.1 mM) or 2 mM of U-^{13}C-glutamine, respectively, for different time periods. Data are shown as mean ± SD, n=6, two independent experiments.*

9.2 Changes in amino acid and glutathione biosynthesis due to neomorphic mutations in *IDH1/2*

Alterations in intracellular amino acid levels in IDH mutant cells have been previously reported [63]. In this section, we characterized the changes in amino acids biosynthesis affected by IDH1/2 mutations. As discussed above, glutamine mainly contributes to the biosynthesis of glutamate, aspartate, and proline by providing the carbon backbone. It can also donate carbons to other amino acids such as ornithine and arginine, however, to a much less extent. Here, we only focus on glutamate, aspartate, and proline. Based on the isotopic steady state analysis performed above, the labeling data originating from U-^{13}C-glutamine tracing after 12h are employed in the following discussion. Figure 49A shows the mean isotopic enrichment of glutamate, aspartate, and proline from tracing with fully ^{13}C-labeled glutamine. IDH1-R132H and IDH2-R172K mutant cells exhibit a significant higher mean isotopic enrichment in glutamate and aspartate compared to the wild-type controls as well as IDH2-R140Q mutant cells (Figure 49A). Interestingly, HCT116 IDH2-R140Q cells act differently compared to cells harboring IDH1-R132H and IDH2-172K mutation regarding the ^{13}C incorporation from glutamine into related amino acids. The same observation was also reported by a previous study [257].

As shown in the isotopologue distribution profile of glutamate in Figure 49B, mutant IDH markedly enhances the conversion of glutamine to glutamate. The [M+5] isotopologue of glutamate is directly derived from U-^{13}C-glutamine. A significantly larger proportion of [M+5] glutamate was observed in IDH1-R132H and IDH2-R172K cells (Figure 49B), which is in agreement with a previous report that cells harboring an neomorphic IDH mutation tend to rely more on glutamine as the carbon source for glutamate biosynthesis via glutaminase (GLS) [8]. Figure 49C shows the labeling pattern of aspartate derived from U-^{13}C-glutamine. Glutamine contributes to the synthesis of aspartate mostly via oxaloacetate by transamination, *i.e.,* aspartate transaminase (AST), also known as glutamic-oxaloacetic transaminase (GOT) [271]. Thus, [M+4] aspartate can be generated from U-^{13}C-glutamine via oxaloacetate in one metabolic cycle. Figure 49C displays a significant higher fraction of [M+4] aspartate in IDH1-R132H and IDH2-R172K cells compared to wild type and IDH2-R140Q cell. This may imply an increased glutamine

oxidative metabolism through TCA cycle in IDH1-R132H and IDH2-R172K mutant cells. On the other hand, [M+3] aspartate fraction can reflect the activity of glutamine reductive metabolism. Glutamine can transfer five labeled carbons to citrate ([M+5] citrate) via its reductive metabolism which can then be converted to oxaloacetate and therefore aspartate, generating [M+3] aspartate. The significantly lower fraction of [M+3] aspartate observed in IDH mutant cell, especially in the IDH1-R132H mutant cell clone, reflects impaired glutamine reductive metabolism (Figure 49C).

Mutant IDH1 has been reported to enhance the production of glutamine-derived proline through pyrroline-5-carboxylate reductase 1 to maintain redox homeostasis in gliomas [272]. Proline is synthesized from glutamate via pyrroline-5-carboxylate synthase (P5C synthase) and pyrroline-5-carboxylate reductase (P5C reductase) [273]. Glutamine-derived glutamate is firstly converted to P5C by P5C synthase. This step requires ATP and NADPH. P5C is then converted to proline by P5C reductase, consuming NADH or NADPH in mitochondria or cytosol, respectively [274]. Increased expression of pyrroline-5-carboxylate reductase 1 was found in IDH1-mutant gliomas [272]. Indeed, in this study, a significant higher peak area ratio of [M+5] proline to [M+5] glutamate was observed in all IDH mutant cells, especially IDH1-R132H mutant cells, compared to wild type (Figure 49D, for statistics see Supplementary Table S12 in Chapter 11). This may reflect an increased expression or enhanced activity of the enzymes involved in the conversion of glutamate to proline in IDH mutant cells. However, differences in isotopic mean enrichment of proline between HCT116 cell lines are not statistically significant (Figure 49A, ANOVA, $p=0.1550$).

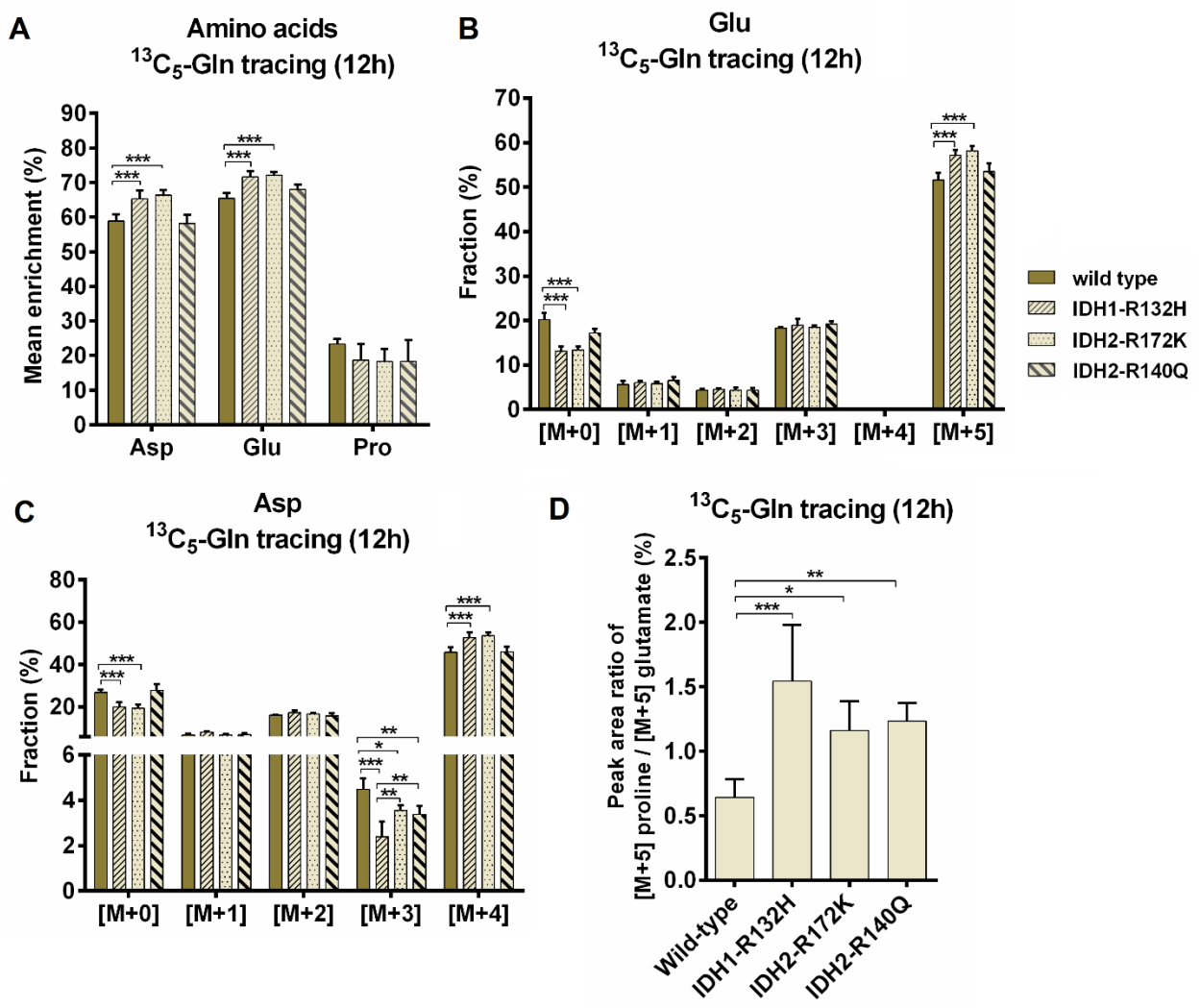

Figure 49. *Amino acid labeling patterns derived from U-^{13}C-glutamine in the HCT116 cell panel.* ***(A)*** *Isotopic mean enrichment in Glu, Asp, and Pro and isotopologue fractions of glutamate* ***(B)*** *and aspartate* ***(C)*** *from U-^{13}C-glutamine tracing at 12 hours.* ***(D)*** *peak area ratio of [M+5] proline to [M+5] glutamate in HCT116 cell panel after 12h incubation with U-^{13}C-glutamine. Data are shown as mean + SD, n=6, two independent experiments. * p< 0.05, ** p< 0.01, *** p< 0.001, for statistics see Supplementary Table S12 in Chapter 11.*

As discussed in section 9.1, amino acids in IDH wild-type cells reached isotopic steady state at 48 h in U-^{13}C-glucose tracing. Labeling data originating from U-^{13}C-glucose tracing at 48h are employed in the following discussion. In contrast to U-^{13}C-glutamine tracing, wild-type cells fed with U-^{13}C-glucose exhibit higher isotopic mean enrichment in glutamate and aspartate compared to IDH1-R132H and IDH2-R172K mutant cells as

shown in Figure 50A (for statistics see Supplementary Table S12 in Chapter 11). However, differences are not significant between wild type and IDH2-R140Q cells (p=0.8803 for glutamate, p=0.0517 for aspartate). Glutamate can be generated from glucose through pyruvate metabolism in mitochondria catabolized either by pyruvate dehydrogenase (PDH) or by pyruvate carboxylase (PC) [275]. Those two pathways will generate different labeling patterns of glutamate. Via PDH, pyruvate is metabolized into acetyl-CoA, transferring two glucose-derived carbons to glutamate ([M+2]) while PC catalyzes the conversion of pyruvate to oxaloacetate, through which three glucose-derived carbons will be transferred into glutamate ([M+3]). Figure 50B shows the labeling pattern of glutamate from the incorporation of labeled glucose. Both PDH- and PC-catalyzed pyruvate metabolism are active in HCT116 cells as indicated by the observation of [M+2] and [M+3] glutamate in Figure 50B. However, significant lower [M+2] and [M+3] glutamate fractions were observed in IDH1-R132H and IDH2-R172K mutant cells compared to wild-type controls and IDH2-R140Q mutant cells, suggesting a possibly decreased activity of both PDH and PC in IDH1-R132H and IDH2-R172K mutant cells. Interestingly, IDH2-R172K mutant cells exhibit the lowest proportion of [M+2] and [M+3] glutamate among all cell lines (Figure 50B). Given that mutant IDH2 localizes to mitochondria, the large amounts of local D-2-HG produced by IDH2-R172K cells may have the highest impact on PDH and PC activities. Even though IDH2-R140Q also localizes to mitochondria, it was reported to produce less 2-HG than IDH2-R172K [257]. A similar labeling pattern was also observed for aspartate in IDH1-R132H and IDH2-R172K mutant cells (Figure 50C).

Besides, as shown in Figure 50A, significant lower mean isotopic enrichment in proline from the ^{13}C incorporation of glucose was observed in IDH1-R132H and IDH2-172K mutant cells. This is could be due to the lower conversion of glucose into glutamate, however, the imbalance of reducing power induced by the IDH mutations may also play a role since the biosynthesis of proline from glutamate needs reducing equivalent. It should be noted that the observation here is in contrast to data reported by Hollinshead et al [272] who showed a higher ^{13}C incorporation into proline from $^{13}C_6$-glucose with glioma cell models. Cell lines as well as circumstances employed in the study may also have impact on cell metabolic characteristics.

Another important glucose-derived amino acid is alanine. When cells were incubated with labeled glucose for 48h, ~80% of the carbon in alanine was ^{13}C labeled in wild-type cells (Figure 50A). Significant lower mean enrichment was observed for the IDH mutant cells. Alanine is synthesized from glucose via pyruvate catalyzed by alanine aminotranferases (ALT). Three labeled carbons derived from glucose will be transferred into alanine. As shown in Figure 50D, IDH1-R132H and IDH2-172K mutant cells exhibit a significant lower fraction of [M+3] alanine compared to the wild-type counterparts. Either lower alanine synthesis or more pyruvate is shuttled in TCA or lactate in IDH1-R132H and IDH2-R172K mutant cells. We then analyzed pyruvate and lactate labeling from $^{13}C_6$-glucose tracing at 48h. IDH1-R132H and IDH2-R172K mutant cells exhibit a significant lower isotopic mean enrichment in pyruvate compared to wild-type cells. However, the lower carbon incorporation of glucose into lactate was only observed in IDH1 mutant cells (Figure 51A). The reduced glycolytic activity in HCT116 IDH1-R132H mutant cells has been reported previously by determining the extracellular acidification rate (ECAR) [263]. ECAR is linearly related to lactate production. Here, we analyzed the glucose uptake and lactate release of each HCT116 cell line to reflect the glycolytic activity. Through glycolysis, one molecule of glucose is converted into two molecules of lactate. As shown in Figure 51B, a lower ratio of lactate release to glucose uptake was observed in IDH1 mutant cells, however, not in IDH2 mutant cells, implying a reduced glycolic activity in IDH1 mutant cells.

Another two important non-essential amino acids derived from glucose are serine and glycine. Serine metabolism plays an essential role cancer cell growth by supplying precursors for protein and nucleic acids synthesis, as well as fueling one-carbon metabolism by providing carbon unit [276]. In cells, glucose serves as the major carbon source for serine biosynthesis via the glycolytic intermediate 3-phosphoglycerate [277], which is oxidized by phosphoglycerate dehydrogenase (PHGDH) and NAD+ to 3-phosphohydroxypyruvate and NADH. 3-phosphohydroxypyruvate is further metabolized by phosphoserine aminotransferase (PSAT1) to phosphoserine and finally by phosphoserine phosphatase (PSPH) to serine [278]. Thus, serine biosynthesis is linked to glycolysis pathway. Isotopic mean enrichment in serine is shown in Figure 50A revealing that IDH1-R132H mutation markedly decreases serine biosynthesis from

glucose, possibly due to a reduced glycolysis activity. Glycine is synthesized from serine. However, a significant higher isotopic mean enrichment in glycine was observed in IDH2-R140Q cells (Figure 50A), while no significant differences were observed for the other mutant cell lines. After cells were incubated with labeled glucose for 48h, 30%~40% of serine were carbon labeled in HCT116 cells (Figure 50A). Extracellular serine in the cell culture medium may replenish serine in cells. Furthermore, protein breakdown is one of the intracellular serine sources [279] and is reported to account for ~20% of the intracellular serine pool [280].

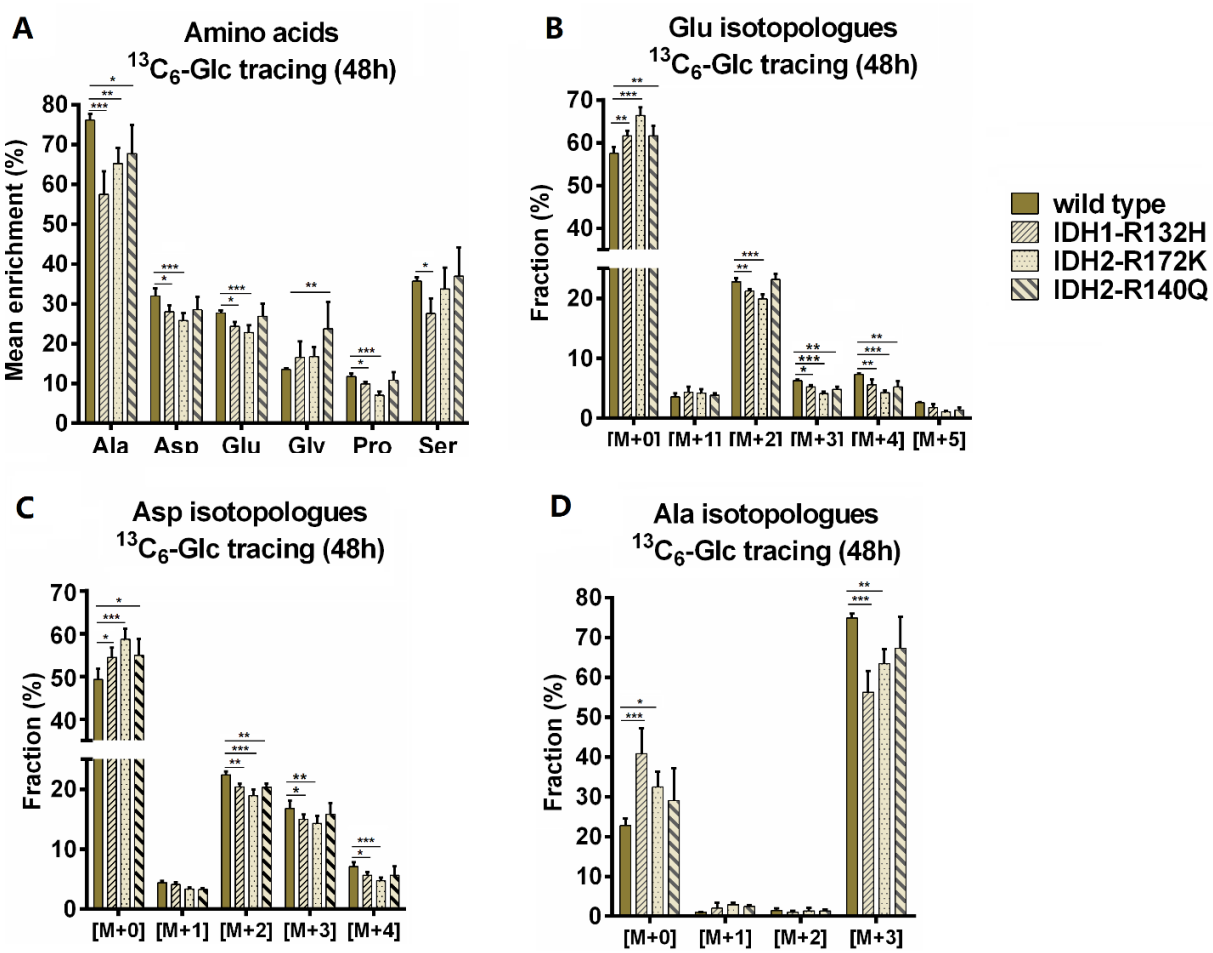

Figure 50. *Amino acids isotope labeling patterns derived from tracer experiments with U-^{13}C-glucose in the HCT116 cell panel.* ***(A)*** *Isotopic mean enrichment in various amino acids.* ***(B-D)*** *show isotopologue fractions for glutamate, aspartate, and alanine. Cells were cultured with U-^{13}C-glucose for 48h (n=6, two independent experiments). Data are shown as mean + SD. * p< 0.05, ** p< 0.01, *** p< 0.001, for statistics see Supplementary Table S12 in Chapter 11.*

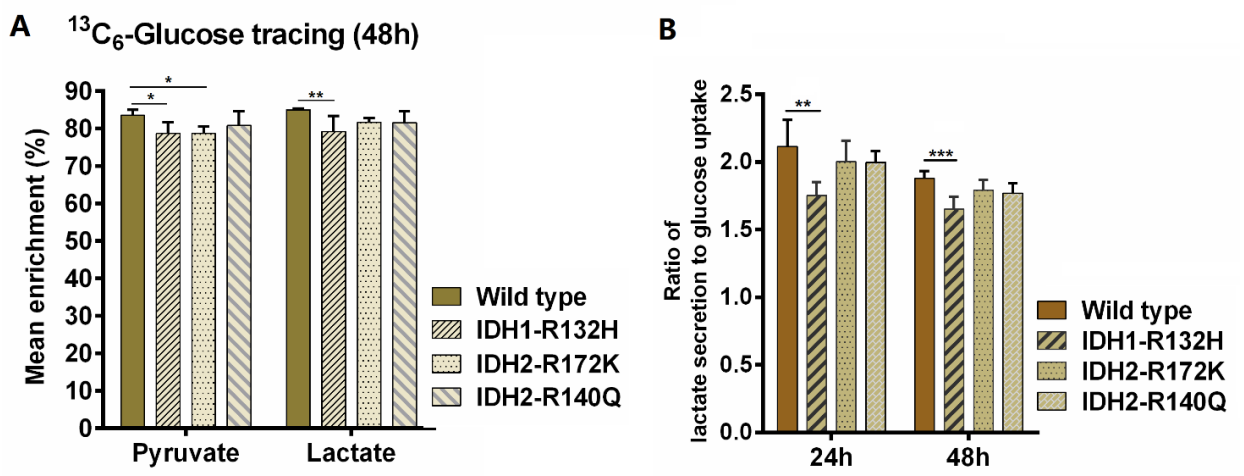

Figure 51. (A) *Isotopic mean enrichment of pyruvate and lactate from U-^{13}C-glucose tracing in HCT116 cell panel cultured for 48 h in the presence of labeled nutrient (n=6, two independent experiments).* ***(B)*** *Ratio of lactate secretion to glucose uptake in HCT116 cells during 24 h / 48 h cell culture (n=6, two independent experiments). The conversion of glucose to lactate reflects the activity of the glycolysis pathway in cells. Lactate and glucose concentrations in cell culture medium were analyzed by NMR. Lactate secretion and glucose uptake were determined by calculating the differences to the blank medium. ANOVA for pyruvate labeling p = 0.0302, wt vs IDH1-R132H p = 0.0150, wt vs IDH2-R172K p = 0.0145; ANOVA for lactate labeling p = 0.0176, wt vs IDH1-132H p = 0.0038; ANOVA for the ratio of lactate secretion to glucose uptake after 24 h cell culture p = 0.0340, wt vs IDH1-R132H p=0,0059; for the ratio after 48 h cell culture ANOVA p = 0.0031, wt vs IDH1-R132H p=0.0003.*

Glutamate, cysteine, and glycine are three substrates for GSH biosynthesis. Thus, glutathione synthesis is also highly related to amino acids metabolism. Figure 52 shows the mean isotopic enrichment of GSH from the ^{13}C incorporation of labeled glucose and glutamine. Mean isotopic enrichment is shown for the intact GSH molecule and the GlyCys and CysGlu fragments (see Chapter 8). IDH1-R132H and IDH2-R172K mutant cells exhibit significant lower carbon incorporation from labeled glucose and significant higher carbon incorporation from labeled glutamine in GSH compared to the wild-type cells. This is consistent with the observation in Chapter 8.

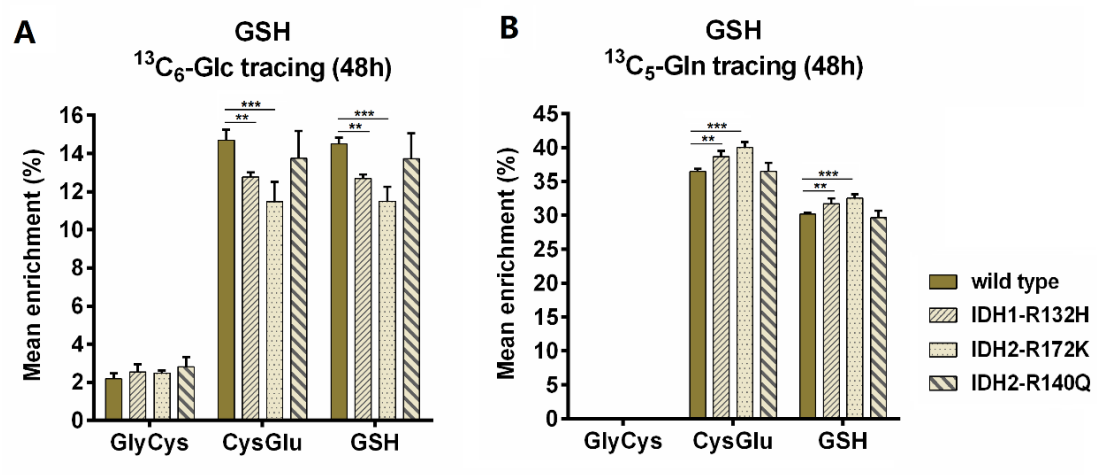

Figure 52. *Mean isotopic enrichment of GSH in HCT116 cell panel when cells were incubated with U-^{13}C-glucose or U-^{13}C-glutamine for 48h, respectively. Data are shown as mean + SD, n=6, two independent experiments, * p< 0.05, ** p< 0.01, *** p< 0.001, for statistics see Supplementary Table S13 in Chapter 11.*

To further investigate the differences in GSH synthesis caused by IDH1/2 mutation, we analyzed the labeling patterns of GSH, as well as its residues GlyCys and CysGlu. Isotopologue fraction analysis of GSH is shown in Figure 53 revealing that glutamine contributes to GSH biosynthesis mainly via glutamate in all cell lines since no detectable GlyCys labeling was observed when cells were incubated with labeled glutamine. On the other hand, the incorporation of glucose into GSH can occur in both GlyCys and CysGlu residues (Figure 54). Only [M+2] labeling was observed in GlyCys residue, indicating that glucose barely contributes to GSH synthesis via its conversion into cysteine (Figure 54). Even cysteine can also be synthesized *de novo* from serine and methionine through transsulfuration pathway, the majority of intracellular cysteine depends on the uptake from the extracellular environment [281]. Besides, the incorporation of glucose into GSH through glycine in wild-type cells is significantly lower than that in IDH mutant cells (Figure 54) which is consistent with the glycine labeling shown in Figure 50A. In addition, the incorporation of glucose-derived carbons into GSH via glutamate is significantly decreased in IDH mutant cells. In contrast, glutamine contributes more carbons to GSH biosynthesis through glutamate in IDH1-R132H and IDH2-R172K mutant cells compared to the wild-type controls as indicated by the higher isotopic enrichment in CysGlu residue

shown in Figure 53. Overall, IDH mutation drives the cells to rely more on glutamine to provide carbons for GSH biosynthesis. This is very likely due to the changes of glutamate synthesis caused by IDH1/2 mutation.

Unfortunately, direct comparison of contributions of glucose and glutamine to GSH biosynthesis is not possible since cells, especially IDH mutant cells, do not reach their GSH isotopic steady state after 48h incubation with $^{13}C_6$-glucose. However, if we look at U-^{13}C-glutamine tracing only at 48h when all cell lines reach their GSH isotopic steady state (Figure 47B), 20% ~ 25% of [M+0] GSH fraction was observed in HCT116 cell panel (Figure 53), indicating that ~75% of GSH carbons are derived from glutamine. This might also be an underestimation due to the presence of unlabeled substrates in cell culture medium. Together, glutamine may play substantially import role in sustaining intracellular redox balance by influencing the *de novo* synthesis of the endogenous anti-oxidant GSH, especially for cells harboring an IDH mutation.

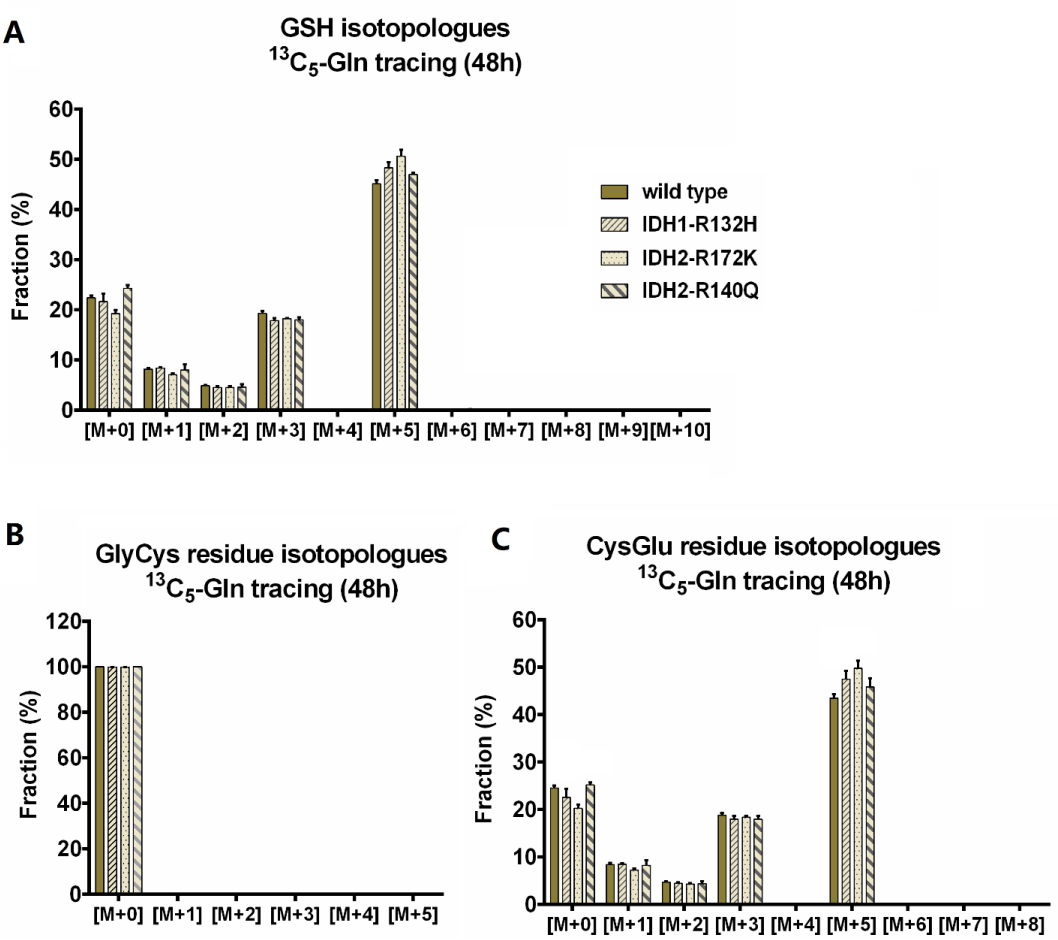

Figure 53. *Isotope labeling distribution of GSH, GlyCys, and CysGlu originating from U-^{13}C-glutamine tracing at 48h. Data are shown as mean + SD, n=6, two independent experiments. * p< 0.05, ** p< 0.01, *** p< 0.001, for statistics see Supplementary Table S13 in Chapter 11.*

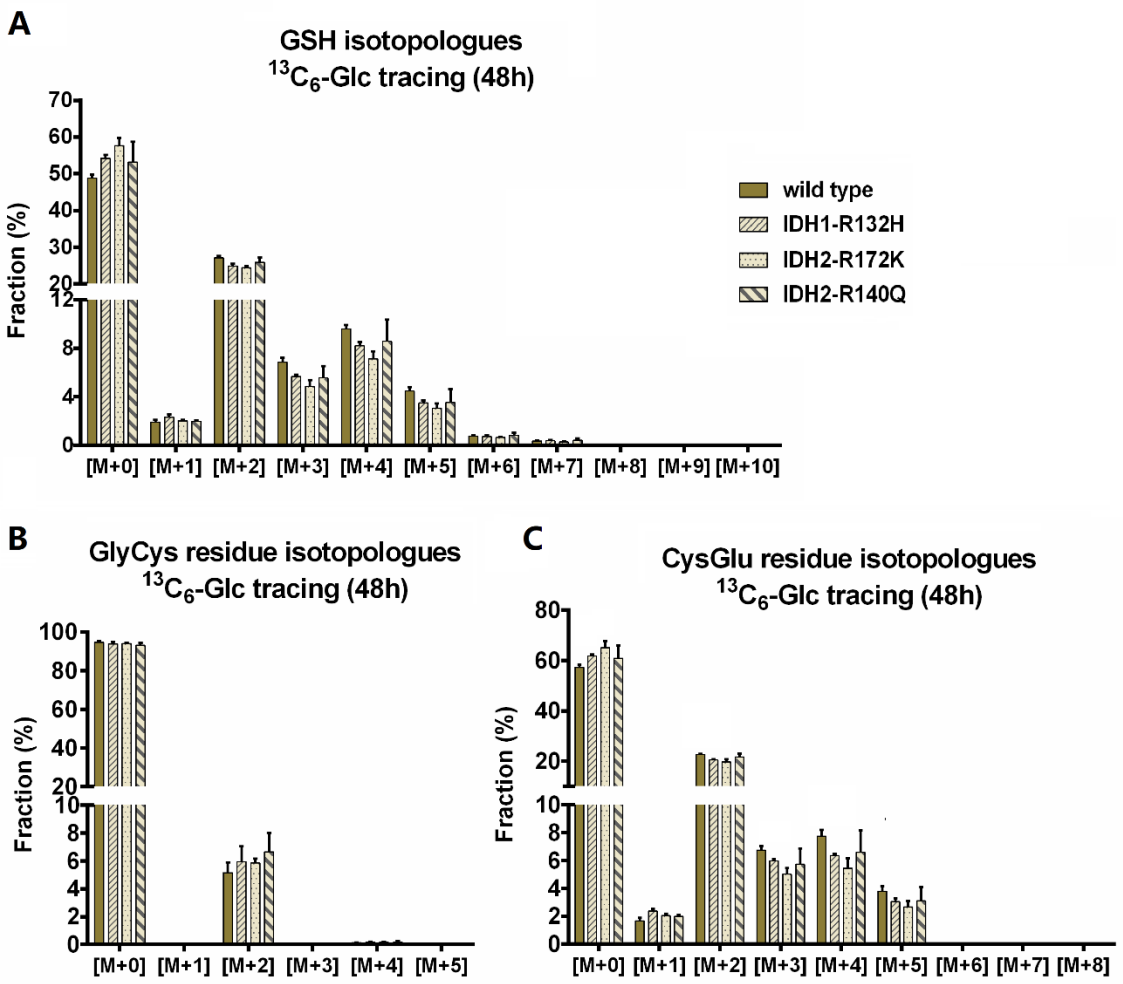

Figure 54. *Isotope labeling distribution of GSH, GlyCys, and CysGlu originating from U-^{13}C-glucose tracing at 48h. Data are shown as mean + SD, n=6, two independent experiments. * p< 0.05, ** p< 0.01, *** p< 0.001, for statistics see Supplementary Table S13 in Chapter 11.*

9.3 Glutamine oxidative metabolism is increased in IDH1/2 mutant cells

Acting as an important energy fuel, glutamine can either undergo complete oxidative metabolism via the TCA cycle, *i.e.*, glutaminolysis, or reductive metabolism (Figure 55).

Using U-^{13}C-glutamine tracing, different labeling patterns of citrate are observed. Through oxidative glutamine metabolism, [M+4] labeled citrate will be generated due to the loss of CO_2 (Figure 55). Glutamine, on the other hand, can directly supply carbons for citrate production via reduction carboxylation catalyzed by IDH, generating [M+5] labeled citrate. As discussed above, the significant lower fraction of [M+3] aspartate observed in IDH1-R132H mutant cells (Figure 49C) may reflect impaired glutamine reductive metabolism. Here, the [M+5] citrate fraction in IDH1-R132H mutant cells is also significantly lower than in wild-type cells (Figure 56A), indicating that IDH1-R132H mutant cells were limited in their ability to generate citrate via reductive carboxylation of glutamine-derived α-KG. Several studies have reported a shift from glutamine oxidation to reductive metabolism in cells cultured under hypoxic conditions or when cells have defective mitochondria in order to maintain citrate levels [282, 283]. However, under normal conditions reductive carboxylation is unlikely to be the major glutamine metabolism route in all cell lines as indicated by the fairly low fraction of [M+5] citrate (~2%) (Figure 56A).

A significant increase in [M+4] citrate was observed in IDH1-R132H and IDH2-R172K cells compared to wild-type and IDH2-R140Q cells, indicating an increased oxidative metabolism of glutamine in those cells (Figure 56A). This is also supported by the higher [M+4] labeling fraction of other TCA cycle intermediates, *i.e.*, succinate, fumarate, and malate, in IDH1-R132H and IDH2-R172K cells (Figure 56B). An overall increase in isotopic mean enrichment in TCA cycle intermediates from glutamine tracing was also observed in IDH1-R132H and IDH2-R172K mutant cells compared to the wild-type cells (Figure 57). It is concluded that mutant IDH increases glutamine oxidative metabolism to fuel the TCA cycle.

As already discussed, glutamine is one of the cellular sources of α-KG. α-KG is further converted to D-2-HG by mutant IDH [47]. A significant higher isotopic mean enrichment in 2-HG was observed in IDH1-R132H and IDH2-R172K mutant cells compared to wild-type cell line as well as IDH2-R140Q mutant cells (Figure 57). It was previously reported that IDH1-R132H and IDH2-172K mutant cells produce higher amounts of 2-HG than IDH2-R140Q mutant cells [257]. The higher consumption of α-KG for the generation of 2-HG may drive more glutamine flux into α-KG. Glucose can also contribute to 2-HG

production (Figure 58). However, ^{13}C incorporation from glucose into 2-HG did not differ significantly between cell lines. This is consistent with previous reports [66, 284]. Besides, the decrease in isotopic mean enrichment in most of the TCA cycle intermediates observed for IDH1-R132H and IDH2-R172K cells when fed with labeled glucose (Figure 58), points to an impact of IDH mutation on the flux of glucose into TCA cycle. However, the decreases are not statistically significant in our data (ANOVA, $p>0.05$ for each metabolite). Glucose-derived carbons are more likely shunted to other metabolic routes, e.g., pentose phosphate pathway, which needs further investigation.

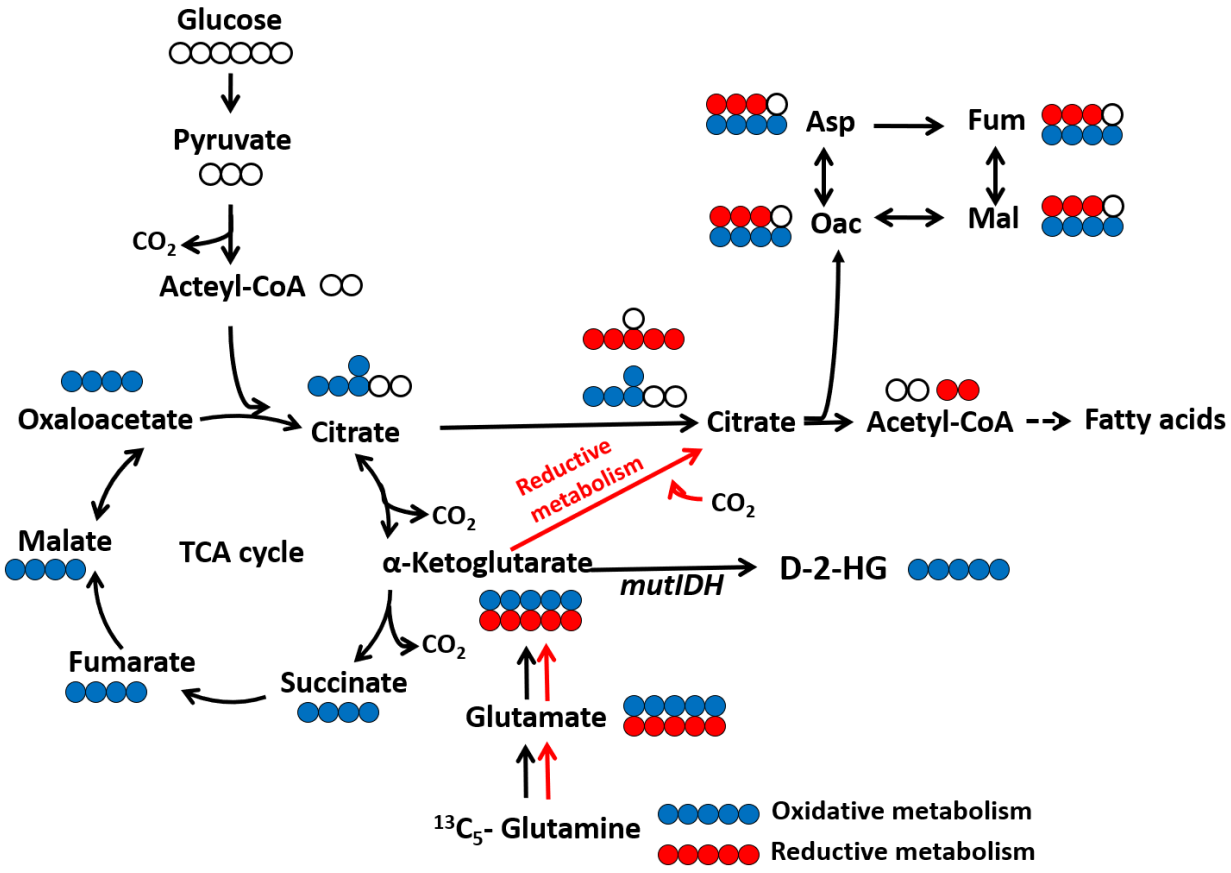

Figure 55. *Scheme depicting the expected isotopologues of intracellular metabolites originated from ^{13}C-glutamine tracing through oxidative or reductive metabolism. Circles represents the number of carbons in each metabolite with white circles for ^{12}C carbon, blue circles for ^{13}C carbon derived from glutamine through oxidative metabolism and red circles for ^{13}C carbons derived from glutamine through reductive metabolism.*

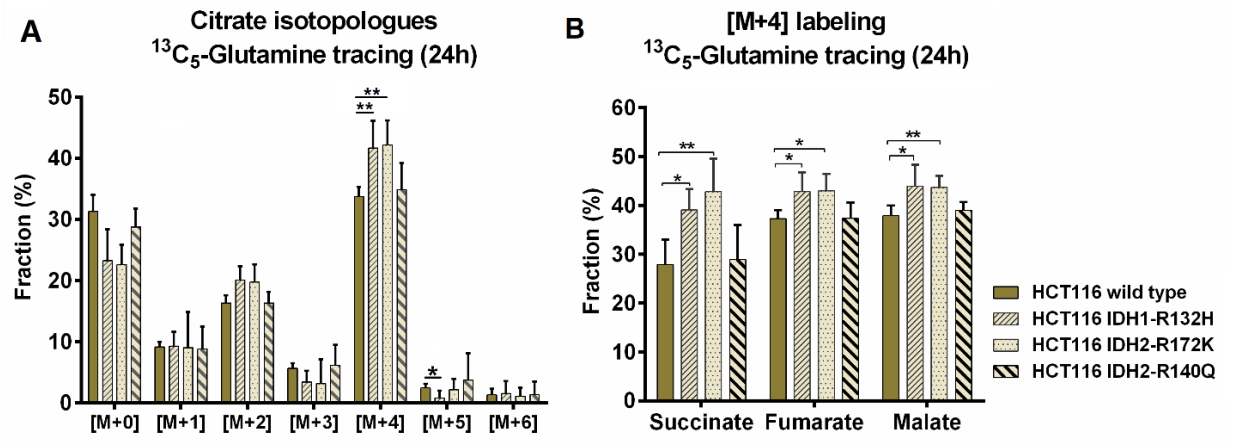

Figure 56. *Isotopologue fractions of citrate and [M+4] fraction of succinate, fumarate, and malate from U-^{13}C-glutamine tracing for 24 h. Significant higher fractions of [M+4] labeling in citrate, succinate, fumarate, and malate were observed in IDH1-R132H and IDH2-R172K cells compared to wild type cells, indicating increased glutamine oxidative metabolism in IDH1-R132H and IDH2-R172K cells. Data are shown as mean + SD, n=5-6, two independent experiments. * p< 0.05, ** p< 0.01, *** p< 0.001, for statistics see Supplementary Table S14 in Chapter 11.*

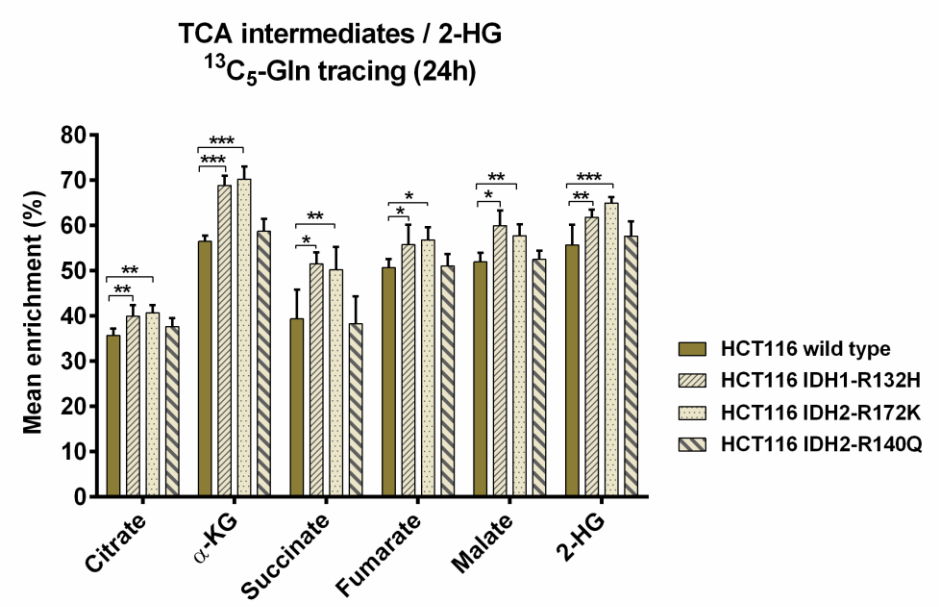

Figure 57. *Isotopic mean enrichment in TCA cycle intermediates and 2-HG from U-^{13}C-glutamine tracing for 24 h. Significant higher isotopic mean enrichments in TCA cycle intermediates and 2-HG were observed in IDH1-R132H and IDH2-R172K cells compared to wild type cells. Data are shown as mean + SD, n=5-6, two independent experiments. * p< 0.05, ** p< 0.01, *** p< 0.001, for statistics see Supplementary Table S14 in Chapter 11.*

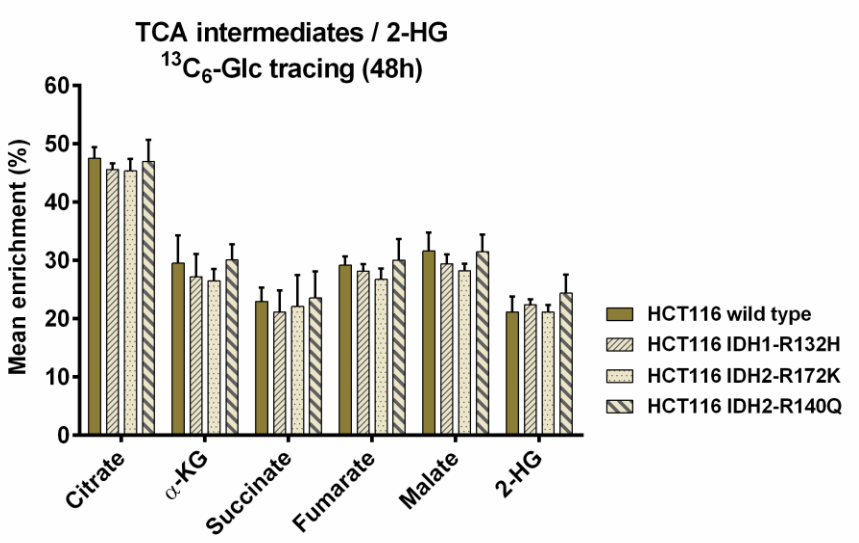

***Figure 58**. Mean isotopic enrichment in TCA cycle intermediates and D-2-HG from U-^{13}C-glucose tracing for 48h. Difference between cell lines are not statistically significant (ANOVA, p>0.05 for each metabolite). Data are shown as mean + SD, n=5-6, two independent experiments.*

9.4 Decreased fatty acids synthesis in mutant IDH cells

To better assess the impact of IDH mutations on the *de novo* biosynthesis of fatty acids, we analyze the labeling of palmitate generated from uniformly ^{13}C-labeled glucose and glutamine, respectively. Acetyl-CoA is the precursor used to synthesize fatty acids through acetyl-CoA carboxylase and fatty acid synthase, yielding palmitate [285]. Figure 59 shows the isotopologue distribution of palmitate in each cell line. The unlabeled [M+0] palmitate attributes to the uptake of serum-derived fatty acids and the *de novo* synthesis of fatty acids from unlabeled substrates. Partially labeled forms including [M+2], [M+4], [M+6], [M+8], [M+10], [M+12], and [M+14] arise from incomplete acetyl-CoA labeling. Together with the fully labeled form [M+16], they are sufficient to determine the fractional labeling of cytosolic acetyl-CoA. The significant different labeled fractions, thus labeled acetyl-CoA, between IDH wild-type and mutant cells indicate the impact of IDH1/2 mutations on the *de novo* synthesis of fatty acids in HCT116 cells (Figure 59, for statistics see Supplementary Table S15 in Chapter 11). The carbon incorporation into fatty acids from both labeled glucose and glutamine are significantly decreased in all IDH mutant cells compared to the wild-type cells (Figure 59 and 60A-B). In addition, compared to

glutamine, glucose contributes more carbons to the *de novo* synthesis of fatty acids as indicated in Figure 60A-B. The mean isotopic enrichment of palmitate in each cell line from labeled glucose is about ten times higher than that from labeled glutamine. Cytosolic acetyl-CoA is mainly produced from glucose-derived citrate under normal conditions and the C2 unit of acetyl-CoA is from pyruvate (Figure 55). Glutamine possibly provides a small amount of carbons to generate acetyl-CoA via citrate after multiple rounds of TCA cycle. When cells are in hypoxia, glutamine has been shown to contribute more to the generation of cytosolic acetyl-CoA for fatty acids synthesis, as under this condition pyruvate dehydrogenase is less active [283]. However, mutant IDH decreases the cells' ability to convert glutamine-derived carbon to citrate, which is required for acetyl-CoA production [59]. This is also consistent with the findings of lower [M+5] citrate and [M+3] aspartate fractions, which indicates reduced glutamine reductive metabolism as discussed above.

IDH1-R132H mutant cells exhibit the lowest isotopic mean enrichment in palmitate in both glucose and glutamine tracing (~two-fold lower mean isotopic enrichment from U-^{13}C-glucose and ~ four-fold lower of mean isotopic enrichment from U-^{13}C-glutamine compared to wild-type cells) (Figure 60A-B). The *de novo* synthesis of fatty acids occurs in the cytosol and requires large amounts of NADPH. The consumption of cytosolic NADPH by mutant IDH1 for the production of D-2-HG may affect NADPH-dependent fatty acid synthesis.

Recently, using isotope tracer analysis, reductive glutamine metabolism catalyzed by IDH has been found to provide considerable fractions of the acetyl-CoA pool in cancer cells, particularly in those with defective mitochondria or grown under hypoxia condition [286]. However, mutant IDH1 compromises the enzyme activity in this metabolic route [287]. Indeed, as discussed above, the low fractions of [M+5] citrate and [M+3] aspartate observed in IDH1 mutant cells indicate decreased glutamine reductive metabolism, therefore, the lower fraction of cytosolic acetyl-CoA from that pathway. More recently, a study revealed that cells switch to increased uptake rather than *de novo* synthesis of fatty acids to meet the large demands of acetyl-CoA under hypoxia condition [288]. It was found that under hypoxia cancer cells increase fatty acids uptake by inducing the

expression of fatty acid binding proteins, namely FABP3 and FABP7, in a HIF-1α-dependent manner [289]. IDH1 mutant cells have been reported to exhibit increased dependence on the uptake of exogenous lipids for cell growth compared to cells expressing wild-type enzyme [290]. We therefore analyzed the uptake of fatty acids from the cell culture medium for each cell line. The uptake data were normalized to the area under the corresponding cell growth curve according to a previous report [291]. The result is shown in Figure 60C. A significant higher uptake of fatty acids was observed in IDH1-R132H mutant cells compared to other cell lines. This may in turn explain the lower isotopic labeling observed in IDH1 mutant cells (Figure 60A-B).

In addition to glucose and glutamine, acetate can also contribute to the production of intracellular acetyl-CoA. Comerford *et al.* reported that acetate provides carbons for acetyl-CoA synthesis in tumors via acetyl-CoA synthetase, ACSS2 [292]. Using ^{13}C-tracer analysis acetate was found to contribute substantially to acetyl-CoA generation in hypoxic cancer cells [293]. Increased uptake of acetate was reported in IDH1-R132H mutant cells in a glioblastoma U251 cell model in both *in vitro* and *in vivo* experiments [6]. To further investigate the impact of IDH1/2 mutations on fatty acids biosynthesis, more extensive and systematic studies need to be carried out.

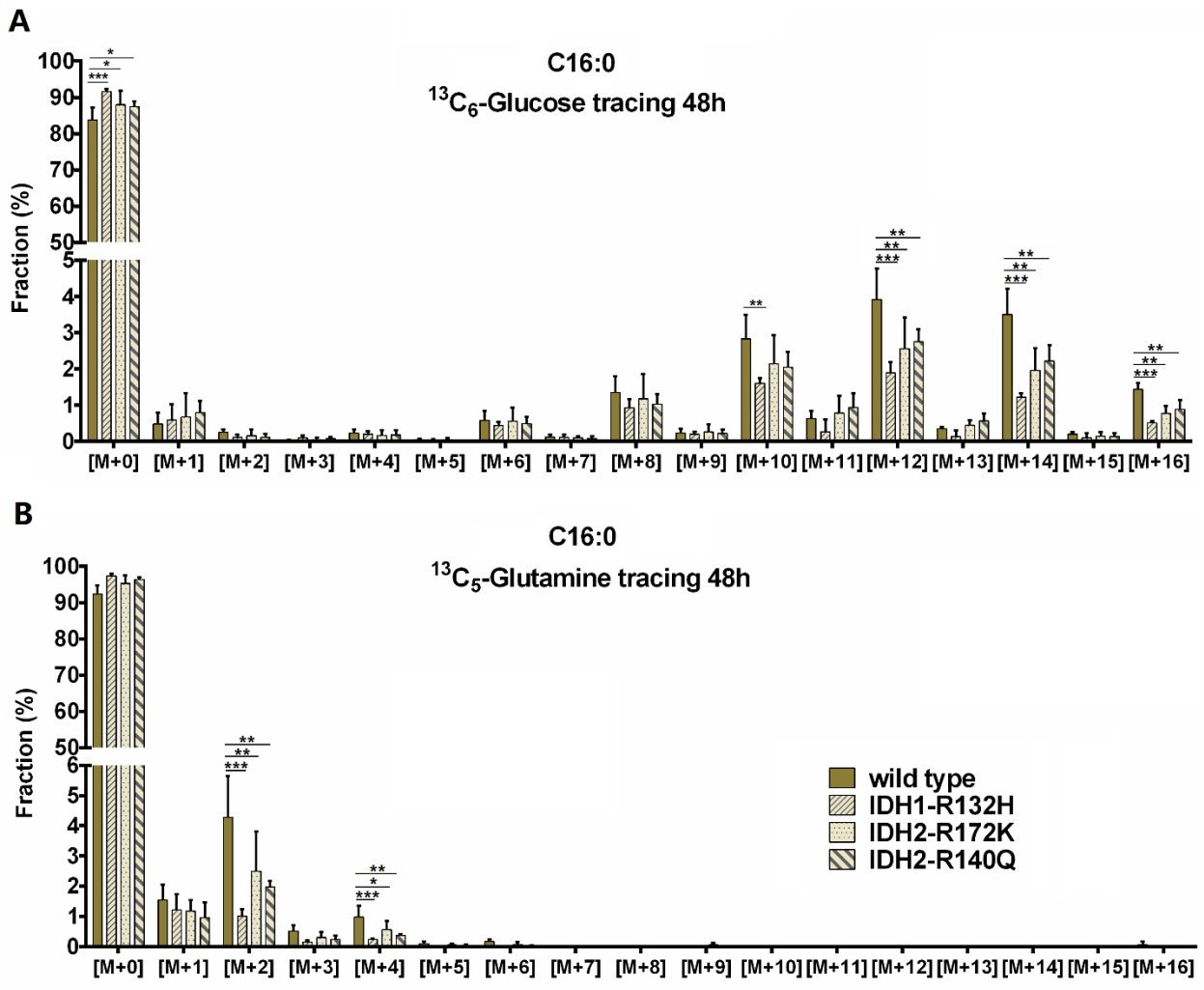

Figure 59. *Isotopologue distribution of palmitate from $^{13}C_6$-glucose **(A)** and $^{13}C_5$-glutamine **(B)** tracing in the HCT116 cell panel. Lower [M+10], [M+12], [M+14], and [M+16] fractions were observed in IDH mutant cells compared to wild-type in $^{13}C_6$-glucose tracing experiments (A), while lower [M+2] and [M+4] fractions can be seen in IDH mutant cells with $^{13}C_5$-glutamine tracing. Data are shown as mean + SD, n=6, two independent experiments. * p< 0.05, ** p< 0.01, *** p< 0.001, for statistics see Supplementary Table S15 in Chapter 11.*

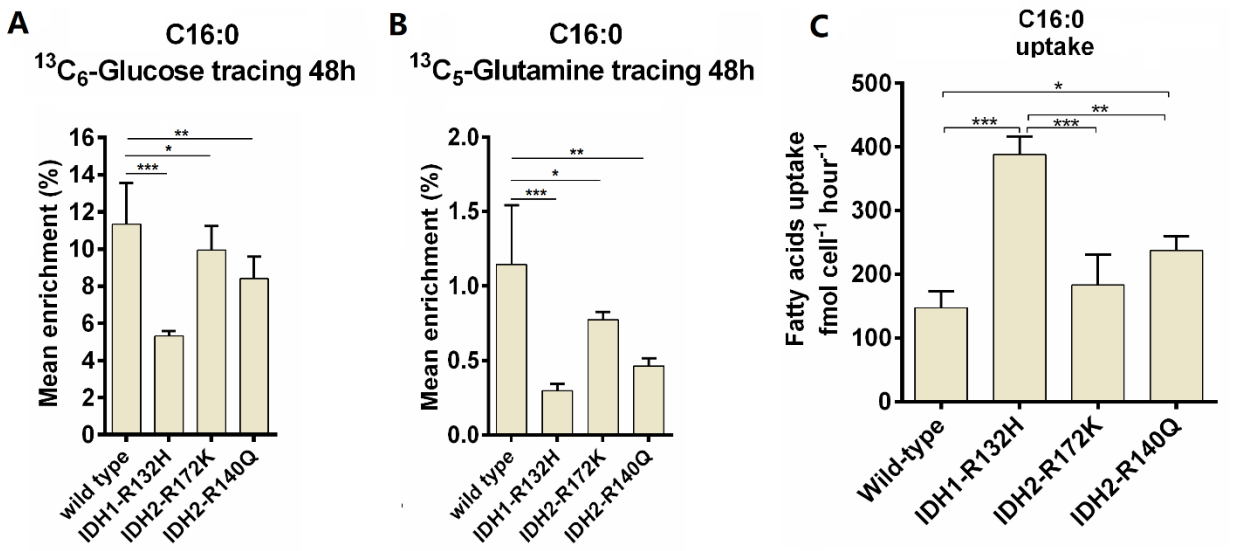

Figure 60. *Mean isotopic enrichment of palmitate from $^{13}C_6$-glucose **(A)** and $^{13}C_5$-glutamine **(B)** tracing and the unlabeled palmitate uptake from the culture medium **(C)** in the HCT116 cell panel. Significant differences in mean enrichment from both ^{13}C-glucose and ^{13}C-glutamine tracing between IDH mutant and wild-type cells were observed. Data are shown as mean + SD, n=6, two independent experiments. * p< 0.05, ** p< 0.01, *** p< 0.001, for statistics see Supplementary Table S15 in Chapter 11.*

10 References

[1] G. Wu, Y.Z. Fang, S. Yang, J.R. Lupton, N.D. Turner, Glutathione Metabolism and Its Implications for Health, J Nutr, 134 (2004) 489-492.

[2] D. Giustarini, F. Galvagni, A. Tesei, A. Farolfi, M. Zanoni, S. Pignatta, A. Milzani, I.M. Marone, I. Dalle-Donne, R. Nassini, R. Rossi, Glutathione, glutathione disulfide, and S-glutathionylated proteins in cell cultures, Free Radic Biol Med, 89 (2015) 972-981.

[3] X. Sun, P. Heinrich, R.S. Berger, P.J. Oefner, K. Dettmer, Quantification and (13)C-Tracer analysis of total reduced glutathione by HPLC-QTOFMS/MS, Anal Chim Acta, 8 (2019) 127-137.

[4] H. Yan, D.W. Parsons, G. Jin, R. McLendon, B.A. Rasheed, W. Yuan, I. Kos, I. Batinic-Haberle, S. Jones, G.J. Riggins, H. Friedman, A. Friedman, D. Reardon, J. Herndon, K.W. Kinzler, V.E. Velculescu, B. Vogelstein, D.D. Bigner, IDH1 and IDH2 mutations in gliomas, N Engl J Med, 360 (2009) 765-773.

[5] K. Lenting, M. Khurshed, T.H. Peeters, C. van den Heuvel, S.A.M. van Lith, T. de Bitter, W. Hendriks, P.N. Span, R.J. Molenaar, D. Botman, K. Verrijp, A. Heerschap, M. Ter Laan, B. Kusters, A. van Ewijk, M.A. Huynen, C.J.F. van Noorden, W.P.J. Leenders, Isocitrate dehydrogenase 1-mutated human gliomas depend on lactate and glutamate to alleviate metabolic stress, FASEB J, 33 (2019) 557-571.

[6] S. Koyasu, Y. Shimizu, A. Morinibu, T. Saga, Y. Nakamoto, K. Togashi, H. Harada, Increased (14)C-acetate accumulation in IDH-mutated human glioblastoma: implications for detecting IDH-mutated glioblastoma with (11)C-acetate PET imaging, J Neurooncol, 145 (2019) 441-447.

[7] T. Mesti, N. Bouchemal, C. Banissi, M.N. Triba, C. Marbeuf-Gueye, M. Cemazar, L.L. Moyec, A.F. Carpentier, P. Savarin, J. Ocvirk, Nuclear magnetic resonance metabolic fingerprint of bevacizumab in mutant IDH1 glioma cells, Radiol Oncol, 52 (2018) 392-398.

[8] S.K. McBrayer, J.R. Mayers, G.J. DiNatale, D.D. Shi, J. Khanal, A.A. Chakraborty, K.A. Sarosiek, K.J. Briggs, A.K. Robbins, T. Sewastianik, S.J. Shareef, B.A. Olenchock, S.J. Parker, K. Tateishi, J.B. Spinelli, M. Islam, M.C. Haigis, R.E. Looper, K.L. Ligon, B.E. Bernstein, R.D. Carrasco, D.P. Cahill, J.M. Asara, C.M. Metallo, N.H. Yennawar, M.G. Vander Heiden, W.G. Kaelin, Jr., Transaminase Inhibition by 2-Hydroxyglutarate Impairs Glutamate Biosynthesis and Redox Homeostasis in Glioma, Cell, 175 (2018) 101-116.

[9] A. Pastore, G. Federici, E. Bertini, F. Piemonte, Analysis of glutathione: implication in redox and detoxification, Clin Chim Acta, 333 (2003) 19-39.

[10] R. Franco, O.J. Schoneveld, A. Pappa, M.I. Panayiotidis, The central role of glutathione in the pathophysiology of human diseases, Arch Physiol Biochem, 113 (2007) 234-258.

[11] A. Bansal, M.C. Simon, Glutathione metabolism in cancer progression and treatment resistance, J Cell Biol, 217 (2018) 2291-2298.

[12] H. Gmunder, W. Droge, Differential effects of glutathione depletion on T cell subsets, Cell Immunol, 138 (1991) 229-237.

[13] D. Giustarini, I. Dalle-Donne, A. Milzani, P. Fanti, R. Rossi, Analysis of GSH and GSSG after derivatization with N-ethylmaleimide, Nat Protoc, 8 (2013) 1660-1669.

[14] F. Tietze, Enzymic method for quantitative determination of nanogram amounts of total and oxidized glutathione: applications to mammalian blood and other tissues, Anal Biochem, 27 (1969) 502-522.

[15] I. Rahman, A. Kode, S.K. Biswas, Assay for quantitative determination of glutathione and glutathione disulfide levels using enzymatic recycling method, Nat Protoc, 1 (2006) 3159-3165.

[16] O.W. Griffith, Determination of glutathione and glutathione disulfide using glutathione reductase and 2-vinylpyridine, Anal Biochem, 106 (1980) 207-212.

[17] D. Giustarini, G. Colombo, M.L. Garavaglia, E. Astori, N.M. Portinaro, F. Reggiani, S. Badalamenti, A.M. Aloisi, A. Santucci, R. Rossi, A. Milzani, I. Dalle-Donne, Assessment of glutathione/glutathione disulphide ratio and S-glutathionylated proteins in human blood, solid tissues, and cultured cells, Free Radic Biol Med, 112 (2017) 360-375.

[18] H. Guntherberg, J. Rost, The true oxidized glutathione content of red blood cells obtained by new enzymic and paper chromatographic methods, Anal Biochem, 15 (1966) 205-210.

[19] S.C. Garcia, K. Schott, M. Charao, A. Moro, R. Bulcao, D. Grotto, J. Valentini, D. Bohrer, S. Cardoso, V. Pomblum, Quantification of reduced glutathione by HPLC-UV in erythrocytes of hemodialysis patients, Biomed Chromatogr, 22 (2008) 460-468.

[20] A.A. Zhloba, E.L. Blashko, Liquid chromatographic determination of total homocysteine in blood plasma with photometric detection, J Chromatogr B Analyt Technol Biome Life Sci, 800 (2004) 275-280.

[21] X. Wang, D. Chi, D. Song, G. Su, L. Li, L. Shao, Quantification of Glutathione in Plasma Samples by HPLC Using 4-Fluoro-7-nitrobenzofurazan as a Fluorescent Labeling Reagent, J Chromatogr Sci, 50 (2012) 119-122.

[22] T.D. Nolin, M.E. McMenamin, J. Himmelfarb, Simultaneous determination of total homocysteine, cysteine, cysteinylglycine, and glutathione in human plasma by high-performance liquid chromatography: Application to studies of oxidative stress, J Chromatogr B Analyt Technol Biomed Life Sci, 852 (2007) 554-561.

[23] C. Cereser, J. Guichard, J. Drai, E. Bannier, I. Garcia, S. Boget, P. Parvaz, A. Revol, Quantitation of reduced and total glutathione at the femtomole level by high-performance

liquid chromatography with fluorescence detection: application to red blood cells and cultured fibroblasts, J Chromatogr B Biomed Sci Appl, 752 (2001) 123-132.

[24] S.G. Lee, J. Yim, Y. Lim, J.H. Kim, Validation of a liquid chromatography tandem mass spectrometry method to measure oxidized and reduced forms of glutathione in whole blood and verification in a mouse model as an indicator of oxidative stress, J Chromatogr B Analyt Technol Biomed Life Sci, 15 (2016) 45-50.

[25] T. Fahrenholz, M.M. Wolle, H.M. Kingston, S. Faber, J.C. Kern, 2nd, M. Pamuku, L. Miller, H. Chatragadda, A. Kogelnik, Molecular speciated isotope dilution mass spectrometric methods for accurate, reproducible and direct quantification of reduced, oxidized and total glutathione in biological samples, Anal Chem, 87 (2015) 1232-1240.

[26] T. Moore, A. Le, A.K. Niemi, T. Kwan, K. Cusmano-Ozog, G.M. Enns, T.M. Cowan, A new LC-MS/MS method for the clinical determination of reduced and oxidized glutathione from whole blood, J Chromatogr B Analyt Technol Biomed Life Sci, 929 (2013) 51-55.

[27] F. Zhang, M.J. Bartels, D.R. Geter, Y.C. Jeong, M.R. Schisler, A.J. Wood, L. Kan, B.B. Gollapudi, Quantitation of glutathione by liquid chromatography/positive electrospray ionization tandem mass spectrometry, Rapid Comm Mass Spectrom, 22 (2008) 3608-3614.

[28] R.L. Norris, G.K. Eaglesham, G.R. Shaw, M.J. Smith, R.K. Chiswell, A.A. Seawright, M.R. Moore, A sensitive and specific assay for glutathione with potential application to glutathione disulphide, using high-performance liquid chromatography-tandem mass spectrometry, J Chromatogr B, 762 (2001) 17-23.

[29] E. Camera, M. Rinaldi, S. Briganti, M. Picardo, S. Fanali, Simultaneous determination of reduced and oxidized glutathione in peripheral blood mononuclear cells by liquid chromatography-electro spray mass spectrometry, J Chromatogr B, 757 (2001) 69-78.

[30] D.J. Reed, J.R. Babson, P.W. Beatty, A.E. Brodie, W.W. Ellis, D.W. Potter, High-performance liquid chromatography analysis of nanomole levels of glutathione, glutathione disulfide, and related thiols and disulfides, Anal Biochem, 106 (1980) 55-62.

[31] G.L. Newton, R. Dorian, R.C. Fahey, Analysis of biological thiols: derivatization with monobromobimane and separation by reverse-phase high-performance liquid chromatography, Anal Biochem, 114 (1981) 383-387.

[32] R.A. Winters, J. Zukowski, N. Ercal, R.H. Matthews, D.R. Spitz, Analysis of glutathione, glutathione disulfide, cysteine, homocysteine, and other biological thiols by high-performance liquid chromatography following derivatization by n-(1-pyrenyl)maleimide, Anal Biochem, 227 (1995) 14-21.

[33] I. Squellerio, D. Caruso, B. Porro, F. Veglia, E. Tremoli, V. Cavalca, Direct glutathione quantification in human blood by LC-MS/MS: comparison with HPLC with electrochemical detection, J Pharm Biomed Anal, 71 (2012) 111-118.

[34] M. Nazari, M.T. Bokhart, P.L. Loziuk, D.C. Muddiman, Quantitative mass spectrometry imaging of glutathione in healthy and cancerous hen ovarian tissue sections by infrared matrix-assisted laser desorption electrospray ionization (IR-MALDESI), Analyst, 143 (2018) 654-661.

[35] J.C. Roberts, D.J. Francetic, The importance of sample preparation and storage in glutathione analysis, Anal Biochem, 211 (1993) 183-187.

[36] R. Rossi, A. Milzani, I. Dalle-Donne, D. Giustarini, L. Lusini, R. Colombo, P. Di Simplicio, Blood glutathione disulfide: In vivo factor or in vitro artifact?, Clin Chem, 48 (2002) 742-753.

[37] E.R. Mardis, L. Ding, D.J. Dooling, D.E. Larson, M.D. McLellan, K. Chen, D.C. Koboldt, R.S. Fulton, K.D. Delehaunty, S.D. McGrath, L.A. Fulton, D.P. Locke, V.J. Magrini, R.M. Abbott, T.L. Vickery, J.S. Reed, J.S. Robinson, T. Wylie, S.M. Smith, L. Carmichael, J.M. Eldred, C.C. Harris, J. Walker, J.B. Peck, F. Du, A.F. Dukes, G.E. Sanderson, A.M. Brummett, E. Clark, J.F. McMichael, R.J. Meyer, J.K. Schindler, C.S. Pohl, J.W. Wallis, X. Shi, L. Lin, H. Schmidt, Y. Tang, C. Haipek, M.E. Wiechert, J.V. Ivy, J. Kalicki, G. Elliott, R.E. Ries, J.E. Payton, P. Westervelt, M.H. Tomasson, M.A. Watson, J. Baty, S. Heath, W.D. Shannon, R. Nagarajan, D.C. Link, M.J. Walter, T.A. Graubert, J.F. DiPersio, R.K. Wilson, T.J. Ley, Recurring mutations found by sequencing an acute myeloid leukemia genome, N Engl J Med, 361 (2009) 1058-1066.

[38] Z.J. Reitman, H. Yan, Isocitrate dehydrogenase 1 and 2 mutations in cancer: alterations at a crossroads of cellular metabolism, J Natl Cancer Inst, 102 (2010) 932-941.

[39] S. Pusch, L. Schweizer, A.C. Beck, J.M. Lehmler, S. Weissert, J. Balss, A.K. Miller, A. von Deimling, D-2-Hydroxyglutarate producing neo-enzymatic activity inversely correlates with frequency of the type of isocitrate dehydrogenase 1 mutations found in glioma, Acta Neuropathol Commun, 2 (2014) 19.

[40] P. Paschka, R.F. Schlenk, V.I. Gaidzik, M. Habdank, J. Kronke, L. Bullinger, D. Spath, S. Kayser, M. Zucknick, K. Gotze, H.A. Horst, U. Germing, H. Dohner, K. Dohner, IDH1 and IDH2 mutations are frequent genetic alterations in acute myeloid leukemia and confer adverse prognosis in cytogenetically normal acute myeloid leukemia with NPM1 mutation without FLT3 internal tandem duplication, J Clin Oncol, 28 (2010) 3636-3643.

[41] L. Zhou, Z. Wang, C. Hu, C. Zhang, P. Kovatcheva-Datchary, D. Yu, S. Liu, F. Ren, X. Wang, Y. Li, X. Hou, H. Piao, X. Lu, Y. Zhang, G. Xu, Integrated metabolomics and lipidomics analyses reveal metabolic reprogramming in human glioma with IDH1 mutation, J Proteome Res, 18 (2019) 960-969.

[42] J.T. Chen, C.C. Liu, J.S. Yu, H.H. Li, M.C. Lai, Integrated omics profiling identifies hypoxia-regulated genes in HCT116 colon cancer cells, J Proteomics, 188 (2018) 139-151.

[43] L. Jiang, A. Boufersaoui, C. Yang, B. Ko, D. Rakheja, G. Guevara, Z. Hu, R.J. DeBerardinis, Quantitative metabolic flux analysis reveals an unconventional pathway of fatty acid synthesis in cancer cells deficient for the mitochondrial citrate transport protein, Metab Eng, 43 (2017) 198-207.

[44] W. Dong, M.A. Keibler, G. Stephanopoulos, Review of metabolic pathways activated in cancer cells as determined through isotopic labeling and network analysis, Metab Eng, 43 (2017) 113-124.

[45] P. Matre, J. Velez, R. Jacamo, Y. Qi, X. Su, T. Cai, S.M. Chan, A. Lodi, S.R. Sweeney, H. Ma, R.E. Davis, N. Baran, T. Haferlach, E.R. Flores, D. Gonzalez, S. Konoplev, I. Samudio, C. DiNardo, R. Majeti, A.D. Schimmer, W. Li, T. Wang, S. Tiziani, M. Konopleva, Inhibiting glutaminase in acute myeloid leukemia: metabolic dependency of selected AML subtypes, Oncotarget, 7 (2016) 79722-79735.

[46] D. Ye, K.L. Guan, Y. Xiong, Metabolism, Activity, and Targeting of D- and L-2-Hydroxyglutarates, Trends Cancer, 4 (2018) 151-165.

[47] L. Dang, D.W. White, S. Gross, B.D. Bennett, M.A. Bittinger, E.M. Driggers, V.R. Fantin, H.G. Jang, S. Jin, M.C. Keenan, K.M. Marks, R.M. Prins, P.S. Ward, K.E. Yen, L.M. Liau, J.D. Rabinowitz, L.C. Cantley, C.B. Thompson, M.G. Vander Heiden, S.M. Su, Cancer-associated IDH1 mutations produce 2-hydroxyglutarate, Nature, 462 (2009) 739-744.

[48] L. Dang, D.W. White, S. Gross, B.D. Bennett, M.A. Bittinger, E.M. Driggers, V.R. Fantin, H.G. Jang, S. Jin, M.C. Keenan, K.M. Marks, R.M. Prins, P.S. Ward, K.E. Yen, L.M. Liau, J.D. Rabinowitz, L.C. Cantley, C.B. Thompson, M.G. Vander Heiden, S.M. Su, Cancer-associated IDH1 mutations produce 2-hydroxyglutarate, Nature, 462 (2009) 739-744.

[49] P.S. Ward, J. Patel, D.R. Wise, O. Abdel-Wahab, B.D. Bennett, H.A. Coller, J.R. Cross, V.R. Fantin, C.V. Hedvat, A.E. Perl, J.D. Rabinowitz, M. Carroll, S.M. Su, K.A. Sharp, R.L. Levine, C.B. Thompson, The common feature of leukemia-associated IDH1 and IDH2 mutations is a neomorphic enzyme activity converting alpha-ketoglutarate to 2-hydroxyglutarate, Cancer Cell, 17 (2010) 225-234.

[50] S. Gross, R.A. Cairns, M.D. Minden, E.M. Driggers, M.A. Bittinger, H.G. Jang, M. Sasaki, S. Jin, D.P. Schenkein, S.M. Su, L. Dang, V.R. Fantin, T.W. Mak, Cancer-associated metabolite 2-hydroxyglutarate accumulates in acute myelogenous leukemia with isocitrate dehydrogenase 1 and 2 mutations, J Exp Med, 207 (2010) 339-344.

[51] D. Ye, K.L. Guan, Y. Xiong, Metabolism, Activity, and Targeting of D- and L-2-Hydroxyglutarates, Trends Cancer, 4 (2018) 151-165.

[52] S. Ma, R. Sun, B. Jiang, J. Gao, W. Deng, P. Liu, R. He, J. Cui, M. Ji, W. Yi, P. Yang, X. Wu, Y. Xiong, Z. Qiu, D. Ye, K.-L. Guan, L2hgdh Deficiency Accumulates l-2-Hydroxyglutarate with Progressive Leukoencephalopathy and Neurodegeneration, Mol Cell Biol, 37 (2017) e00492.

[53] E.-H. Shim, C.B. Livi, D. Rakheja, J. Tan, D. Benson, V. Parekh, E.-Y. Kho, A.P. Ghosh, R. Kirkman, S. Velu, S. Dutta, B. Chenna, S.L. Rea, R.J. Mishur, Q. Li, T.L. Johnson-Pais, L. Guo, S. Bae, S. Wei, K. Block, S. Sudarshan, L-2-Hydroxyglutarate: an epigenetic modifier and putative oncometabolite in renal cancer, Cancer Discov, 4 (2014) 1290-1298.

[54] A. Borodovsky, M.J. Seltzer, G.J. Riggins, Altered cancer cell metabolism in gliomas with mutant IDH1 or IDH2, Curr Opin Oncol, 24 (2012) 83-89.

[55] G. Karpel-Massler, T.T.T. Nguyen, E. Shang, M.D. Siegelin, Novel IDH1-Targeted Glioma Therapies, CNS Drugs, 33 (2019) 1155-1166.

[56] D. Golub, N. Iyengar, S. Dogra, T. Wong, D. Bready, K. Tang, A.S. Modrek, D.G. Placantonakis, Mutant Isocitrate Dehydrogenase Inhibitors as Targeted Cancer Therapeutics, Front Oncol, 9 (2019) 417.

[57] L. Dimitrov, C.S. Hong, C. Yang, Z. Zhuang, J.D. Heiss, New developments in the pathogenesis and therapeutic targeting of the IDH1 mutation in glioma, Int J Med Sci, 12 (2015) 201-213.

[58] F. Ohka, M. Ito, M. Ranjit, T. Senga, A. Motomura, K. Motomura, K. Saito, K. Kato, Y. Kato, T. Wakabayashi, T. Soga, A. Natsume, Quantitative metabolome analysis profiles activation of glutaminolysis in glioma with IDH1 mutation, Tumour Biol, 35 (2014) 5911-5920.

[59] A.R. Grassian, S.J. Parker, S.M. Davidson, A.S. Divakaruni, C.R. Green, X. Zhang, K.L. Slocum, M. Pu, F. Lin, C. Vickers, C. Joud-Caldwell, F. Chung, H. Yin, E.D. Handly, C. Straub, J.D. Growney, M.G. Vander Heiden, A.N. Murphy, R. Pagliarini, C.M. Metallo, IDH1 mutations alter citric acid cycle metabolism and increase dependence on oxidative mitochondrial metabolism, Cancer Res, 74 (2014) 3317-3331.

[60] M. Esmaeili, B.C. Hamans, A.C. Navis, R. van Horssen, T.F. Bathen, I.S. Gribbestad, W.P. Leenders, A. Heerschap, IDH1 R132H mutation generates a distinct phospholipid metabolite profile in glioma, Cancer Res, 74 (2014) 4898-4907.

[61] C. Chesnelong, M.M. Chaumeil, M.D. Blough, M. Al-Najjar, O.D. Stechishin, J.A. Chan, R.O. Pieper, S.M. Ronen, S. Weiss, H.A. Luchman, J.G. Cairncross, Lactate dehydrogenase A silencing in IDH mutant gliomas, Neuro Oncol, 16 (2014) 686-695.

[62] M.M. Chaumeil, P.E. Larson, S.M. Woods, L. Cai, P. Eriksson, A.E. Robinson, J.M. Lupo, D.B. Vigneron, S.J. Nelson, R.O. Pieper, J.J. Phillips, S.M. Ronen, Hyperpolarized [1-13C] glutamate: a metabolic imaging biomarker of IDH1 mutational status in glioma, Cancer Res, 74 (2014) 4247-4257.

[63] Z.J. Reitman, G. Jin, E.D. Karoly, I. Spasojevic, J. Yang, K.W. Kinzler, Y. He, D.D. Bigner, B. Vogelstein, H. Yan, Profiling the effects of isocitrate dehydrogenase 1 and 2 mutations on the cellular metabolome, Proc Natl Acad Sci U S A, 108 (2011) 3270-3275.

[64] B.S. Winkler, N. DeSantis, F. Solomon, Multiple NADPH-producing pathways control glutathione (GSH) content in retina, Exp Eye Res, 43 (1986) 829-847.

[65] J. Shi, B. Sun, W. Shi, H. Zuo, D. Cui, L. Ni, J. Chen, Decreasing GSH and increasing ROS in chemosensitivity gliomas with IDH1 mutation, Tumour Biol, 36 (2015) 655-662.

[66] S.J. Gelman, F. Naser, N.G. Mahieu, L.D. McKenzie, G.P. Dunn, M.G. Chheda, G.J. Patti, Consumption of NADPH for 2-HG Synthesis Increases Pentose Phosphate Pathway Flux and Sensitizes Cells to Oxidative Stress, Cell Rep, 22 (2018) 512-522.

[67] M.J. Seltzer, B.D. Bennett, A.D. Joshi, P. Gao, A.G. Thomas, D.V. Ferraris, T. Tsukamoto, C.J. Rojas, B.S. Slusher, J.D. Rabinowitz, C.V. Dang, G.J. Riggins, Inhibition of glutaminase preferentially slows growth of glioma cells with mutant IDH1, Cancer Res, 70 (2010) 8981-8987.

[68] S. Venneti, C.B. Thompson, Metabolic modulation of epigenetics in gliomas, Brain Pathol, 23 (2013) 217-221.

[69] S.J. Kim, S.H. Kim, J.H. Kim, S. Hwang, H.J. Yoo, Understanding Metabolomics in Biomedical Research, Endocrinol Metab (Seoul), 31 (2016) 7-16.

[70] K. Dettmer, B.D. Hammock, Metabolomics--a new exciting field within the "omics" sciences, Environ Health Perspect, 112, (2004) A396-397.

[71] J. Piestansky, D. Olesova, J. Galba, K. Marakova, V. Parrak, P. Secnik, P. Secnik, Jr., B. Kovacech, A. Kovac, Z. Zelinkova, P. Mikus, Profiling of Amino Acids in Urine Samples of Patients Suffering from Inflammatory Bowel Disease by Capillary Electrophoresis-Mass Spectrometry, Molecules, 24 (2019) 3345-3360.

[72] K. Dettmer, P.A. Aronov, B.D. Hammock, Mass spectrometry-based metabolomics, Mass Spectrom Rev, 26 (2007) 51-78.

[73] M. Zhou, J.F. McDonald, F.M. Fernandez, Optimization of a direct analysis in real time/time-of-flight mass spectrometry method for rapid serum metabolomic fingerprinting, J Am Soc Mass Spectrom, 21 (2010) 68-75.

[74] H. Song, L. Wang, H.L. Liu, X.B. Wu, H.S. Wang, Z.H. Liu, Y. Li, D.C. Diao, H.L. Chen, J.S. Peng, Tissue metabolomic fingerprinting reveals metabolic disorders associated with human gastric cancer morbidity, Oncol Rep, 26 (2011) 431-438.

[75] W. Wiechert, M. Mollney, S. Petersen, A.A. de Graaf, A universal framework for C-13 metabolic flux analysis, Metab Eng, 3 (2001) 265-283.

[76] C. Wittmann, Metabolic flux analysis using mass spectrometry, Adv Biochem Eng Biotechnol, 74 (2002) 39-64.

[77] U. Sauer, High-throughput phenomics: experimental methods for mapping fluxomes, Curr Opin Biotechnol, 15 (2004) 58-63.

[78] W. Wiechert, K. Noh, Isotopically non-stationary metabolic flux analysis: complex yet highly informative, Curr Opin Biotechnol, 24 (2013) 979-986.

[79] S. Niedenfuhr, W. Wiechert, K. Noh, How to measure metabolic fluxes: a taxonomic guide for (13)C fluxomics, Curr Opin Biotechnol, 34 (2015) 82-90.

[80] M.R. Antoniewicz, 13C metabolic flux analysis: optimal design of isotopic labeling experiments, Curr Opin Biotechnol, 24 (2013) 1116-1121.

[81] J.M. Buescher, M.R. Antoniewicz, L.G. Boros, S.C. Burgess, H. Brunengraber, C.B. Clish, R.J. DeBerardinis, O. Feron, C. Frezza, B. Ghesquiere, E. Gottlieb, K. Hiller, R.G. Jones, J.J. Kamphorst, R.G. Kibbey, A.C. Kimmelman, J.W. Locasale, S.Y. Lunt, O.D.K. Maddocks, C. Malloy, C.M. Metallo, E.J. Meuillet, J. Munger, K. Nöh, J.D. Rabinowitz, M. Ralser, U. Sauer, G. Stephanopoulos, J. St-Pierre, D.A. Tennant, C. Wittmann, M.G. Vander Heiden, A. Vazquez, K. Vousden, J.D. Young, N. Zamboni, S.-M. Fendt, A roadmap for interpreting 13C metabolite labeling patterns from cells, Curr Opin Biotechnol, 34 (2015) 189-201.

[82] P. Heinrich, C. Kohler, L. Ellmann, P. Kuerner, R. Spang, P.J. Oefner, K. Dettmer, Correcting for natural isotope abundance and tracer impurity in MS-, MS/MS- and high-resolution-multiple-tracer-data from stable isotope labeling experiments with IsoCorrectoR, Sci Rep, 8 (2018) 17910-17919.

[83] S. Klein, E. Heinzle, Isotope labeling experiments in metabolomics and fluxomics, Wiley Interdiscip Rev Syst Biol Med, 4 (2012) 261-272.

[84] Z. Dai, J.W. Locasale, Understanding metabolism with flux analysis: From theory to application, Metab Eng, 43 (2017) 94-102.

[85] M. Horl, J. Schnidder, U. Sauer, N. Zamboni, Non-stationary (13)C-metabolic flux ratio analysis, Biotechnol Bioeng, 110 (2013) 3164-3176.

[86] A. Amberg, B. Riefke, G. Schlotterbeck, A. Ross, H. Senn, F. Dieterle, M. Keck, NMR and MS Methods for Metabolomics, Methods Mol Biol, (2017) 229-258.

[87] J.L. Markley, R. Bruschweiler, A.S. Edison, H.R. Eghbalnia, R. Powers, D. Raftery, D.S. Wishart, The future of NMR-based metabolomics, Curr Opin Biotechnol, 43 (2017) 34-40.

[88] G.A. Gowda, D. Djukovic, Overview of mass spectrometry-based metabolomics: opportunities and challenges, Methods Mol Biol, (2014) 3-12.

[89] A. Zhang, H. Sun, P. Wang, Y. Han, X. Wang, Modern analytical techniques in metabolomics analysis, Analyst, 137 (2012) 293-300.

[90] H. Jaurila, V. Koivukangas, M. Koskela, F. Gäddnäs, S. Myllymaa, A. Kullaa, T. Salo, T.I. Ala-Kokko, (1)H NMR Based Metabolomics in Human Sepsis and Healthy Serum, Metabolites, 10 (2020) 70-82.

[91] M. Cuperlovic-Culf, D. Ferguson, A. Culf, P. Morin, Jr., M. Touaibia, 1H NMR metabolomics analysis of glioblastoma subtypes: correlation between metabolomics and gene expression characteristics, J Biol Chem, 287 (2012) 20164-20175.

[92] L. Bervoets, G. Massa, W. Guedens, G. Reekmans, J.-P. Noben, P. Adriaensens, Identification of metabolic phenotypes in childhood obesity by (1)H NMR metabolomics of blood plasma, Future Sci OA, 4 (2018) 310-323.

[93] A.K. Kosmides, K. Kamisoglu, S.E. Calvano, S.A. Corbett, I.P. Androulakis, Metabolomic fingerprinting: challenges and opportunities, Crit Rev Biomed Eng, 41 (2013) 205-221.

[94] E.M. Lenz, I.D. Wilson, Analytical strategies in metabonomics, J Proteome Res, 6 (2007) 443-458.

[95] G.A. Nagana Gowda, D. Raftery, Recent Advances in NMR-Based Metabolomics, Anal Chem, 89 (2017) 490-510.

[96] G.A. Nagana Gowda, Y.N. Gowda, D. Raftery, Expanding the limits of human blood metabolite quantitation using NMR spectroscopy, Anal Chem, 87 (2015) 706-715.

[97] A.-H. Emwas, R. Roy, R.T. McKay, L. Tenori, E. Saccenti, G.A.N. Gowda, D. Raftery, F. Alahmari, L. Jaremko, M. Jaremko, D.S. Wishart, NMR Spectroscopy for Metabolomics Research, Metabolites, 9 (2019) 123-161.

[98] C.E. McHugh, T.L. Flott, C.R. Schooff, Z. Smiley, M.A. Puskarich, D.D. Myers, J.G. Younger, A.E. Jones, K.A. Stringer, Rapid, Reproducible, Quantifiable NMR Metabolomics: Methanol and Methanol: Chloroform Precipitation for Removal of Macromolecules in Serum and Whole Blood, Metabolites, 8 (2018) 93-107.

[99] J. Rodriguez-Morato, O.J. Pozo, J. Marcos, Targeting human urinary metabolome by LC-MS/MS: a review, Bioanalysis, 10 (2018) 489-516.

[100] K. Pietrowska, D.A. Dmuchowska, P. Samczuk, T. Kowalczyk, P. Krasnicki, M. Wojnar, A. Skowronska, Z. Mariak, A. Kretowski, M. Ciborowski, LC-MS-Based Metabolic Fingerprinting of Aqueous Humor, J Anal Methods Chem, 2017 (2017) 6745932-6745944.

[101] M. Woollam, M. Teli, P. Angarita-Rivera, S. Liu, A.P. Siegel, H. Yokota, M. Agarwal, Detection of Volatile Organic Compounds (VOCs) in Urine via Gas Chromatography-Mass Spectrometry QTOF to Differentiate Between Localized and Metastatic Models of Breast Cancer, Sci Rep, 9 (2019) 2526-2537.

[102] O. Fiehn, Metabolomics by Gas Chromatography-Mass Spectrometry: Combined Targeted and Untargeted Profiling, Curr Protoc Mol Biol, 114 (2016) 1-30.

[103] S. Ishikawa, M. Sugimoto, K. Kitabatake, A. Sugano, M. Nakamura, M. Kaneko, S. Ota, K. Hiwatari, A. Enomoto, T. Soga, M. Tomita, M. Iino, Identification of salivary metabolomic biomarkers for oral cancer screening, Sci Rep, 6 (2016) 31520-31256.

[104] T. Soga, Y. Kakazu, M. Robert, M. Tomita, T. Nishioka, Qualitative and quantitative analysis of amino acids by capillary electrophoresis-electrospray ionization-tandem mass spectrometry, Electrophoresis, 25 (2004) 1964-1972.

[105] T.M. Annesley, Ion suppression in mass spectrometry, Clin Chem, 49 (2003) 1041-1044.

[106] K. Bingol, R. Bruschweiler, NMR/MS Translator for the Enhanced Simultaneous Analysis of Metabolomics Mixtures by NMR Spectroscopy and Mass Spectrometry: Application to Human Urine, J Proteome Res, 14 (2015) 2642-2648.

[107] A. Leggett, C. Wang, D.-W. Li, A. Somogyi, L. Bruschweiler-Li, R. Brüschweiler, Identification of Unknown Metabolomics Mixture Compounds by Combining NMR, MS, and Cheminformatics, Methods Enzymol, 615 (2019) 407-422.

[108] W.M.A. Niessen, D. Falck, Introduction to Mass Spectrometry, a Tutorial, Analyzing Biomolecular Interactions by Mass Spectrometry, (2015) 1-54.

[109] F.A. Mellon, Mass spectrometry, Principles and Instrumentation, Encyclopedia of Food Sciences and Nutrition (Second Edition), (2003).

[110] W.B. Dunn, Mass spectrometry in systems biology an introduction, Methods Enzymol, 500 (2011) 15-35.

[111] W. Clarke, Mass spectrometry in the clinical laboratory: determining the need and avoiding pitfalls, Mass Spectrometry for the Clinical Laboratory (First Edition), Chapter 1 (2017) 1-15.

[112] V.M. Doroshenko, R.J. Cotter, Ideal velocity focusing in a reflectron time-of-flight mass spectrometer, J Am Soc Mass Spectrom, 10 (1999) 992-999.

[113] www.chromacademy.com, Mass spectrometry fundamental LC-MS mass analysers, e-learning for the analytical chemistry community.

[114] A. Radionova, I. Filippov, P.J. Derrick, In pursuit of resolution in time-of-flight mass spectrometry: A historical perspective, Mass Spectrom Rev, 35 (2016) 738-757.

[115] A.A. Makarov, Mass spectrometer, Patent, 5886346 (1999).

[116] Q. Hu, R.J. Noll, H. Li, A. Makarov, M. Hardman, R. Graham Cooks, The Orbitrap: a new mass spectrometer, J Mass Spectrom, 40 (2005) 430-443.

[117] M. Hardman, A.A. Makarov, Interfacing the orbitrap mass analyzer to an electrospray ion source, Anal Chem, 75 (2003) 1699-1705.

[118] A. Makarov, Electrostatic axially harmonic orbital trapping: a high-performance technique of mass analysis, Anal Chem, 72 (2000) 1156-1162.

[119] M. Scigelova, A. Makarov, Orbitrap mass analyzer--overview and applications in proteomics, Proteomics, 2 (2006) 16-21.

[120] A. Makarov, E. Denisov, O. Lange, S. Horning, Dynamic range of mass accuracy in LTQ Orbitrap hybrid mass spectrometer, J Am Soc Mass Spectrom, 17 (2006) 977-982.

[121] A. Makarov, M. Scigelova, Coupling liquid chromatography to Orbitrap mass spectrometry, J Chromatogr A, 1217 (2010) 3938-3945.

[122] H. Zhou, Y.M. Cao, S. Miao, L. Lan, M. Chen, W.T. Li, X.H. Mao, S. Ji, Qualitative screening and quantitative determination of 569 pesticide residues in honeysuckle using ultrahigh-performance liquid chromatography coupled to quadrupole-Orbitrap high resolution mass spectrometry, J Chromatogr A, 16 (2019) 460374.

[123] C.L. Yao, Z.M. Qian, W.S. Tian, X.Q. Xu, Y. Yan, Y. Shen, S.M. Lu, W.J. Li, D.A. Guo, Profiling and identification of aqueous extract of Cordyceps sinensis by ultra-high performance liquid chromatography tandem quadrupole-orbitrap mass spectrometry, Chin J Nat Med, 17 (2019) 631-640.

[124] N. Vu-Duc, T. Nguyen-Quang, T. Le-Minh, X. Nguyen-Thi, T.M. Tran, H.A. Vu, L.A. Nguyen, T. Doan-Duy, B. Van Hoi, C.T. Vu, D. Le-Van, L.A. Phung-Thi, H.A. Vu-Thi, D.B. Chu, Multiresidue Pesticides Analysis of Vegetables in Vietnam by Ultrahigh-Performance Liquid Chromatography in Combination with High-Resolution Mass Spectrometry (UPLC-Orbitrap MS), J Anal Methods Chem, 2019 (2019) 3489634-3489645.

[125] S.A. Ugrin, A.M. English, J.E.P. Syka, D.L. Bai, L.C. Anderson, J. Shabanowitz, D.F. Hunt, Ion-Ion Proton Transfer and Parallel Ion Parking for the Analysis of Mixtures of Intact Proteins on a Modified Orbitrap Mass Analyzer, J Am Soc Mass Spectrom, 7 (2019) 2163-2173.

[126] A. Lommen, A. Elaradi, A. Vonaparti, M. Blokland, M.W. Nielen, K.A. Saad, W.M. Abushreeda, P. Horvatovich, A.E. Al-Muraikhi, M. Al-Maadheed, C. Georgakopoulos, Ultra-fast retroactive processing of liquid chromatography high-resolution full-scan Orbitrap mass spectrometry data in anti-doping screening of human urine, Rapid Commun Mass Spectrom, 33 (2019) 1578-1588.

[127] M.H. Lucie Nováková, Robert Jirásko and Miroslav Lísa, UHPLC/MS Coupling: How to Select a Suitable Configuration?, UHPLC in Life Sciences, Chapter 7 (2012) 186-210.

[128] R.A. Yost, R.K. Boyd, Tandem mass spectrometry: quadrupole and hybrid instruments, Methods Enzymol, 193 (1990) 154-200.

[129] Q. Wu, A. Hua, Y. Sun, C. Ma, W. Tian, C. Huang, H. Yu, P. Jiao, S. Wang, H. Tong, W. Qiu, Determination and pharmacokinetic study of AZD-3759 in rat plasma by ultra performance liquid chromatography with triple quadrupole mass spectrometer, Thorac Cancer, 9 (2018) 1383-1389.

[130] S. El Balkhi, M. Chaslot, N. Picard, S. Dulaurent, M. Delage, O. Mathieu, F. Saint-Marcoux, Characterization and identification of eight designer benzodiazepine metabolites by incubation with human liver microsomes and analysis by a triple quadrupole mass spectrometer, Int J Legal Med, 131 (2017) 979-988.

[131] E.H. Wang, P.C. Combe, K.A. Schug, Multiple Reaction Monitoring for Direct Quantitation of Intact Proteins Using a Triple Quadrupole Mass Spectrometer, J Am Soc Mass Spectrom, 27 (2016) 886-896.

[132] S.A. Mackintosh, A. Perez-Fuentetaja, L.R. Zimmerman, G. Pacepavicius, M. Clapsadl, M. Alaee, D.S. Aga, Analytical performance of a triple quadrupole mass spectrometer compared to a high resolution mass spectrometer for the analysis of polybrominated diphenyl ethers in fish, Anal Chim Acta, 747 (2012) 67-75.

[133] B. Ruisch, T. Konig, Liquid chromatography with accurate mass measurement on a triple quadrupole mass spectrometer for the identification and quantification of N-lactoyl ethanolamine in wine, Mol Nutr Food Res, 54 (2010) 304-305.

[134] J.H. Kennedy, J.M. Wiseman, Evaluation and performance of desorption electrospray ionization using a triple quadrupole mass spectrometer for quantitation of pharmaceuticals in plasma, Rapid Commun Mass Spectrom, 24 (2010) 309-314.

[135] A. Makarov, E. Denisov, A. Kholomeev, W. Balschun, O. Lange, K. Strupat, S. Horning, Performance evaluation of a hybrid linear ion trap/orbitrap mass spectrometer, Anal Chem, 78 (2006) 2113-2120.

[136] I.V. Chernushevich, A.V. Loboda, B.A. Thomson, An introduction to quadrupole-time-of-flight mass spectrometry, J Mass Spectrom, 36 (2001) 849-865.

[137] I.V. Chernushevich, Duty Cycle Improvement for a Quadrupole-Time-of-Flight Mass Spectrometer and its Use for Precursor Ion Scans, Eur J Mass Spectrom, 6 (2000) 471-479.

[138] W. Ens, K.G. Standing, Hybrid quadrupole/time-of-flight mass spectrometers for analysis of biomolecules, Methods Enzymol, 402 (2005) 49-78.

[139] N. Couto, L. Davlyatova, C.A. Evans, P.C. Wright, Application of the broadband collision-induced dissociation (bbCID) mass spectrometry approach for protein glycosylation and phosphorylation analysis, Rapid Commun Mass Spectrom, 32 (2018) 75-85.

[140] S. Vikingsson, T. Rautio, J. Wallgren, A. Astrand, S. Watanabe, J. Dahlen, A. Wohlfarth, P. Konradsson, X. Wu, R. Kronstrand, H. Green, LC-QTOF-MS Identification of Major Urinary Cyclopropylfentanyl Metabolites Using Synthesized Standards, J Anal Toxicol, 43 (2019) 607-614.

[141] X. Su, Y. Wu, Y. Li, Y. Huang, Y. Liu, P. Luo, Z. Zhang, Effect of Different Post-Harvest Processing Methods on the Chemical Constituents of Notopterygium franchetii by an UHPLC-QTOF-MS-MS Metabolomics Approach, Molecules, 24 (2019) 3188-3203.

[142] K. Nagai, B. Uranbileg, Z. Chen, A. Fujioka, T. Yamazaki, Y. Matsmoto, H. Tsukamoto, H. Ikeda, Y. Yatomi, H. Chiba, S.P. Hui, T. Nakazawa, R. Saito, S. Koshiba, J. Aoki, D. Saigusa, Y. Tomioka, Identification of novel biomarkers of hepatocellular carcinoma by a high definition mass spectrometry; UHPLC-QTOF/MS and DESI-MSI, Rapid Commun Mass Spectrom, 34 (2019) e8551-8559.

[143] L.A.L. da Silva, L.P. Sandjo, A. Misturini, G.F. Caramori, M.W. Biavatti, ESI-QTof-MS characterization of hirsutinolide and glaucolide sesquiterpene lactones: fragmentation mechanisms and differentiation based on Na(+) /H(+) adducts interactions in complex mixture, J Mass Spectrom, 54 (2019) 915-932.

[144] H.M. Cornthwaite, C.S. McDonald, J.H. Watterson, Analysis of Dextromethorphan and Three Metabolites in Decomposed Skeletal Tissues by UPLC-QToF-MS: Comparison of Acute and Repeated Drug Exposures, J Anal Toxicol, 43 (2019) 726-733.

[145] J.Q. Zhang, C.C. Zhao, Q.Y. Yang, S. Liang, F. Wu, B.L. Ma, Y. Feng, Pharmacokinetics, bioavailability and tissue distribution studies of rhodojaponin III in mice using QTRAP LC-MS/MS, Biomed Chromatogr, 33 (2019) e4649.

[146] A.L. Heffernan, K. Thompson, G. Eaglesham, S. Vijayasarathy, J.F. Mueller, P.D. Sly, M.J. Gomez, Rapid, automated online SPE-LC-QTRAP-MS/MS method for the simultaneous analysis of 14 phthalate metabolites and 5 bisphenol analogues in human urine, Talanta, 151 (2016) 224-233.

[147] S. Louw, M. Njoroge, N. Chigorimbo-Murefu, K. Chibale, Comparison of electrospray ionisation, atmospheric pressure chemical ionisation and atmospheric pressure photoionisation for the identification of metabolites from labile artemisinin-based anti-malarial drugs using a QTRAP(R) mass spectrometer, Rapid Commun Mass Spectrom, 26 (2012) 2431-2442.

[148] W. Bu, T. Akama, S. Chanda, D. Sullivan, V. Ciaravino, K. Jarnagin, Y. Freund, V. Sanders, C.W. Chen, X. Fan, I. Heyman, L. Liu, Early rapid identification of in vivo rat metabolites of AN6414, a novel boron-containing PDE4 inhibitor by QTRAP LC/MS/MS to support drug discovery, J Pharm Biomed Anal, 70 (2012) 344-353.

[149] M. Gros, M. Petrovic, D. Barcelo, Tracing pharmaceutical residues of different therapeutic classes in environmental waters by using liquid chromatography/quadrupole-linear ion trap mass spectrometry and automated library searching, Anal Chem, 81 (2009) 898-912.

[150] R. King, C. Fernandez-Metzler, The use of Qtrap technology in drug metabolism, Curr Drug Metab, 7 (2006) 541-545.

[151] C.A. Mueller, W. Weinmann, S. Dresen, A. Schreiber, M. Gergov, Development of a multi-target screening analysis for 301 drugs using a QTrap liquid chromatography/tandem mass spectrometry system and automated library searching, Rapid Commun Mass Spectrom, 19 (2005) 1332-1338.

[152] G.L. Herrin, H.H. McCurdy, W.H. Wall, Investigation of an LC-MS-MS (QTrap) method for the rapid screening and identification of drugs in postmortem toxicology whole blood samples, J Anal Toxicol, 29 (2005) 599-606.

[153] B.A. Parks, L. Jiang, P.M. Thomas, C.D. Wenger, M.J. Roth, M.T. Boyne, 2nd, P.V. Burke, K.E. Kwast, N.L. Kelleher, Top-down proteomics on a chromatographic time scale using linear ion trap fourier transform hybrid mass spectrometers, Anal Chem, 79 (2007) 7984-7991.

[154] J. Chen, L. Canales, R.E. Neal, Multi-Segment Direct Inject nano-ESI-LTQ-FT-ICR-MS/MS For Protein Identification, Proteome Sci, 9 (2011) 38-45.

[155] J.E.P. Syka, J.A. Marto, D.L. Bai, S. Horning, M.W. Senko, J.C. Schwartz, B. Ueberheide, B. Garcia, S. Busby, T. Muratore, J. Shabanowitz, D.F. Hunt, Novel Linear Quadrupole Ion Trap/FT Mass Spectrometer: Performance Characterization and Use in the Comparative Analysis of Histone H3 Post-translational Modifications, J Proteome Res, 3 (2004) 621-626.

[156] M. Ghaste, R. Mistrik, V. Shulaev, Applications of Fourier Transform Ion Cyclotron Resonance (FT-ICR) and Orbitrap Based High Resolution Mass Spectrometry in Metabolomics and Lipidomics, Int J Mol Sci, 17 (2016) 816-837.

[157] A. Kalli, G.T. Smith, M.J. Sweredoski, S. Hess, Evaluation and optimization of mass spectrometric settings during data-dependent acquisition mode: focus on LTQ-Orbitrap mass analyzers, J Proteome Res, 12 (2013) 3071-3086.

[158] M.S. Bereman, T.I. Williams, D.C. Muddiman, Development of a nanoLC LTQ orbitrap mass spectrometric method for profiling glycans derived from plasma from healthy, benign tumor control, and epithelial ovarian cancer patients, Anal Chem, 81 (2009) 1130-1136.

[159] E. Hurtado-Fernandez, T. Pacchiarotta, E. Longueira-Suarez, O.A. Mayboroda, A. Fernandez-Gutierrez, A. Carrasco-Pancorbo, Evaluation of gas chromatography-atmospheric pressure chemical ionization-mass spectrometry as an alternative to gas chromatography-electron ionization-mass spectrometry: avocado fruit as example, J Chromatogr A, 25 (2013) 228-244.

[160] X. Feng, X. Liu, Q. Luo, B.F. Liu, Mass spectrometry in systems biology: an overview, Mass Spectrom Rev, 27 (2008) 635-660.

[161] J.N. Wei, D. Belanger, R.P. Adams, D. Sculley, Rapid Prediction of Electron-Ionization Mass Spectrometry Using Neural Networks, ACS Cent Sci, 5 (2019) 700-708.

[162] G.A. Newsome, F.L. Steinkamp, B.C. Giordano, Isobutane Made Practical as a Reagent Gas for Chemical Ionization Mass Spectrometry, J Am Soc Mass Spectrom, 27 (2016) 1789-1795.

[163] J.B. Fenn, M. Mann, C.K. Meng, S.F. Wong, C.M. Whitehouse, Electrospray ionization for mass spectrometry of large biomolecules, Science, 246 (1989) 64-71.

[164] J.S. Andersen, B. Svensson, P. Roepstorff, Electrospray ionization and matrix assisted laser desorption/ionization mass spectrometry: powerful analytical tools in recombinant protein chemistry, Nat Biotechnol, 14 (1996) 449-457.

[165] I. Jardine, Electrospray ionization mass spectrometry of biomolecules, Nature, 345 (1990) 747-748.

[166] M. Geisow, Electrospray ionization mass spectrometry--a powerful new analytical tool, Trends Biotechnol, 8 (1990) 301-303.

[167] C.G. Edmonds, R.D. Smith, Electrospray ionization mass spectrometry, Methods Enzymol, 193 (1990) 412-431.

[168] A. Kiontke, S. Billig, C. Birkemeyer, Response in Ambient Low Temperature Plasma Ionization Compared to Electrospray and Atmospheric Pressure Chemical Ionization for Mass Spectrometry, Int J Anal Chem, 18 (2018) 5647536-5647553.

[169] F. Gosetti, E. Mazzucco, D. Zampieri, M.C. Gennaro, Signal suppression / enhancement in high-performance liquid chromatography tandem mass spectrometry, J Chromatogr A, 18 (2010) 3929-3937.

[170] L. Zheng, F. Zheng, Development and validation of an LC-APCI-MS/MS method for the determination of phenethyl isothiocyanate in human plasma, Biomed Chromatogr, 29 (2015) 619-625.

[171] J.B. Powers, S.R. Campagna, Design and Evaluation of a Gas Chromatograph-Atmospheric Pressure Chemical Ionization Interface for an Exactive Orbitrap Mass Spectrometer, J Am Soc Mass Spectrom, 11 (2019) 2369-2379.

[172] M. Karas, D. Bachmann, U. Bahr, F. Hillenkamp, Matrix-assisted ultraviolet laser desorption of non-volatile compounds, Int J Mass Spectrom Ion Proc, 78 (1987) 53-68.

[173] M. Karas, F. Hillenkamp, Matrix-assisted laser desorption/ionisation, an experience, Int J Mass Spectrom 200 (2000) 71-77.

[174] C.E. Costello, Time, life, and mass spectrometry. New techniques to address biological questions, Biophys Chem, 68 (1997) 173-188.

[175] Z. Takats, J.M. Wiseman, B. Gologan, R.G. Cooks, Mass spectrometry sampling under ambient conditions with desorption electrospray ionization, Science, 306 (2004) 471-473.

[176] R.G. Cooks, Z. Ouyang, Z. Takats, J.M. Wiseman, Detection Technologies. Ambient mass spectrometry, Science, 311 (2006) 1566-1570.

[177] C.S. Clendinen, M.E. Monge, F.M. Fernandez, Ambient mass spectrometry in metabolomics, Analyst, 142 (2017) 3101-3117.

[178] A.K. Jarmusch, V. Pirro, Z. Baird, E.M. Hattab, A.A. Cohen-Gadol, R.G. Cooks, Lipid and metabolite profiles of human brain tumors by desorption electrospray ionization-MS, Proc Natl Acad Sci U S A, 113 (2016) 1486-1491.

[179] A. Lubin, D. Cabooter, P. Augustijns, F. Cuyckens, One drop chemical derivatization--DESI-MS analysis for metabolite structure identification, J Mass Spectrom, 50 (2015) 871-878.

[180] H. Chen, Z. Pan, N. Talaty, D. Raftery, R.G. Cooks, Combining desorption electrospray ionization mass spectrometry and nuclear magnetic resonance for differential metabolomics without sample preparation, Rapid Commun Mass Spectrom, 20 (2006) 1577-1584.

[181] J.M. Wiseman, D.R. Ifa, Y. Zhu, C.B. Kissinger, N.E. Manicke, P.T. Kissinger, R.G. Cooks, Desorption electrospray ionization mass spectrometry: Imaging drugs and metabolites in tissues, Proc Natl Acad Sci U S A, 105 (2008) 18120-18125.

[182] M.C.McMaster, HPLC, a practical user's guide, Wiley, (2007).

[183] W.S. Sawyer, L. Wang, T. Uehara, P. Tamrakar, R. Prathapam, M. Mostafavi, L.E.t. Metzger, B. Feng, C.M. Baxter Rath, Targeted lipopolysaccharide biosynthetic intermediate analysis with normal-phase liquid chromatography mass spectrometry, PLoS One, 14 (2019) e0211803.

[184] J. Zhou, Y. Yin, Strategies for large-scale targeted metabolomics quantification by liquid chromatography-mass spectrometry, Analyst, 141 (2016) 6362-6373.

[185] Z.Z. Fang, F.J. Gonzalez, LC-MS-based metabolomics: an update, Arch Toxicol, 88 (2014) 1491-1502.

[186] D. Rojo, C. Barbas, F.J. Ruperez, LC-MS metabolomics of polar compounds, Bioanalysis, 4 (2012) 1235-1243.

[187] H. Farwanah, J. Wirtz, T. Kolter, K. Raith, R.H. Neubert, K. Sandhoff, Normal phase liquid chromatography coupled to quadrupole time of flight atmospheric pressure chemical ionization mass spectrometry for separation, detection and mass spectrometric profiling of neutral sphingolipids and cholesterol, J Chromatogr B Analyt Technol Biomed Life Sci, 877 (2009) 2976-2982.

[188] W.B. Wilson, H.V. Hayes, L.C. Sander, A.D. Campiglia, S.A. Wise, Normal-phase liquid chromatography retention behavior of polycyclic aromatic sulfur heterocycles and

alkyl-substituted polycyclic aromatic sulfur heterocycle isomers on an aminopropyl stationary phase, Anal Bioanal Chem, 410 (2018) 1511-1524.

[189] C.H. Grun, S. Besseau, Normal-phase liquid chromatography-atmospheric-pressure photoionization-mass spectrometry analysis of cholesterol and phytosterol oxidation products, J Chromatogr A, 25 (2016) 74-81.

[190] H. Poppe, Optimization of detectors for modern liquid chromatography, J Pharm Biomed Anal, 2 (1984) 233-240.

[191] N. Sillner, A. Walker, E.M. Harrieder, P. Schmitt-Kopplin, M. Witting, Development and application of a HILIC UHPLC-MS method for polar fecal metabolome profiling, J Chromatogr B Analyt Technol Biomed Life Sci, 1 (2019) 142-148.

[192] S. Arase, S. Kimura, T. Ikegami, Method optimization of hydrophilic interaction chromatography separation of nucleotides using design of experiment approaches I: Comparison of several zwitterionic columns, J Pharm Biomed Anal, 158 (2018) 307-316.

[193] R. Zhang, D.G. Watson, L. Wang, G.D. Westrop, G.H. Coombs, T. Zhang, Evaluation of mobile phase characteristics on three zwitterionic columns in hydrophilic interaction liquid chromatography mode for liquid chromatography-high resolution mass spectrometry based untargeted metabolite profiling of Leishmania parasites, J Chromatogr A, 3 (2014) 168-179.

[194] R.A. Sonnenberg, S. Naz, L. Cougnaud, D. Vuckovic, Comparison of underivatized silica and zwitterionic sulfobetaine hydrophilic interaction liquid chromatography stationary phases for global metabolomics of human plasma, J Chromatogr A, 8 (2019) 460419.

[195] P. Hemström, K. Irgum, Hydrophilic interaction chromatography, J Sep Sci, 29 (2006) 1784-1821.

[196] B. Buszewski, S. Noga, Hydrophilic interaction liquid chromatography (HILIC)--a powerful separation technique, Anal Bioanal Chem, 402 (2012) 231-247.

[197] P. Galeano Garcia, B.H. Zimmermann, C. Carazzone, Hydrophilic Interaction Liquid Chromatography Coupled to Mass Spectrometry and Multivariate Analysis of the De Novo Pyrimidine Pathway Metabolites, Biomolecules, 9 (2019) 328-342.

[198] D.Q. Tang, L. Zou, X.X. Yin, C.N. Ong, HILIC-MS for metabolomics: An attractive and complementary approach to RPLC-MS, Mass Spectrom Rev, 35 (2016) 574-600.

[199] K. Spagou, H. Tsoukali, N. Raikos, H. Gika, I.D. Wilson, G. Theodoridis, Hydrophilic interaction chromatography coupled to MS for metabonomic/metabolomic studies, J Sep Sci, 33 (2010) 716-727.

[200] L. Zhang, Q. Dai, X. Qiao, C. Yu, X. Qin, H. Yan, Mixed-mode chromatographic stationary phases: Recent advancements and its applications for high-performance liquid chromatography, TrAC Trends Anal Chem, 82 (2016) 143-163.

[201] Y. Yang, X. Geng, Mixed-mode chromatography and its applications to biopolymers, J Chromatogr A, 1218 (2011) 8813-8825.

[202] A.P. Vilches, S.H. Norström, D. Bylund, Direct analysis of free amino acids by mixed-mode chromatography with tandem mass spectrometry, J Sep Sci, 40 (2017) 1482-1492.

[203] M.S. Choi, S.U. Rehman, I.S. Kim, H.J. Park, M.Y. Song, H.H. Yoo, Development of a mixed-mode chromatography with tandem mass spectrometry method for the quantitative analysis of 23 underivatized amino acids in human serum, J Pharm Biomed Anal, 145 (2017) 52-58.

[204] H. Hinterwirth, M. Lämmerhofer, B. Preinerstorfer, A. Gargano, R. Reischl, W. Bicker, O. Trapp, L. Brecker, W. Lindner, Selectivity issues in targeted metabolomics: Separation of phosphorylated carbohydrate isomers by mixed-mode hydrophilic interaction/weak anion exchange chromatography, J Sep Sci, 33 (2010) 3273-3282.

[205] E. Apfelthaler, W. Bicker, M. Lämmerhofer, M. Sulyok, R. Krska, W. Lindner, R. Schuhmacher, Retention pattern profiling of fungal metabolites on mixed-mode reversed-phase/weak anion exchange stationary phases in comparison to reversed-phase and weak anion exchange separation materials by liquid chromatography-electrospray ionisation-tandem mass spectrometry, J Chromatogr A, 1191 (2008) 171-181.

[206] Y. Mu, Y. Zhou, Y. Wang, W. Li, L. Zhou, X. Lu, P. Gao, M. Gao, Y. Zhao, Q. Wang, G. Xu, Serum Metabolomics Study of Nonsmoking Female Patients with Non-Small Cell Lung Cancer Using Gas Chromatography-Mass Spectrometry, J Proteome Res, 18 (2019) 2175-2184.

[207] C.L. Silva, R. Perestrelo, P. Silva, H. Tomas, J.S. Camara, Volatile metabolomic signature of human breast cancer cell lines, Sci Rep, 7 (2017) 43969-43976.

[208] M.P. Papadimitropoulos, C.G. Vasilopoulou, C. Maga-Nteve, M.I. Klapa, Untargeted GC-MS Metabolomics, Methods Mol Biol, (2018) 133-147.

[209] K.K. Pasikanti, P.C. Ho, E.C. Chan, Gas chromatography/mass spectrometry in metabolic profiling of biological fluids, J Chromatogr B Analyt Technol Biomed Life Sci, 871 (2008) 202-211.

[210] L.N. Williamson, M.G. Bartlett, Quantitative gas chromatography/time-of-flight mass spectrometry: a review, Biomed Chromatogr, 21 (2007) 664-669.

[211] D.J. Beale, F.R. Pinu, K.A. Kouremenos, M.M. Poojary, V.K. Narayana, B.A. Boughton, K. Kanojia, S. Dayalan, O.A.H. Jones, D.A. Dias, Review of recent

developments in GC-MS approaches to metabolomics-based research, Metabolomics, 14 (2018) 152.

[212] A.I. Ruiz-Matute, O. Hernandez-Hernandez, S. Rodriguez-Sanchez, M.L. Sanz, I. Martinez-Castro, Derivatization of carbohydrates for GC and GC-MS analyses, J Chromatogr B Analyt Technol Biomed Life Sci, 879 (2011) 1226-1240.

[213] K. Singer, K. Dettmer, P. Unger, G. Schonhammer, K. Renner, K. Peter, P.J. Siska, M. Berneburg, W. Herr, P.J. Oefner, S. Karrer, M. Kreutz, E. Datz, Topical Diclofenac Reprograms Metabolism and Immune Cell Infiltration in Actinic Keratosis, Front Oncol, 9 (2019) 605-617.

[214] I. Hayek, F. Fischer, J. Schulze-Luehrmann, K. Dettmer, K. Sobotta, V. Schatz, L. Kohl, K. Boden, R. Lang, P.J. Oefner, S. Wirtz, J. Jantsch, A. Luhrmann, Limitation of TCA Cycle Intermediates Represents an Oxygen-Independent Nutritional Antibacterial Effector Mechanism of Macrophages, Cell Rep, 26 (2019) 3502-3510.

[215] H.H. Chiu, C.H. Kuo, Gas chromatography-mass spectrometry-based analytical strategies for fatty acid analysis in biological samples, J Food Drug Anal, 28 (2020) 60-73.

[216] K. Schmidt, I. Podmore, Current Challenges in Volatile Organic Compounds Analysis as Potential Biomarkers of Cancer, J Biomark, 2015 (2015) 981458-981473.

[217] P. Fuchs, C. Loeseken, J.K. Schubert, W. Miekisch, Breath gas aldehydes as biomarkers of lung cancer, Int J Cancer, 126 (2010) 2663-2670.

[218] J. Rudnicka, T. Kowalkowski, T. Ligor, B. Buszewski, Determination of volatile organic compounds as biomarkers of lung cancer by SPME-GC-TOF/MS and chemometrics, J Chromatogr B Analyt Technol Biomed Life Sci, 879 (2011) 3360-3366.

[219] M. Phillips, R.N. Cataneo, T. Cheema, J. Greenberg, Increased breath biomarkers of oxidative stress in diabetes mellitus, Clin Chim Acta, 344 (2004) 189-194.

[220] X. Sun, K. Shao, T. Wang, Detection of volatile organic compounds (VOCs) from exhaled breath as noninvasive methods for cancer diagnosis, Anal Bioanal Chem, 408 (2016) 2759-2780.

[221] V. Gabelica, E. Marklund, Fundamentals of ion mobility spectrometry, Curr Opin Chem Biol, 42 (2018) 51-59.

[222] V. Gabelica, A.A. Shvartsburg, C. Afonso, P. Barran, J.L.P. Benesch, C. Bleiholder, M.T. Bowers, A. Bilbao, M.F. Bush, J.L. Campbell, I.D.G. Campuzano, T. Causon, B.H. Clowers, C.S. Creaser, E. De Pauw, J. Far, F. Fernandez-Lima, J.C. Fjeldsted, K. Giles, M. Groessl, C.J. Hogan, Jr., S. Hann, H.I. Kim, R.T. Kurulugama, J.C. May, J.A. McLean, K. Pagel, K. Richardson, M.E. Ridgeway, F. Rosu, F. Sobott, K. Thalassinos, S.J. Valentine, T. Wyttenbach, Recommendations for reporting ion mobility mass spectrometry measurements, Mass Spectrom Rev, 38 (2019) 291-320.

[223] R. Cumeras, E. Figueras, C.E. Davis, J.I. Baumbach, I. Gràcia, Review on ion mobility spectrometry. Part 1: current instrumentation, Analyst, 140 (2015) 1376-1390.

[224] A.A. Shvartsburg, R.D. Smith, Fundamentals of traveling wave ion mobility spectrometry, Anal Chem, 80 (2008) 9689-9699.

[225] A. Garabedian, P. Benigni, C.E. Ramirez, E.S. Baker, T. Liu, R.D. Smith, F. Fernandez-Lima, Towards Discovery and Targeted Peptide Biomarker Detection Using nanoESI-TIMS-TOF MS, J Am Soc Mass Spectrom, 29 (2018) 817-826.

[226] J.E. Kyle, N. Aly, X. Zheng, K.E. Burnum-Johnson, R.D. Smith, E.S. Baker, Evaluating lipid mediator structural complexity using ion mobility spectrometry combined with mass spectrometry, Bioanalysis, 10 (2018) 279-289.

[227] A.A. Shvartsburg, G. Isaac, N. Leveque, R.D. Smith, T.O. Metz, Separation and classification of lipids using differential ion mobility spectrometry, J Am Soc Mass Spectrom, 22 (2011) 1146-1155.

[228] R. Pérez-Míguez, B. Bruyneel, M. Castro-Puyana, M.L. Marina, G.W. Somsen, E. Domínguez-Vega, Chiral Discrimination of DL-Amino Acids by Trapped Ion Mobility Spectrometry after Derivatization with (+)-1-(9-Fluorenyl)ethyl Chloroformate, Anal Chem, 91 (2019) 3277-3285.

[229] K.M. Szykuła, J. Meurs, M.A. Turner, C.S. Creaser, J.C. Reynolds, Combined hydrophilic interaction liquid chromatography-scanning field asymmetric waveform ion mobility spectrometry-time-of-flight mass spectrometry for untargeted metabolomics, Anal Bioanal Chem, 411 (2019) 6309-6317.

[230] H. Maleki, A.K. Karanji, S. Majuta, M.M. Maurer, S.J. Valentine, Ion Mobility Spectrometry-Mass Spectrometry Coupled with Gas-Phase Hydrogen/Deuterium Exchange for Metabolomics Analyses, J Am Soc Mass Spectrom, 29 (2018) 230-241.

[231] S.N. Majuta, H. Maleki, A. Kiani Karanji, K. Attanyake, E. Loch, S.J. Valentine, Magnifying ion mobility spectrometry-mass spectrometry measurements for biomolecular structure studies, Curr Opin Chem Biol, 42 (2018) 101-110.

[232] X. Zheng, R.D. Smith, E.S. Baker, Recent advances in lipid separations and structural elucidation using mass spectrometry combined with ion mobility spectrometry, ion-molecule reactions and fragmentation approaches, Curr Opin Chem Biol, 42 (2018) 111-118.

[233] P.D. Rainville, I.D. Wilson, J.K. Nicholson, G. Isaac, L. Mullin, J.I. Langridge, R.S. Plumb, Ion mobility spectrometry combined with ultra performance liquid chromatography/mass spectrometry for metabolic phenotyping of urine: Effects of column length, gradient duration and ion mobility spectrometry on metabolite detection, Anal Chim Acta, 982 (2017) 1-8.

[234] T.J. Causon, L. Si-Hung, K. Newton, R.T. Kurulugama, J. Fjeldsted, S. Hann, Fundamental study of ion trapping and multiplexing using drift tube-ion mobility time-of-flight mass spectrometry for non-targeted metabolomics, Anal Bioanal Chem, 411 (2019) 6265-6274.

[235] X. Zhang, K. Kew, R. Reisdorph, M. Sartain, R. Powell, M. Armstrong, K. Quinn, C. Cruickshank-Quinn, S. Walmsley, S. Bokatzian, E. Darland, M. Rain, K. Imatani, N. Reisdorph, Performance of a High-Pressure Liquid Chromatography-Ion Mobility-Mass Spectrometry System for Metabolic Profiling, Anal Chem, 89 (2017) 6384-6391.

[236] X. Zheng, N.A. Aly, Y. Zhou, K.T. Dupuis, A. Bilbao, V.L. Paurus, D.J. Orton, R. Wilson, S.H. Payne, R.D. Smith, E.S. Baker, A structural examination and collision cross section database for over 500 metabolites and xenobiotics using drift tube ion mobility spectrometry, Chem Sci, 8 (2017) 7724-7736.

[237] M. Sans, C.L. Feider, L.S. Eberlin, Advances in mass spectrometry imaging coupled to ion mobility spectrometry for enhanced imaging of biological tissues, Curr Opin Chem Biol, 42 (2018) 138-146.

[238] A.T. van der Goot, W. Zhu, R.P. Vazquez-Manrique, R.I. Seinstra, K. Dettmer, H. Michels, F. Farina, J. Krijnen, R. Melki, R.C. Buijsman, M. Ruiz Silva, K.L. Thijssen, I.P. Kema, C. Neri, P.J. Oefner, E.A. Nollen, Delaying aging and the aging-associated decline in protein homeostasis by inhibition of tryptophan degradation, Proc Natl Acad Sci U S A, 109 (2012) 14912-14917.

[239] K. Dettmer, N. Nurnberger, H. Kaspar, M.A. Gruber, M.F. Almstetter, P.J. Oefner, Metabolite extraction from adherently growing mammalian cells for metabolomics studies: optimization of harvesting and extraction protocols, Anal Bioanal Chem, 399 (2011) 1127-1139.

[240] A. Masood, K.D. Stark, N. Salem, Jr., A simplified and efficient method for the analysis of fatty acid methyl esters suitable for large clinical studies, J Lipid Res, 46 (2005) 2299-2305.

[241] M. Jain, R. Nilsson, S. Sharma, N. Madhusudhan, T. Kitami, A.L. Souza, R. Kafri, M.W. Kirschner, C.B. Clish, V.K. Mootha, Metabolite profiling identifies a key role for glycine in rapid cancer cell proliferation, Science, 336 (2012) 1040-1044.

[242] D. Giustarini, I. Dalle-Donne, R. Colombo, A. Milzani, R. Rossi, An improved HPLC measurement for GSH and GSSG in human blood, Free Radic Biol Med, 35 (2003) 1365-1372.

[243] L. Hakuna, B. Doughan, J.O. Escobedo, R.M. Strongin, A simple assay for glutathione in whole blood, Analyst, 140 (2015) 3339-3342.

[244] S. Bravo-Veyrat, G. Hopfgartner, High-throughput liquid chromatography differential mobility spectrometry mass spectrometry for bioanalysis: determination of reduced and oxidized form of glutathione in human blood, Anal Bioanal Chem, 410 (2018) 7153-7161.

[245] L. Blahova, J. Kohoutek, J. Lebedova, L. Blaha, Z. Vecera, M. Buchtova, I. Misek, K. Hilscherova, Simultaneous determination of reduced and oxidized glutathione in tissues by a novel liquid chromatography-mass spectrometry method: application in an inhalation study of Cd nanoparticles, Anal Bioanal Chem, 406 (2014) 5867-5876.

[246] D. Giustarini, I. Dalle-Donne, D. Tsikas, R. Rossi, Oxidative stress and human diseases: Origin, link, measurement, mechanisms, and biomarkers, Crit Rev Clin Lab Sci, 46 (2009) 241-281.

[247] I. Dalle-Donne, R. Rossi, R. Colombo, D. Giustarini, A. Milzani, Biomarkers of oxidative damage in human disease, Clin Chem, 52 (2006) 601-623.

[248] Guidance for industry: bioanalytical method validation, (2001).

[249] I.H. Shaik, R. Mehvar, Rapid determination of reduced and oxidized glutathione levels using a new thiol-masking reagent and the enzymatic recycling method: application to the rat liver and bile samples, Anal Bioanal Chem, 385 (2006) 105-113.

[250] I. Marchiq, R. Le Floch, D. Roux, M.P. Simon, J. Pouyssegur, Genetic disruption of lactate/H+ symporters (MCTs) and their subunit CD147/BASIGIN sensitizes glycolytic tumor cells to phenformin, Cancer Res, 75 (2015) 171-180.

[251] J.R. Doherty, C. Yang, K.E. Scott, M.D. Cameron, M. Fallahi, W. Li, M.A. Hall, A.L. Amelio, J.K. Mishra, F. Li, M. Tortosa, H.M. Genau, R.J. Rounbehler, Y. Lu, C.V. Dang, K.G. Kumar, A.A. Butler, T.D. Bannister, A.T. Hooper, K. Unsal-Kacmaz, W.R. Roush, J.L. Cleveland, Blocking lactate export by inhibiting the Myc target MCT1 Disables glycolysis and glutathione synthesis, Cancer Res, 74 (2014) 908-920.

[252] C.S. Hong, N.A. Graham, W. Gu, C. Espindola Camacho, V. Mah, E.L. Maresh, M. Alavi, L. Bagryanova, P.A.L. Krotee, B.K. Gardner, I.S. Behbahan, S. Horvath, D. Chia, I.K. Mellinghoff, S.A. Hurvitz, S.M. Dubinett, S.E. Critchlow, S.K. Kurdistani, L. Goodglick, D. Braas, T.G. Graeber, H.R. Christofk, MCT1 Modulates Cancer Cell Pyruvate Export and Growth of Tumors that Co-express MCT1 and MCT4, Cell Rep, 14 (2016) 1590-1601.

[253] D. Anastasiou, G. Poulogiannis, J.M. Asara, M.B. Boxer, J.K. Jiang, M. Shen, G. Bellinger, A.T. Sasaki, J.W. Locasale, D.S. Auld, C.J. Thomas, M.G. Vander Heiden, L.C. Cantley, Inhibition of pyruvate kinase M2 by reactive oxygen species contributes to cellular antioxidant responses, Science, 334 (2011) 1278-1283.

[254] N.M. Gruning, D. Du, M.A. Keller, B.F. Luisi, M. Ralser, Inhibition of triosephosphate isomerase by phosphoenolpyruvate in the feedback-regulation of glycolysis, Open Biol, 4 (2014) 130232-130242.

[255] Y. Contreras-Baeza, P.Y. Sandoval, R. Alarcon, A. Galaz, F. Cortes-Molina, K. Alegria, F. Baeza-Lehnert, R. Arce-Molina, A. Guequen, C.A. Flores, A. San Martin, L.F. Barros, Monocarboxylate transporter 4 (MCT4) is a high affinity transporter capable of exporting lactate in high-lactate microenvironments, J Biol Chem, 294 (2019) 20135-20147.

[256] A. Stincone, A. Prigione, T. Cramer, M.M. Wamelink, K. Campbell, E. Cheung, V. Olin-Sandoval, N.M. Gruning, A. Kruger, M. Tauqeer Alam, M.A. Keller, M. Breitenbach, K.M. Brindle, J.D. Rabinowitz, M. Ralser, The return of metabolism: biochemistry and physiology of the pentose phosphate pathway, Biol Rev Camb Philos Soc, 90 (2015) 927-963.

[257] R.S. Berger, Development and application of analytical tools to study the origin, fate and impact of the oncometabolite 2-hydroxyglutarate and its lactone, Dissertation, University of Regensburg, Germany.

[258] S. Borra, D.E. Featherstone, S.A. Shippy, Total cysteine and glutathione determination in hemolymph of individual adult D. melanogaster, Anal Chim Acta, 853 (2015) 660-667.

[259] E.B. Getz, M. Xiao, T. Chakrabarty, R. Cooke, P.R. Selvin, A comparison between the sulfhydryl reductants tris(2-carboxyethyl)phosphine and dithiothreitol for use in protein biochemistry, Anal Biochem, 273 (1999) 73-80.

[260] I.K. Abukhalaf, N.A. Silvestrov, J.M. Menter, D.A. von Deutsch, M.A. Bayorh, R.R. Socci, A.A. Ganafa, High performance liquid chromatographic assay for the quantitation of total glutathione in plasma, J Pharm Biomed Anal, 28 (2002) 637-643.

[261] H.H. Bailey, L-S,R-buthionine sulfoximine: historical development and clinical issues, Chem Biol Interact, 112 (1998) 239-254.

[262] O.W. Griffith, A. Meister, Potent and specific inhibition of glutathione synthesis by buthionine sulfoximine (S-n-butyl homocysteine sulfoximine), J Biol Chem, 254 (1979) 7558-7560.

[263] M. Khurshed, R.J. Molenaar, K. Lenting, W.P. Leenders, C.J.F. van Noorden, In silico gene expression analysis reveals glycolysis and acetate anaplerosis in IDH1 wild-type glioma and lactate and glutamate anaplerosis in IDH1-mutated glioma, Oncotarget, 8 (2017) 49165-49177.

[264] D.A. Mustafa, S.M. Swagemakers, L. Buise, P.J. van der Spek, J.M. Kros, Metabolic alterations due to IDH1 mutation in glioma: opening for therapeutic opportunities?, Acta Neuropathol Commun, 2 (2014) 6.

[265] K. Tateishi, H. Wakimoto, A.J. Iafrate, S. Tanaka, F. Loebel, N. Lelic, D. Wiederschain, O. Bedel, G. Deng, B. Zhang, T. He, X. Shi, R.E. Gerszten, Y. Zhang, J.J. Yeh, W.T. Curry, D. Zhao, S. Sundaram, F. Nigim, M.V.A. Koerner, Q. Ho, D.E. Fisher, E.M. Roider, L.V. Kemeny, Y. Samuels, K.T. Flaherty, T.T. Batchelor, A.S. Chi, D.P. Cahill, Extreme Vulnerability of IDH1 Mutant Cancers to NAD+ Depletion, Cancer Cell, 28 (2015) 773-784.

[266] S.J. Parker, C.M. Metallo, Metabolic consequences of oncogenic IDH mutations, Pharmacol Ther, 152 (2015) 54-62.

[267] K. Jing, K. Lim, Why is autophagy important in human diseases?, Exp Mol Med, 44 (2012) 69-72.

[268] M.R. Gilbert, Y. Liu, J. Neltner, H. Pu, A. Morris, M. Sunkara, T. Pittman, N. Kyprianou, C. Horbinski, Autophagy and oxidative stress in gliomas with IDH1 mutations, Acta Neuropathol, 127 (2014) 221-233.

[269] R.J. DeBerardinis, Proliferating Cells Conserve Nitrogen to Support Growth, Cell Metab, 23 (2016) 957-958.

[270] S.M. Fendt, E.L. Bell, M.A. Keibler, B.A. Olenchock, J.R. Mayers, T.M. Wasylenko, N.I. Vokes, L. Guarente, M.G. Vander Heiden, G. Stephanopoulos, Reductive glutamine metabolism is a function of the alpha-ketoglutarate to citrate ratio in cells, Nat Commun, 4 (2013) 2236-2256.

[271] E.L. Lieu, T. Nguyen, S. Rhyne, J. Kim, Amino acids in cancer, Exp Mol Med, 52 (2020) 15-30.

[272] K.E.R. Hollinshead, H. Munford, K.L. Eales, C. Bardella, C. Li, C. Escribano-Gonzalez, A. Thakker, Y. Nonnenmacher, K. Kluckova, M. Jeeves, R. Murren, F. Cuozzo, D. Ye, G. Laurenti, W. Zhu, K. Hiller, D.J. Hodson, W. Hua, I.P. Tomlinson, C. Ludwig, Y. Mao, D.A. Tennant, Oncogenic IDH1 Mutations Promote Enhanced Proline Synthesis through PYCR1 to Support the Maintenance of Mitochondrial Redox Homeostasis, Cell Rep, 22 (2018) 3107-3114.

[273] J.M. Phang, W. Liu, C.N. Hancock, J.W. Fischer, Proline metabolism and cancer: emerging links to glutamine and collagen, Curr Opin Clin Nutr Metab Care, 18 (2015) 71-77.

[274] J. De Ingeniis, M.D. Kazanov, K. Shatalin, M.S. Gelfand, A.L. Osterman, L. Sorci, Glutamine versus ammonia utilization in the NAD synthetase family, PLoS One, 7 (2012) e39115-39126.

[275] L.R. Gray, S.C. Tompkins, E.B. Taylor, Regulation of pyruvate metabolism and human disease, Cell Mol Life Sci, 71 (2014) 2577-2604.

[276] I. Amelio, F. Cutruzzola, A. Antonov, M. Agostini, G. Melino, Serine and glycine metabolism in cancer, Trends Biochem Sci, 39 (2014) 191-198.

[277] K. Snell, Enzymes of serine metabolism in normal, developing and neoplastic rat tissues, Adv Enzyme Regul, 22 (1984) 325-400.

[278] J.P. Murphy, M.A. Giacomantonio, J.A. Paulo, R.A. Everley, B.E. Kennedy, G.P. Pathak, D.R. Clements, Y. Kim, C. Dai, T. Sharif, S.P. Gygi, S. Gujar, The NAD(+) Salvage Pathway Supports PHGDH-Driven Serine Biosynthesis, Cell Rep, 24 (2018) 2381-2391.

[279] S.C. Kalhan, L.L. Gruca, P.S. Parimi, A. O'Brien, L. Dierker, E. Burkett, Serine metabolism in human pregnancy, Am J Physiol Endocrinol Metab, 284 (2003) 733-740.

[280] S.C. Kalhan, R.W. Hanson, Resurgence of serine: an often neglected but indispensable amino acid, J Biol Chem, 287 (2012) 19786-19791.

[281] I. Romero, J. Tellez, L.E. Yamanaka, M. Steindel, A.J. Romanha, E.C. Grisard, Transsulfuration is an active pathway for cysteine biosynthesis in *Trypanosoma rangeli*, Parasit Vectors, 7 (2014) 197-207.

[282] A.R. Mullen, W.W. Wheaton, E.S. Jin, P.H. Chen, L.B. Sullivan, T. Cheng, Y. Yang, W.M. Linehan, N.S. Chandel, R.J. DeBerardinis, Reductive carboxylation supports growth in tumour cells with defective mitochondria, Nature, 481 (2011) 385-388.

[283] C.M. Metallo, P.A. Gameiro, E.L. Bell, K.R. Mattaini, J. Yang, K. Hiller, C.M. Jewell, Z.R. Johnson, D.J. Irvine, L. Guarente, J.K. Kelleher, M.G. Vander Heiden, O. Iliopoulos, G. Stephanopoulos, Reductive glutamine metabolism by IDH1 mediates lipogenesis under hypoxia, Nature, 481 (2011) 380-384.

[284] J.L. Izquierdo-Garcia, P. Viswanath, P. Eriksson, L. Cai, M. Radoul, M.M. Chaumeil, M. Blough, H.A. Luchman, S. Weiss, J.G. Cairncross, J.J. Phillips, R.O. Pieper, S.M. Ronen, IDH1 Mutation Induces Reprogramming of Pyruvate Metabolism, Cancer Res, 75 (2015) 2999-3009.

[285] F. Rohrig, A. Schulze, The multifaceted roles of fatty acid synthesis in cancer, Nat Rev Cancer, 16 (2016) 732-749.

[286] F.V. Filipp, D.A. Scott, Z.A. Ronai, A.L. Osterman, J.W. Smith, Reverse TCA cycle flux through isocitrate dehydrogenases 1 and 2 is required for lipogenesis in hypoxic melanoma cells, Pigment Cell Melanoma Res, 25 (2012) 375-383.

[287] R. Leonardi, C. Subramanian, S. Jackowski, C.O. Rock, Cancer-associated isocitrate dehydrogenase mutations inactivate NADPH-dependent reductive carboxylation, J Biol Chem, 287 (2012) 14615-14620.

[288] J. Fan, J.J. Kamphorst, J.D. Rabinowitz, T. Shlomi, Fatty acid labeling from glutamine in hypoxia can be explained by isotope exchange without net reductive isocitrate dehydrogenase (IDH) flux, J Biol Chem, 288 (2013) 31363-31369.

[289] K. Bensaad, E. Favaro, C.A. Lewis, B. Peck, S. Lord, J.M. Collins, K.E. Pinnick, S. Wigfield, F.M. Buffa, J.L. Li, Q. Zhang, M.J.O. Wakelam, F. Karpe, A. Schulze, A.L. Harris, Fatty acid uptake and lipid storage induced by HIF-1alpha contribute to cell growth and survival after hypoxia-reoxygenation, Cell Rep, 9 (2014) 349-365.

[290] M.G. Badur, T. Muthusamy, S.J. Parker, S. Ma, S.K. McBrayer, T. Cordes, J.H. Magana, K.L. Guan, C.M. Metallo, Oncogenic R132 IDH1 Mutations Limit NADPH for De Novo Lipogenesis through (D)2-Hydroxyglutarate Production in Fibrosarcoma Sells, Cell Rep, 25 (2018) 1018-1026.

[291] M. Jain, R. Nilsson, S. Sharma, N. Madhusudhan, T. Kitami, A.L. Souza, R. Kafri, M.W. Kirschner, C.B. Clish, V.K. Mootha, Metabolite Profiling Identifies a Key Role for Glycine in Rapid Cancer Cell Proliferation, Science, 336 (2012) 1040-1044.

[292] S.A. Comerford, Z. Huang, X. Du, Y. Wang, L. Cai, A.K. Witkiewicz, H. Walters, M.N. Tantawy, A. Fu, H.C. Manning, J.D. Horton, R.E. Hammer, S.L. McKnight, B.P. Tu, Acetate dependence of tumors, Cell, 159 (2014) 1591-1602.

[293] J.J. Kamphorst, M.K. Chung, J. Fan, J.D. Rabinowitz, Quantitative analysis of acetyl-CoA production in hypoxic cancer cells reveals substantial contribution from acetate, Cancer Metab, 2 (2014) 23-30.

11 Supplementary information

Table S1. Parameters used for amino acid isotopologue detection in MRM mode by HPLC-ESI-QqQ-MS/MS. The numbers next to each amino acid represent the mass shift for the precursor and product ion, respectively, *e.g.*, Glu_4.3 represents a mass shift of 4 in the precursor ion and 3 in the product ion in a glutamate molecule.

ID	Q1 Mass (Da)	Q3 Mass (Da)	Time (msec)	DP (volts)	CE (volts)	CXP (volts)
Arg_0.0	303.200	243.000	40	26	25	14
Ser_0.0	234.130	174.080	40	50	14	10
Ser_1.0	235.130	175.080	40	50	14	10
Ser_2.0	236.130	176.080	40	50	14	10
Ser_3.0	237.130	177.080	40	50	14	10
Asn_0.0	243.130	157.100	40	66	14	11
Asn_1.1	244.130	158.100	40	66	14	11
Asn_2.2	245.130	159.100	40	66	14	11
Asn_3.3	246.130	160.100	40	66	14	11
Asn_4.4	247.130	161.100	40	66	14	11
Gly_0.0	204.120	144.070	40	56	12	12
Gly_1.1	205.120	145.070	40	56	12	12
Gly_2.2	206.120	146.070	40	56	12	12
Ala_0.0	218.13	130.09	40	59	17	10
Arg_1.1	304.200	244.000	40	26	25	14
Arg_2.2	305.200	245.000	40	26	25	14
Arg_3.3	306.200	246.000	40	26	25	14
Arg_4.4	307.200	247.000	40	26	25	14
Arg_5.5	308.200	248.000	40	26	25	14
Arg_6.6	309.200	249.000	40	26	25	14
Ala_1.0	219.130	130.090	40	59	17	10
Ala_1.1	219.130	131.090	40	59	17	10
Ala_2.1	220.130	131.090	40	59	17	10
Pro_0.0	244.150	184.100	40	50	12	10
Orn_0.0	347.120	287.160	40	67	14	8
Orn_1.1	348.210	288.160	40	67	14	8
Orn_2.2	349.120	289.160	40	67	14	8
Orn_3.3	350.120	290.160	40	67	14	8
Orn_4.4	351.120	291.160	40	67	14	8
Orn_5.5	352.120	292.160	40	67	14	8
Asp_0.0	304.170	216.120	40	61	18	11
Glu_0.0	318.180	230.140	40	64	18	12
Glu_5.4	323.180	234.140	40	64	18	12
Glu_4.3	322.180	233.140	40	64	18	12
Glu_4.4	322.180	234.140	40	64	18	12
Glu_3.3	321.180	233.140	40	64	18	12
Glu_3.2	321.180	232.140	40	64	18	12
Glu_2.2	320.180	232.140	40	64	18	12
Glu_2.1	320.180	231.140	40	64	18	12
Glu_1.1	319.180	231.140	40	64	18	12
Glu_1.0	319.180	231.140	40	64	18	12
Pro_1.1	245.150	185.100	40	50	12	10
Pro_2.2	246.150	186.100	40	50	12	10
Pro_3.3	247.150	187.100	40	50	12	10
Pro_4.4	248.150	188.100	40	50	12	10
Pro_5.5	249.150	189.100	40	50	12	10
Asp_1.0	305.170	216.120	40	61	18	11
Asp_1.1	305.170	217.120	40	61	18	11
Asp_2.1	306.170	217.120	40	61	18	11
Asp_2.2	306.170	218.120	40	61	18	11
Asp_3.2	307.170	218.120	40	61	18	11
Asp_3.3	307.170	219.120	40	61	18	11
Asp_4.3	308.170	219.120	40	61	18	11

Table S2. Density of HCT116 cells seeded per well for each cell line in 6-well plates.

Cell culture time	wild type	IDH1-R132H	IDH2-R172K / IDH2-R140Q
0h	380,000	400,000	380,000
12h	300,000	350,000	300,000
24h	300,000	350,000	250,000
48h	200,000	300,000	200,000
72h	150,000	200,000	150,000

Table S3. "Analysis of variance (ANOVA) of GSH/GSSG ratio between MCT-competent and MCT-deficient LS174T cells under normal or H_2O_2 treatment conditions was performed in R (version 3.5.1). Pairwise comparisons between cell lines under each condition were performed with Tukey's post hoc test. A paired t-test (EXCEL 2013) was used to test the impact of H_2O_2 treatment in each cell line. A p-value of less than 0.05 was statistically significant. n.s., not significant." *(Sun et al., in submission)*

Normal condition (overall p-value = 0.0004)				
	WT	*MCT1-/-*	*MCT4-/-*	*MCT1-/- MCT4-/-*
WT	--	--	--	--
MCT1-/-	n.s.	--	--	--
MCT4-/-	n.s.	n.s.	--	--
MCT1-/- MCT4-/-	0.0016	0.0027	0.0011	--
H_2O_2 treatment (overall p-value = 4.86E-05)				
	WT	*MCT1-/-*	*MCT4-/-*	*MCT1-/- MCT4-/-*
WT	--	--	--	--
MCT1-/-	n.s.	--	--	--
MCT4-/-	3.40E-05	0.0037	--	--
MCT1-/- MCT4-/-	0.0022	n.s.	0.0014	--
Normal condition versus H_2O_2 treatment				
	WT	*MCT1-/-*	*MCT4-/-*	*MCT1-/- MCT4-/-*
WT	9.73E-05	--	--	--
MCT1-/-	--	5.89E-05	--	--
MCT4-/-	--	--	3.61E-05	--
MCT1-/- MCT4-/-	--	--	--	1.05E-07

Table S4. "Analysis of variance (ANOVA) of pyruvate secretion, lactate release, glucose uptake, and intracellular glucose and G6P content between MCT-competent and MCT-deficient LS174T cells under normal conditions were performed in R (version 3.5.1). Pairwise comparisons between cell lines under each condition were performed with Tukey's post hoc test. A p-value of less than 0.05 was statistically significant. n.s., not significant." *(Sun et al., in submission)*

Under normal condition (overall p-value = 2.86×10^{-13}) – pyruvate secretion				
	WT	*MCT1-/-*	*MCT4-/-*	*MCT1-/- MCT4-/-*
WT	--	--	--	--
MCT1-/-	1.33×10^{-8}	--	--	--
MCT4-/-	9.38×10^{-5}	6.86×10^{-4}	--	--
MCT1-/- MCT4-/-	2.28×10^{-13}	1.33×10^{-8}	5.77×10^{-11}	--
Under normal condition (overall p-value = 9.67×10^{-9}) – lactate release				
	WT	*MCT1-/-*	*MCT4-/-*	*MCT1-/- MCT4-/-*
WT	--	--	--	--
MCT1-/-	n.s	--	--	--
MCT4-/-	n.s	n.s	--	--
MCT1-/- MCT4-/-	1.57×10^{-7}	5.33×10^{-8}	1.19×10^{-7}	--
Under normal condition (overall p-value = 1.29×10^{-9}) – glucose uptake				
	WT	*MCT1-/-*	*MCT4-/-*	*MCT1-/- MCT4-/-*
WT	--	--	--	--
MCT1-/-	n.s	--	--	--
MCT4-/-	n.s.	n.s.	--	--
MCT1-/- MCT4-/-	2.70×10^{-8}	4.67×10^{-8}	3.81×10^{-9}	--
Under normal condition (overall p-value = 2.43×10^{-6}) – intracellular glucose				
	WT	*MCT1-/-*	*MCT4-/-*	*MCT1-/- MCT4-/-*
WT	--	--	--	--
MCT1-/-	2.01×10^{-5}	--	--	--
MCT4-/-	n.s.	3.80×10^{-6}	--	--
MCT1-/- MCT4-/-	n.s.	2.90×10^{-4}	n.s.	--
Under normal condition (overall p-value = 2.81×10^{-5}) – intracellular G6P				
	WT	*MCT1-/-*	*MCT4-/-*	*MCT1-/- MCT4-/-*
WT	--	--	--	--
MCT1-/-	n.s.	--	--	--
MCT4-/-	n.s.	4.72×10^{-3}	--	--
MCT1-/- MCT4-/-	6.14×10^{-4}	1.62×10^{-2}	2.54×10^{-5}	--

Table S5. “Analysis of variance (ANOVA) of GSH/GSSG ratios between HCT116 cell lines was performed in R (version 3.5.1) with Tukey’s post hoc test. A p-value of less than 0.05 was statistically significant. n.s., not significant.” *(Sun et al., in submission)*

overall p-value = 0.0004				
	WT	IDH1-R132H	IDH2-R172K	IDH2-R140Q
WT	--	--	--	--
IDH1-R132H	0.0004	--	--	--
IDH2-R172K	0.0040	0.0021	--	--
IDH2-R140Q	0.0106	0.0004	n.s.	--

Table S6. “Analysis of variance (ANOVA) of peak area ratio between different measurement conditions (concentrations and Q1 window widths) was performed using the R/Bioconductor software package limma (version 3.4.1). P-values adjusted according to the method proposed by Benjamini and Hochberg of pairwise comparisons are given. Differences were considered significant, if the p-value was less than 0.05.” [3]

	179/182	**308/311**
10 µM 8 Da vs 10 Da	2.50E-12	7.45E-18
10 µM 8 Da vs 12 Da	6.66E-17	1.65E-22
10 µM 8 Da vs 20 Da	3.41E-17	3.28E-23
10 µM 10 Da vs 12 Da	2.59E-13	6.45E-19
10 µM 10 Da vs 20 Da	7.82E-14	3.82E-20
10 µM 12 Da vs 20 Da	2.34E-02	2.40E-10
20 µM 8 Da vs 10 Da	2.80E-20	3.23E-20
20 µM 8 Da vs 12 Da	1.62E-28	1.62E-28
20 µM 8 Da vs 20 Da	1.27E-29	1.27E-29
20 µM 10 Da vs 12 Da	3.81E-22	3.81E-22
20 µM 10 Da vs 20 Da	4.58E-24	1.63E-24
20 µM 12 Da vs 20 Da	1.82E-07	2.80E-09
40 µM 8 Da vs 10 Da	6.37E-13	9.75E-18
40 µM 8 Da vs 12 Da	7.01E-18	1.11E-22
40 µM 8 Da vs 20 Da	1.53E-18	1.50E-23
40 µM 10 Da vs 12 Da	2.18E-14	4.02E-19
40 µM 10 Da vs 20 Da	1.64E-15	1.34E-20
40 µM 12 Da vs 20 Da	1.56E-05	2.32E-11

Table S7. “RPMI 1640 medium components from PAN-Biotech website.”[3]

	Components	mg/L
Inorganic Salts	Calcium nitrate × $4H_2O$	100.00
	Potassium chloride	400.00
	Magnesium sulfate anhydrous	48.83
	Sodium chloride	6000.00
	di-Sodium hydrogen phosphate	800.49
Other Components	D(+)-Glucose anhydrous	2000.00
	Glutathione (red.)	1.00
	Phenol red	5.00
Amino acids	L-Arginine × HCl	241.86
	L-Asparagine × H_2O	50.00
	L-Aspartic acid	20.00
	L-Cystine × 2HCl	65.19
	L-Glutamine	0.00
	L-Glutamic acid	20.00
	Glycine	10.00
	L-Histidine × HCl × H_2O	20.27
	L-Hydroxyproline	20.00
	L-Isoleucine	50.00
	L-Leucine	50.00
	L-Lysine × HCl	40.00
	L-Methionine	15.00
	L-Phenylalanine	15.00
	L-Proline	20.00
	L-Serine	30.00
	L-Threonine	20.00
	L-Tryptophan	5.00
	L-Tyrosine × 2Na	28.83
	L-Valine	20.00
Vitamins	p-Aminobenzoic acid	1.00
	D-(+)-Biotin	0.20
	D-Calcium pantothenate	0.25
	Choline chloride	3.00
	Folic acid	1.00
	myo-Inositol	35.00
	Nicotinamide	1.00
	Pyridoxine × HCl	1.00
	Riboflavin	0.20
	Thiamine × HCl	1.00
	Vitamine B12	0.005

Table S8. “Analysis of variance (ANOVA) of isotopic mean enrichment of GSH between groups from the ^{13}C-tracer experiments was performed using the R/Bioconductor software package limma (version 3.4.1). P-values adjusted according to the method proposed by Benjamini and Hochberg of pairwise comparisons are given. Differences were considered significant, if the p-value was less than 0.05. No significant difference: n.s.” [3]

U-^{13}C-Glucose tracing (48 h)				
	Par ctrl vs par BSO	**Par ctrl vs 132H ctrl**	**Par BSO vs 132H BSO**	**132H ctrl vs 132H BSO**
GlyCys	6.10E-04	1.35E-06	2.56E-07	4.24E-03
CysGlu	2.55E-03	7.80E-06	9.49E-07	1.34E-02
GSH	1.93E-03	5.43E-06	1.55E-06	1.24E-02
U-^{13}C-Glutamine tracing (48 h)				
	Par ctrl vs par BSO	**Par ctrl vs 132H ctrl**	**Par BSO vs 132H BSO**	**132H ctrl vs 132H BSO**
CysGlu	*n.s.*	0.0401	*n.s.*	*n.s.*
GSH	*n.s.*	0.0401	*n.s.*	*n.s.*

Table S9. Analysis of variance (ANOVA) of isotopic mean enrichment of amino acids from U-^{13}C-glucose / glutamine tracing experiments were performed in R (version 3.5.1). Pairwise comparisons between cell lines were performed with Tukey’s post hoc test. A p-value of less than 0.05 was considered statistically significant.

U-^{13}C-Glucose tracing (wild-type)				
	Overall p-value	**12h vs 24h**	**24h vs 48h**	**48h vs 72h**
Alanine	1.48E-15	1.00E-08	6.00E-07	6.90E-01
Aspartate	4.96E-15	1.00E-08	1.10E-06	8.66E-01
Glutamate	2.96E-15	1.00E-08	8.00E-07	2.34E-01
Glycine	4.21E-07	2.49E-02	1.09E-01	3.59E-02
Proline	5.18E-13	2.20E-06	1.00E-06	2.76E-01
Serine	2.03E-14	1.13E-05	1.00E-08	3.33E-03
U-^{13}C-Glutamine tracing (wild-type)				
Aspartate	2.84E-10	4.63E-04	2.47E-04	1.23E-01
Glutamate	2.55E-08	4.38E-02	1.41E-03	1.50E-01
Proline	9.75E-11	9.11E-04	4.40E-06	9.33E-01
U-^{13}C-Glucose tracing (IDH1-R132H)				
Alanine	4.92E-09	1.84E-02	1.54E-03	3.00E-02
Aspartate	3.39E-10	4.69E-03	4.13E-04	7.74E-03
Glutamate	1.56E-15	7.20E-06	1.00E-07	2.00E-07
Glycine	5.61E-06	2.16E-01	4.41E-02	2.24E-02
Proline	6.42E-12	1.63E-02	9.60E-06	2.07E-04
Serine	1.50E-12	6.19E-03	1.00E-07	3.91E-02
U-^{13}C-Glutamine tracing (IDH1-R132H)				
Aspartate	2.00E-16	3.51E-03	0.00E+00	3.86E-04

Glutamate	3.52E-10	7.14E-01	1.33E-05	3.84E-03
Proline	9.36E-01	--	--	--
U-^{13}C-Glucose tracing (IDH2-R172K)				
Alanine	6.12E-15	2.00E-07	0.00E+00	3.32E-03
Aspartate	2.00E-16	2.00E-07	0.00E+00	0.00E+00
Glutamate	2.00E-16	2.12E-05	0.00E+00	0.00E+00
Glycine	7.28E-12	1.28E-04	7.05E-02	5.00E-07
Proline	1.25E-10	1.56E-02	1.24E-03	9.97E-05
Serine	7.29E-09	7.29E-09	1.19E-05	6.65E-01
U-^{13}C-Glutamine tracing (IDH2-R172K)				
Aspartate	2.00E-16	6.00E-07	0.00E+00	0.00E+00
Glutamate	4.81E-14	2.97E-01	5.00E-07	1.00E-07
Proline	6.85E-01	--	--	--
U-^{13}C-Glucose tracing (IDH2-R140Q)				
Alanine	1.49E-11	5.83E-05	2.73E-05	4.58E-02
Aspartate	8.55E-14	3.83E-04	3.00E-07	5.05E-05
Glutamate	1.61E-11	1.27E-02	2.63E-05	4.00E-04
Glycine	3.20E-07	3.39E-01	6.86E-02	3.15E-03
Proline	1.85E-08	2.69E-01	1.91E-03	9.58E-03
Serine	6.32E-11	1.88E-01	1.00E-06	7.14E-02
U-^{13}C-Glutamine tracing (IDH2-R140Q)				
Aspartate	2.24E-16	3.00E-07	0.00E+00	5.20E-06
Glutamate	2.00E-16	1.12E-03	0.00E+00	0.00E+00
Proline	9.40E-01	--	--	--

Table S10. Analysis of variance (ANOVA) of isotopic mean enrichment of organic acids from U-^{13}C-glucose / glutamine tracing experiments were performed in R (version 3.5.1). Pairwise comparisons between cell lines were performed with Tukey's post hoc test. A p-value of less than 0.05 was considered statistically significant.

U-^{13}C-Glucose tracing (wild-type)				
	Overall p-value	**12h vs 24h**	**24h vs 48h**	**48h vs 72h**
Pyruvate	4.41E-08	4.45E-05	1.83E-01	7.76E-01
Lactate	1.85E-10	1.00E-07	2.26E-01	7.00E-01
Succinate	9.06E-04	6.43E-02	2.05E-01	1.11E-02
Fumarate	2.19E-15	1.00E-08	8.10E-06	1.48E-01
Malate	8.88E-12	2.00E-07	1.93E-04	9.78E-01
Citrate	1.37E-14	1.00E-08	3.60E-05	7.58E-01
α-KG	7.90E-06	2.57E-03	2.49E-01	9.76E-01
Glycerol-3-P	2.00E-16	1.00E-08	1.00E-08	4.50E-06
2-HG	2.53E-03	4.33E-02	4.49E-02	4.98E-02
U-^{13}C-Glutamine tracing (wild-type)				
Succinate	2.23E-02	9.95E-01	3.64E-01	7.81E-01
Fumarate	1.07E-05	4.67E-01	1.62E-02	3.60E-01
Malate	1.07E-07	2.39E-01	8.60E-04	3.25E-01

Citrate	6.64E-05	2.05E-01	8.58E-02	7.56E-01
α-KG	1.32E-03	1.26E-01	9.74E-01	1.82E-01
2-HG	7.02E-03	7.26E-01	3.23E-01	8.58E-01
U-^{13}C-Glucose tracing (IDH1-R132H)				
Pyruvate	6.17E-02	--	--	--
Lactate	9.51E-06	3.87E-03	7.35E-01	2.40E-01
Succinate	1.26E-04	5.46E-02	6.92E-01	2.56E-02
Fumarate	2.64E-13	2.97E-03	9.00E-07	2.49E-05
Malate	2.40E-09	4.35E-03	1.33E-03	4.96E-02
Citrate	1.68E-06	1.95E-03	1.99E-01	4.66E-02
α-KG	3.42E-09	2.12E-01	8.86E-03	1.67E-04
Glycerol-3-P	2.21E-15	1.00E-16	1.00E-07	1.32E-01
2-HG	6.92E-14	3.08E-05	1.10E-06	4.74E-05
U-^{13}C-Glutamine tracing (IDH1-R132H)				
Succinate	5.60E-05	9.99E-01	2.94E-03	9.62E-01
Fumarate	6.07E-06	9.53E-01	9.01E-03	8.81E-02
Malate	3.04E-10	8.74E-01	1.00E-07	8.67E-02
Citrate	1.82E-07	9.83E-01	1.93E-04	2.51E-01
α-KG	1.68E-04	6.67E-01	1.54E-03	9.82E-01
2-HG	9.08E-05	1.77E-03	2.68E-01	7.97E-03
U-^{13}C-Glucose tracing (IDH2-R172K)				
Pyruvate	3.29E-01	--	--	--
Lactate	3.60E-09	2.35E-04	7.90E-04	9.31E-01
Succinate	6.16E-05	8.90E-01	9.07E-02	1.03E-02
Fumarate	1.15E-09	1.05E-01	4.37E-03	1.49E-04
Malate	1.21E-12	2.47E-04	9.51E-05	1.18E-05
Citrate	1.49E-11	2.10E-06	3.53E-04	1.38E-02
α-KG	4.13E-10	4.67E-02	7.19E-04	5.60E-04
Glycerol-3-P	1.04E-10	1.18E-05	1.79E-04	3.02E-01
2-HG	2.00E-16	0.00E+00	0.00E+00	0.00E+00
U-^{13}C-Glutamine tracing (IDH2-R172K)				
Succinate	5.48E-03	9.74E-01	5.91E-01	2.47E-01
Fumarate	1.90E-11	2.44E-02	1.69E-04	2.75E-05
Malate	3.35E-10	2.94E-02	2.98E-03	1.06E-04
Citrate	4.16E-11	5.49E-01	8.40E-06	2.54E-04
α-KG	1.97E-07	4.70E-01	8.25E-04	4.71E-03
2-HG	1.99E-12	0.00E+00	1.88E-01	0.00E+00
U-^{13}C-Glucose tracing (IDH2-R140Q)				
Pyruvate	8.88E-04	7.16E-01	1.16E-02	7.76E-01
Lactate	4.36E-09	4.71E-05	1.03E-02	7.05E-01
Succinate	1.73E-04	7.03E-01	9.93E-01	2.16E-03
Fumarate	4.29E-11	5.28E-04	1.62E-04	5.20E-04
Malate	1.09E-10	6.12E-03	1.68E-04	2.49E-03
Citrate	6.29E-09	8.93E-03	3.23E-04	3.14E-02
α-KG	2.46E-11	8.31E-02	4.80E-06	2.55E-04
Glycerol-3-P	1.05E-10	5.70E-06	3.28E-04	2.50E-01
2-HG	1.51E-13	2.46E-04	2.05E-05	1.00E-06
U-^{13}C-Glutamine tracing (IDH2-R140Q)				
Succinate	2.29E-01	--	--	--

Fumarate	1.88E-08	6.52E-01	1.59E-04	7.10E-02
Malate	1.04E-14	3.98E-01	0.00E+00	4.90E-06
Citrate	3.94E-08	6.16E-01	1.47E-04	6.49E-03
α-KG	2.20E-04	9.93E-01	2.02E-02	3.71E-01
2-HG	6.46E-05	2.41E-02	5.15E-01	1.16E-03

Table S11. Analysis of variance (ANOVA) of isotopic mean enrichment of glutathione from U-^{13}C-glucose / glutamine tracing experiments were performed in R (version 3.5.1). Pairwise comparisons between cell lines were performed with Tukey's post hoc test. A p-value of less than 0.05 was considered statistically significant.

U-^{13}C-Glucose tracing				
	Overall p-value	**12h vs 24h**	**24h vs 48h**	**48h vs 72h**
Wild-type	2.00E-16	1.00E-16	1.00E-16	3.08E-04
IDH1-R132H	2.00E-16	2.00E-16	2.00E-16	2.00E-16
IDH2-R172K	2.00E-16	2.00E-16	2.00E-16	2.00E-16
IDH2-R140Q	2.00E-16	3.00E-06	2.00E-16	2.34E-05
U-^{13}C-Glutamine tracing				
Wild-type	8.54E-05	1.91E-04	9.84E-01	6.20E-02
IDH1-R132H	1.66E-11	2.00E-16	9.65E-01	3.00E-07
IDH2-R172K	2.00E-16	2.00E-16	2.00E-01	2.00E-16
IDH2-R140Q	3.80E-10	2.00E-16	3.49E-01	1.00E-07

Table S12. Analysis of variance (ANOVA) of isotopic mean enrichment and isotopologues of amino acids from U-^{13}C-glucose / glutamine tracing experiments were performed in R (version 3.5.1). Pairwise comparisons between cell lines were performed with Tukey's post hoc test. A p-value of less than 0.05 was considered statistically significant.

U-^{13}C-Glucose tracing 48 h (mean enrichment)							
	overall p-value	**wt vs 132H**	**wt vs 172K**	**wt vs 140Q**	**132H vs 172K**	**132H vs 140Q**	**172K vs 140Q**
Ala	4.03E-05	1.73E-05	6.54E-03	4.29E-02	--	1.07E-02	--
Asp	9.58E-04	2.34E-02	4.89E-04	--	--	--	--
Glu	1.17E-03	3.64E-02	1.83E-03	--	--	--	9.73E-03
Gly	2.49E-03	--	--	1.67E-03	--	2.86E-02	3.47E-02
Pro	1.10E-05	--	8.70E-06	--	3.04E-03	--	1.74E-04
Ser	1.75E-02	4.46E-02	--	--	--	1.74E-02	--
U-^{13}C-Glucose tracing 48 h (isotopologues)							
m0_Ala	1.89E-04	9.75E-05	3.32E-02	--	--	8.07E-03	--
m1_Ala	2.40E-03	1.18E-01	1.66E-03	1.95E-02	--	--	--
m3_Ala	4.82E-05	2.42E-05	5.48E-03	--	--	7.14E-03	--
m0_Glu	5.62E-07	3.79E-03	2.00E-07	3.43E-03	7.76E-04	--	8.58E-04

m2_Glu	4.16E-07	5.99E-03	5.60E-06	--	2.38E-02	7.78E-04	9.00E-07
m3_Glu	1.06E-08	2.27E-04	1.00E-08	2.60E-06	1.05E-04	--	1.16E-02
m4_Glu	3.02E-06	1.98E-03	1.50E-06	2.18E-04	1.68E-02	--	--
m5_Glu	8.44E-06	4.65E-03	8.10E-06	9.69E-05	4.38E-02	--	--
m0_Asp	1.72E-04	2.37E-02	7.52E-05	1.28E-02	--	--	--
m1_Asp	1.44E-06	--	2.14E-05	6.90E-06	1.67E-03	4.90E-04	--
m2_Asp	7.38E-07	4.43E-04	3.00E-07	3.98E-04	1.03E-02	--	1.15E-02
m3_Asp	2.51E-02	--	2.14E-02	--	--	--	--
m4_Asp	2.42E-03	--	1.28E-03	--	--	--	--
U-^{13}C-Glutamine tracing 12 h (mean enrichment)							
	overall p-value	**wt vs 132H**	**wt vs 172K**	**wt vs 140Q**	**132H vs 172K**	**132H vs 140Q**	**172K vs 140Q**
Asp	8.98E-07	2.33E-04	3.49E-05	--	--	7.04E-05	1.11E-05
Glu	2.12E-07	2.30E-06	7.00E-07	2.49E-02	--	2.13E-03	5.05E-04
U-^{13}C-Glutamine tracing 12 h (isotopologues)							
m0_Glu	8.66E-10	1.00E-11	1.00E-11	7.22E-04	--	2.27E-05	6.39E-05
m5_Glu	3.55E-07	1.15E-05	1.00E-06	--	--	1.68E-03	1.15E-04
m0_Asp	4.07E-07	1.08E-04	3.51E-05	--	--	1.79E-05	6.10E-06
m1_Asp	1.39E-03	3.94E-03	--	--	3.21E-03	8.34E-03	--
m2_Asp	1.30E-02	--	--	--	--	1.26E-02	--
m3_Asp	2.66E-06	1.00E-06	1.21E-02	2.59E-03	1.70E-03	7.99E-03	--
m4_Asp	2.49E-06	1.75E-04	4.19E-05	--	--	2.99E-04	7.05E-05
m5 Pro/m5 Glu	1.06E-04	5.12E-05	1.45E-02	4.98E-03	8.93E-02	2.11E-01	9.63E-01

Table S13. Analysis of variance (ANOVA) of isotopic mean enrichment and isotopologues of GSH from U-^{13}C-glucose / glutamine tracing experiments were performed in R (version 3.5.1). Pairwise comparisons between cell lines were performed with Tukey's post hoc test. A p-value of less than 0.05 was considered statistically significant.

U-^{13}C-Glucose tracing 48 h (mean enrichment)							
	overall p-value	**wt vs 132H**	**wt vs 172K**	**wt vs 140Q**	**132H vs 172K**	**132H vs 140Q**	**172K vs 140Q**
CysGlu	6.60E-05	1.00E-02	4.74E-05	--	--	--	2.33E-03
GSH	1.41E-05	3.86E-03	1.22E-05	--	--	--	5.02E-04
U-^{13}C-Glucose tracing 48 h (isotopologues)							
m0_GSH	6.06E-04	2.53E-02	2.87E-04	--	---	--	--
m1_GSH	3.65E-04	3.66E-04	--	--	--	--	--
m2_GSH	1.42E-05	2.26E-04	1.43E-05	3.56E-02	--	--	1.08E-02
m3_GSH	9.54E-05	1.08E-02	4.58E-05	4.98E-03	--	--	--
m4_GSH	3.06E-03	--	1.58E-03	--	--	--	--
m5_GSH	4.82E-03	4.96E-02	3.01E-03	--	--	--	--
m0_CysGlu	1.68E-03	--	8.08E-04	--	--	--	--
m1_CysGlu	4.04E-06	1.50E-06	3.04E-03	--	1.14E-02	1.92E-03	--
m2_CysGlu	5.89E-05	1.68E-03	6.24E-05	--	--	--	5.53E-03
m3_CysGlu	1.32E-03	--	6.50E-04	4.86E-02	--	--	--

m4_CysGlu	2.67E-03	--	1.35E-03	--	--	--	--
m5_CysGlu	2.40E-02	--	1.52E-02	--	--	--	--
U-^{13}C-Glutamine tracing 48 h (mean enrichment)							
	overall p-value	**wt vs 132H**	**wt vs 172K**	**wt vs 140Q**	**132H vs 172K**	**132H vs 140Q**	**172K vs 140Q**
CysGlu	9.16E-07	1.66E-03	5.00E-06	--	--	1.89E-03	5.60E-06
GSH	1.72E-06	4.89E-03	5.88E-05	--	--	3.00E-04	4.30E-06
U-^{13}C-Glutamine tracing 48 h (isotopologues)							
m0_GSH	2.72E-07	--	9.88E-05	1.52E-02	2.34E-03	6.44E-04	1.00E-07
m1_GSH	4.31E-03	--	1.53E-02	--	4.58E-03	--	4.92E-02
m3_GSH	7.63E-05	1.08E-04	4.02E-03	3.65E-04	--	--	--
m5_GSH	2.46E-08	4.27E-05	1.00E-08	9.72E-03	2.06E-03	--	9.80E-06
m0_CysGlu	2.97E-07	1.80E-02	4.10E-06	--	5.68E-03	1.49E-03	5.00E-07
m1_CysGlu	4.05E-03	--	1.01E-02	--	6.11E-03	--	3.58E-02
m5_CysGlu	9.22E-06	1.22E-03	5.40E-06	--	--	--	1.77E-03

Table S14. Analysis of variance (ANOVA) of isotopic mean enrichment and isotopologue distribution in TCA cycle intermediates and 2-HG from U-^{13}C-glucose / glutamine tracing experiments were performed in R (version 3.5.1). Pairwise comparisons between cell lines were performed with Tukey's post hoc test. A p-value of less than 0.05 was considered statistically significant.

U-^{13}C-Glutamine tracing 24 h (mean enrichment)							
	overall p-value	**wt vs 132H**	**wt vs 172K**	**wt vs 140Q**	**132H vs 172K**	**132H vs 140Q**	**172K vs 140Q**
2-HG	2.65E-06	3.84E-04	2.90E-06	--	--	3.53E-02	2.23E-04
Citrate	8.37E-04	5.51E-03	1.09E-03	--	--	--	--
α-KG	8.77E-09	3.00E-07	1.00E-07	--	--	4.61E-05	5.80E-06
Succinate	1.74E-03	4.40E-02	9.42E-03	--	--	4.51E-02	4.68E-03
Fumarate	2.99E-03	3.90E-02	1.17E-02	--	--	--	1.83E-02
Malate	1.89E-03	2.12E-02	8.15E-03	--	--	4.37E-02	1.73E-02
U-^{13}C-Glutamine tracing 24 h (isotopologues)							
m0_Citrate	9.64E-04	5.12E-03	2.61E-03	--	--	--	3.91E-02
m2_Citrate	6.45E-03	3.35E-02	--	--	--	3.25E-02	--
m4_Citrate	9.62E-04	8.64E-03	5.19E-03	--	--	2.60E-02	1.59E-02
m5_Citrate	2.67E-02	2.14E-02	--	--	--	--	--
m4_Succinate	1.98E-03	3.92E-02	5.36E-03	--	--	--	9.52E-03
m4_Fumarate	3.74E-03	3.06E-02	2.57E-02	--	--	3.41E-02	2.87E-02
m4_Malate	1.68E-03	1.02E-02	7.06E-03	--	--	3.21E-02	4.53E-02

Table S15. Analysis of variance (ANOVA) of isotopic mean enrichment and isotopologues of fatty acids (C16:0) from U-^{13}C-glucose / glutamine tracing experiments, as well as uptake of fatty acids of the cells after 48 h incubation were performed in R (version 3.5.1). Pairwise comparisons between cell lines were performed with Tukey's post hoc test. A p-value of less than 0.05 was considered statistically significant.

C16:0 mean enrichment							
	overall p-value	**wt vs 132H**	**wt vs 172K**	**wt vs 140Q**	**132H vs 172K**	**132H vs 140Q**	**172K vs 140Q**
Glc tracing_48h	3.24E-06	2.40E-06	--	9.28E-03	8.85E-05	6.10E-03	--
Gln tracing_48h	2.67E-06	2.90E-06	2.25E-02	5.80E-05	3.03E-03	--	--
U-^{13}C-Glucose tracing (48 h)							
	overall p-value	**wt vs 132H**	**wt vs 172K**	**wt vs 140Q**	**132H vs 172K**	**132H vs 140Q**	**172K vs 140Q**
[M+0]	8.81E-04	3.92E-04	--	--	--	--	--
[M+10]	9.82E-03	5.55E-03	--	--	--	--	--
[M+12]	2.70E-04	1.39E-04	8.12E-03	2.44E-02	--	--	--
[M+14]	3.19E-06	1.50E-06	2.83E-04	2.00E-03	--	1.67E-02	--
[M+16]	4.57E-07	3.00E-07	2.99E-05	3.21E-04	--	1.27E-02	--
U-^{13}C-Glutamine tracing (48 h)							
	overall p-value	**wt vs 132H**	**wt vs 172K**	**wt vs 140Q**	**132H vs 172K**	**132H vs 140Q**	**172K vs 140Q**
[M+0]	3.46E-04	2.89E-04	3.37E-02	2.69E-03	--	--	--
[M+2]	9.28E-05	5.20E-05	2.14E-02	2.54E-03	--	--	--
[M+4]	1.83E-04	1.65E-04	2.85E-02	1.41E-03	--	--	--
[M+6]	4.52E-04	6.94E-04	4.13E-02	1.34E-03	--	**--**	--
C16:0 uptake (48 h)							
	overall	**wt vs 132H**	**wt vs 172K**	**wt vs 140Q**	**132H vs 172K**	**132H vs 140Q**	**172K vs 140Q**
uptake	9.01E-05	8.71E-05	--	3.97E-02	2.76E-04	2.23E-03	--

12 Publications and Presentations

Peer-Reviewed Journal Articles

1. **Sun X**, Heinrich P, Berger RS, Oefner PJ, Dettmer K.
   Quantification and ^{13}C-Tracer Analysis of Total Reduced Glutathione by HPLC-QTOFMS/MS, *Anal Chim Acta*, 2019, 1080, 127-137.
2. **Sun X**, Berger RS, Heinrich P, Marchiq I, Pouyssegur J, Renner K, Oefner PJ, Dettmer K.
   Simultaneous determination of GSH and GSSG in cultured cells by LC-UV-QTOFMS after in situ derivatization with N-ethylmaleimide. *Metabolites*. In revision.
3. Arlt A, von Bonin F, Rehberg T, Perez-Rubio P, Engelmann JC, Limm K, Reinke S, Dullin C, **Sun X**, Specht R, Maulhardt M, Linke F, Bunt G, Klapper W, Vockerodt M, Wilting J, Pukrop T, Dettmer K, Gronwald W, Oefner PJ, Spang R, Kube D.
   High CD206 levels in Hodgkin lymphoma-educated macrophages are linked to matrix-remodeling and lymphoma dissemination, *Molecular Oncology*, 2020, 14, 571-589.
4. Blazquez R, Rietkötter E, Wenske B, Wlochowitz D, Sparrer D, Vollmer E, Müller G, Seegerer J, **Sun X**, Dettmer K, Barrantes-Freer A, Stange L, Utpatel K, Bleckmann A, Treiber H, Bohnenberger H, Lenz C, Schulz M, Reimelt C, Hackl C, Grade M, Büyüktas D, Siam L, Balkenhol M, Stadelmann C, Kube D, Krahn MP, Proescholdt MA, Riemenschneider MJ, Evert M, Oefner PJ, Klein CA, Hanisch UK, Binder C, Pukrop T.
   LEF1 supports metastatic brain colonization by regulating glutathione metabolism and increasing ROS resistance in breast cancer, *Int J Cancer*, 2020, 146, 3170-3183.
5. Feist M, Schwarzfischer P, Heinrich P, **Sun X**, Kemper J, von Bonin F, Perez-Rubio P, Taruttis F, Rehberg T, Dettmer K, Gronwald W, Reinders J, Engelmann JC, Dudek J, Klapper W, Trümper L, Spang R, Oefner PJ, Kube D.

Cooperative STAT/NF-κB signaling regulates lymphoma metabolic reprogramming and aberrant GOT2 expression, *Nature Communications*, 2018, 9, 1514-1527.

Oral presentations

1. Thessaloniki 2019 - 5th workshop on analytical metabolomics
   Title: “Quantification and ^{13}C-Tracer Analysis of Total Reduced Glutathione by HPLC-QTOF MS/MS”
2. Doktorandenseminar Hohenroda 2020 - 30. Doktorandenseminar des AK Separation Science
   Title: “Glutathione determination and ^{13}C-tracer analysis in cell cultures by HPLC-QTOF MS/MS”

13 Summary

This thesis describes the development and optimization of mass spectrometry-based methods for glutathione determination and ^{13}C-tracer analysis in cultured cells. Glutathione is an essential endogenous antioxidant and plays an important role in cellular defense against oxidative damage. In this thesis, an HPLC-UV-MS method was developed for the simultaneous determination of GSH and GSSG in cultured cells following derivatization of GSH with N-ethylmaleimide (NEM) to prevent GSH autooxidation. LC-UV was used to detect the GS-NEM conjugate by monitoring its UV absorbance at 210 nm. Subsequently, GSSG and the corresponding stable isotope labeled internal standard (glutathione-(glycine-$^{13}C_4$,$^{15}N_2$)) were detected by mass spectrometry. Here, direct GSSG determination can be achieved without additional sample preparation. The method implemented in this thesis provides a straightforward and rapid approach for GSH and GSSG determination in cell culture samples and other biospecimens that may require minor adaption of the method. In some cases, only the total glutathione pool is of the interest. To that end, an optimized reduction procedure, employing dithiothreitol (DTT), was developed to achieve quantification of total reduced glutathione (tGSH) in cultured cells by LC-MS. Both of the developed methods introduced above were validated by testing LOD, LLOQ, intra-/inter-day precision, as well as recoveries with spike-in experiments.

In addition to quantitative metabolite analysis, ^{13}C-tracer experiments to study metabolism are a major component of this thesis. In this context, a wide window MRM strategy on a QTOF instrument was introduced to perform ^{13}C-tracer analysis of glutathione. With this approach, isotopologue profiles of both precursor and product ions can be obtained simultaneously with high resolution, thus obviating the need to set up individual transitions. Q1 window width was adjusted to achieve accurate determination and to reduce potential interferences as much as possible. The developed method was applied to U-^{13}C-glucose / U-^{13}C-glutamine tracer analysis of glutathione in wild-type and IDH1-R132H mutant HCT116 cells to study the contributions of glucose and glutamine to glutathione biosynthesis in the absence or presence of IDH1 mutation. Interestingly, IDH1-R132H cells exhibited a higher dependence on glutamine for glutathione

biosynthesis than wild-type controls. The strategy introduced here can also be employed to the tracer analysis of other metabolites after a metabolite specific optimization of the MRM window width.

Finally, by combining U-^{13}C-glucose / glutamine tracing experiments with mass spectrometry-based ^{13}C labeling profile analysis, the effects of different IDH1/2 mutations on cellular metabolism were systematically investigated by comparing ^{13}C enrichment and isotopologue distribution in various metabolites including amino acids, organic acids, fatty acids, and GSH in the HCT116 cell panel. Changes in metabolism observed due to IDH1/2 mutation included different pathways and substrates that the cells use to supply TCA cycle intermediates, fatty acids, amino acids, as well as endogenous antioxidant glutathione. Cells harboring an IDH mutation tend to rely more on glutamine to refuel intracellular amino acids such as glutamate and aspartate, GSH, as well as TCA intermediates. In addition, the *de novo* biosynthesis of fatty acids is significantly decreased in IDH mutant cells.

Affidavit

I hereby declare that I have written the present doctoral thesis myself without the use of any other sources and tools than those explicitly stated.

_____ _____

Place, date Signature